

Study of different Dark Matter models with extended Higgs sector

by

Amit Dutta Banik

Enrolment No.: PHYS05201004004

**Saha Institute of Nuclear Physics
Kolkata**

*A thesis submitted to the
Board of Studies in Physical Science Discipline
In partial fulfillment of requirements
For the Degree of*

DOCTOR OF PHILOSOPHY

of

HOMI BHABHA NATIONAL INSTITUTE

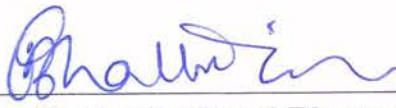


June, 2016

Homi Bhabha National Institute

Recommendations of the Viva Voce Committee

As members of the Viva Voce Committee, we certify that we have read the dissertation prepared by Amit Dutta Banik entitled "Study of different Dark Matter models with extended Higgs sector" and recommend that it may be accepted as fulfilling the thesis requirement for the award of Degree of Doctor of Philosophy.



Date : 10/08/2016

Chairman : Prof. Pijushpani Bhattacharjee, SINP



Date : 10/08/2016

Guide & Convener : Prof. Debasish Majumdar, SINP



Date : 10/08/2016

Examiner : Prof. Narendra Sahu, IIT Hyderabad



Date : 10/8/2016

Member : Prof. Subhendu Rakshit, IIT Indore



Date : 10/08/2016

Member : Prof. Ambar Ghosal, SINP

Final approval and acceptance of this thesis is contingent upon the candidate's submission of the final copies of the thesis to HBNI.

I hereby certify that I have read this thesis prepared under my direction and recommend that it may be accepted as fulfilling the thesis requirement.

Date : Aug, 10, 2016
Place : Kolkata

Guide



STATEMENT BY AUTHOR

This dissertation has been submitted in partial fulfillment of requirements for an advanced degree at Homi Bhabha National Institute (HBNI) and is deposited in the Library to be made available to borrowers under rules of the HBNI.

Brief quotations from this dissertation are allowable without special permission, provided that accurate acknowledgement of source is made. Requests for permission for extended quotation from or reproduction of this manuscript in whole or in part may be granted by the Competent Authority of HBNI when in his or her judgment the proposed use of the material is in the interests of scholarship. In all other instances, however, permission must be obtained from the author.

AMIT DUTTA BANIK

DECLARATION

I, hereby declare that the investigation presented in the thesis has been carried out by me. The work is original and has not been submitted earlier as a whole or in part for a degree / diploma at this or any other Institution / University.

AMIT DUTTA BANIK

List of Publications arising from the thesis

Journal

1. **“Extension of minimal fermionic dark matter model: A study with two Higgs doublet model”**
A. D. Banik and D. Majumdar,
Eur. Phys. J. C **75**, 364 (2015).
2. **“Inert doublet dark matter with an additional scalar singlet and 125 GeV Higgs boson”**
A. D. Banik and D. Majumdar,
Eur. Phys. J. C **74**, 3142 (2014).
3. **“Low Energy Gamma Ray Excess Confronting a Singlet Scalar Extended Inert Doublet Dark Matter Model”**
A. D. Banik and D. Majumdar,
Phys. Lett. B **743**, 420 (2015).
4. **“Possible Explanation of Indirect Gamma Ray Signatures from Hidden Sector Fermionic Dark Matter”**
A. D. Banik, D. Majumdar and A. Biswas,
Eur. Phys. J. C **76**, 346(2016).

AMIT DUTTA BANIK

DEDICATIONS

To My Family

ACKNOWLEDGMENTS

I express my sincere gratitude to all those people who have helped me to complete the six years long journey and made this dissertation possible. Foremost, I would like to express my deepest gratitude to my advisor, Prof. Debasish Majumdar for his motivation, enthusiasm and guidance that helped me all the time to complete the journey and writing of this thesis. I deeply thank him for sharing his knowledge with me and introducing me to the research field of dark matter. I would also like to express my sincere gratitude to my teachers who helped me to build a successful research career providing their immense knowledge, excellent teaching which enriched my knowledge and understanding of physics. This list includes Prof. Palash Baran Pal, Prof. Anirban Kundu, Prof. Rabindra Nath Chatterjee (Retired Professor, St. Paul's College), Prof. Arup Roy (Retired Professor, Scottish Church College). Their teaching with great effort and devotion helped me to shape my academic career and motivated me in my research. Besides that I would also like to thank my collaborator and colleague Anirban Biswas for many fruitful discussions on various academic issues which surely strengthen my knowledge about my research field.

I have been blessed with a cheerful group of friends at Saha Institute of Nuclear Physics with whom I shared precious moments throughout the journey. I would like to thank all the members of room numbers 3319 and 346 and also fellow labmates Biswarup Paul, Kalyanmoy Chatterjee, Souvik Priyam Adhya, Rajani Raman, Hitesh Rahangdale, Mahatsab Mandal, Sourav Dey, Palash Khan for discussions on various topics in physics and beyond and bringing jovial moments in my Ph.D. career. I also thank my friends Tanmoy Datta, Chirantan Singha, Arpan Pal and Chiranjib Chakrabarti for being with me till the very end of this journey and providing

refreshments in difficult times.

Most importantly, I would like to thank my family who encouraged me in all the way to achieve my goal and supported me unconditionally to prosper in life. I thank all the members of my family, to whom this dissertation is dedicated to, has been a constant source of love, concern, inspiration and strength all these years.

Finally, I would like to thank Saha Institute of Nuclear Physics, for providing me excellent opportunity to pursue my research work and also Department of Atomic Energy (DAE), Govt. of INDIA for giving me financial support as a research fellowship for the entire period of my Ph.D. work.

AMIT DUTTA BANIK

Contents

Synopsis	xvii
List of Figures	xxv
List of Tables	xxix
1 Prelude to dark matter	1
1.1 Astrophysical evidences for dark matter	2
1.2 Distribution of dark matter	6
1.3 Candidates for dark matter	7
2 Standard Model	11
2.1 Electroweak theory of Standard Model	12
2.2 Shortcoming of Standard Model	22
3 Physics of Dark Matter	27
3.1 Thermal evolution of dark matter and relic density	28
3.2 Dark matter direct detection	35
3.3 Dark matter indirect detection	36
3.4 Collider searches of dark matter	39
4 Fermionic dark matter in two Higgs doublet model	41
4.1 Introduction	41
4.2 The Model	43
4.3 Collider physics phenomenology	47
4.4 DM annihilation and relic density	50
4.5 Results	55
4.5.1 Direct detection measurements	56
4.6 Discussion	61
5 Singlet scalar extension of inert doublet model (IDM) part-I	63
5.1 Introduction	63
5.2 The Model	65
5.2.1 Scalar Sector	65
5.2.2 Constraints	67
5.3 Dark matter	70

5.3.1	Relic density	70
5.3.2	Annihilation cross section	70
5.3.3	Modification of $R_{\gamma\gamma}$ and $R_{\gamma Z}$	71
5.4	Analysis of $R_{\gamma\gamma}$ and $R_{\gamma Z}$	73
5.5	Direct Detection	77
5.6	Summary and Outlook	83
6	Singlet scalar extension of inert doublet model (IDM) part-II	85
6.1	Introduction	85
6.2	Dark matter in inert doublet model and Fermi-LAT observed gamma ray excess	87
6.3	Inert doublet model with additional singlet scalar	93
6.4	Calculation of gamma ray flux	98
6.5	Summary	101
7	Hidden sector Fermionic dark matter Model	103
7.1	Introduction	103
7.2	The Model	104
7.3	Constraints	108
7.4	Calculational procedures and Results	123
7.4.1	Constraining the model parameter space	123
7.4.2	Calculation of gamma ray signals from galactic centre and dwarf galaxies	127
7.5	Discussions and Conclusions	134
8	Summary	137
A	Diphoton and γZ decay width of scalar bosons	143

SYNOPSIS

One of the most challenging and unsolved puzzles in the present day physics is the existence of unknown matter or dark matter (DM) in the Universe. They do not emit any visible light or other electromagnetic radiation and are all pervading the Universe. Study of the cosmic microwave background radiation (CMBR) data by PLANCK [3] and WMAP [4] satellite borne experiments claim that about 26.5% of our Universe is made up of this mysterious dark matter. However, evidence for the existence of dark matter are purely through their gravitational effects such as the study of spiral galaxies (rotation curve), gravitational lensing effects of distant galaxies and the galaxy clusters etc. The particle nature of this mysterious and unobserved dark matter is overwhelmingly unknown. But they must be neutral, stable and most likely very weakly interacting massive particles (WIMPs). Although the Standard Model of particle physics (SM) is established successfully with the recent findings of SM-like Higgs, the dark matter or at least a large part of it are possibly not made up of SM particles. Also the possibility of having more than one Higgs like scalar is not ruled out by ATLAS and CMS experiments performed at Large Hadron Collider (LHC). There are shortcomings of Standard Model of particle physics and extension of SM is hence called for, in order to provide a viable explanation to the particle nature of dark matter. In this thesis, I have explored different particle physics dark matter models with SM extension in the Higgs sector. As stated earlier, dark matter particle, though possibly interacts very weakly with the matter (SM sector) may scatter nucleus of target materials via a mediator (scalar or boson). Based on this simple idea of DM-nucleon scattering, different direct detection experiments such as XENON100 [27], LUX [28], CDMS [29], CoGeNT [31], DAMA [32] etc. are designed. Direct detection experiments measure the recoil energy of the nucleus resulting from the elastic scattering of the dark matter particle off the target nucleus. The result

is then interpreted as DM-nucleon scattering for uniform comparison of the results from different experiments. Since, no such conclusive events have been observed yet, direct detection experiments provide upper limit on DM-nucleon elastic scattering cross-section (for both spin dependent and spin independent scattering) for different values of DM mass. Although direct detection experiments like CDMS, CoGeNT etc. claimed to have observed a few events supporting low mass dark matter ($\sim 10\text{-}30$ GeV), possibility of the existence of such low mass dark matter is not supported by XENON100 and latest results from LUX DM direct search experiment. Besides the direct search experiments of dark matter, there are different earth based and satellite borne experiments as well for indirect search of dark matter. Dark matter particle after suffering several scattering events inside a massive body loses its velocity to such an extent that it cannot escape the gravitational influence of the body and dark matter gets trapped within it. This may happen at the core of the astrophysical objects such as galactic centre, solar core etc. If accumulated in sufficient number these captured dark matter particles may pair annihilate into gamma rays or fermion-antifermion $f\bar{f}$ pairs ($p\bar{p}$, e^+e^- , $\nu\bar{\nu}$ etc.). Hence, any excess in observed gamma rays, $f\bar{f}$ flux detected from such objects that cannot be explained by known astrophysical processes (such as inverse Compton effect, synchrotron radiation etc.) may indicate to have produced from DM annihilation at these astrophysical sites. Satellite borne γ -ray experiments such as Fermi-LAT has reported such excess of γ -rays from the direction of galactic centre, dwarf galaxies etc. These sites are potentially thought to be rich in dark matter. Terrestrial experiments such as HESS [39], MAGIC [40] etc. also look for γ -rays from various cosmic sources (both galactic and extragalactic). Other indirect detection experiments like AMS [45], PAMELA [46] search for the excess antiparticle such as positron, antiproton etc. while ANTARES [43] experiment measures the observed cosmic neutrino flux. Fluxes of gamma ray, e^+e^- , $p\bar{p}$ etc. observed by these different experiments provide significant bound on DM annihilation cross-section $\langle\sigma v\rangle$

and mass of dark matter. In the thesis, the viabilities of the different dark matter models have been addressed. The model parameters of the proposed theoretical models are first constrained by theoretical conditions and then from experimental results and PLANCK results for dark matter relic density. It is also ensured that limits obtained from the LHC on SM Higgs and DM direct detection is obeyed.

Two Higgs doublet model (THDM) is one of the most general non-supersymmetric extensions of SM scalar sector, where an extra scalar doublet of same hypercharge is invoked in the SM. Both the doublet fields Φ_1 and Φ_2 acquire vacuum expectation values under spontaneous symmetry breaking (SSB). There are several advantages of THDM over SM as it can address the problems such as baryon asymmetry in the Universe and provide source of CP violation. The scalar sector of THDM is rich with charged scalars H^\pm , two CP even scalars h and H and one CP odd scalar A . In the thesis work, a model for singlet fermionic dark matter in two Higgs doublet model framework has been explored. For simplicity, only CP conserving THDM is taken into account which can be achieved by introducing a discrete Z_2 symmetry between the doublet fields Φ_1 and Φ_2 . There are four different types of CP conserved THDM (namely type I, II, III and IV) depending on the coupling of the doublet fields with the fermions (quarks and leptons). Out of these four types of THDM, type I and type II THDM are explored in the thesis work. The stability of dark matter fermion is ensured by an another discrete symmetry Z'_2 under which all the THDM sector including fermions and gauge bosons are odd. The singlet fermionic dark matter χ in THDM proposed in the thesis couples to Higgs doublets through a dimension five coupling and a new physics scale Λ is introduced. Throughout the work, one of the CP even scalar h is treated as SM-like Higgs discovered at LHC while the other scalar H gives the essence of new physics and this is the non-SM scalar. The Boltzmann equation is solved for the fermionic dark matter χ in the framework of type I and type II THDM for the constrained model parameter space obtained from

vacuum stability, LHC limits on SM Higgs signal strength (denoted by R), invisible decay branching ratio of SM scalar. The relic density is obtained by solving the Boltzmann equation and the direct detection cross-section and other observables are theoretically calculated for the dark matter candidate χ . The unknown parameters (such as couplings etc.) for the fermionic dark matter χ in both type I and type II THDM are then constrained by the relic density observed by PLANCK, bounds from direct dark matter search experiments, vacuum stability, SM Higgs signal strength etc.

Among other different scalar dark matter models, inert doublet model (IDM) is a simple extension of SM of particle physics which includes an additional Higgs doublet that acquires no VEV. The newly added Higgs doublet is protected by a discrete Z_2 symmetry under which all the SM sector is odd. As a result, the lightest inert particle (LIP) of the inert Higgs doublet can serve as a potential candidate for dark matter. Most importantly inert doublet model is UV complete and does not contain any non-renormalisable terms. There are also other advantages of IDM as it can generate tiny neutrino mass and deal with problems like leptogenesis when right handed Majorana neutrinos are added to the model. However, in the present thesis, only the scalar sector of the IDM is investigated in order to achieve a viable particle candidate for dark matter. In the thesis scalar sector of IDM is extended by adding a singlet scalar s to the model itself. In the proposed model added scalar receives a VEV after spontaneous symmetry breaking (SSB) and mixes up with the SM Higgs producing two Higgs like physical scalar particles h_1 and h_2 while the dark Higgs doublet (the LIP in IDM) remains intact. The particle spectrum of IDM involves charged scalars H^\pm , one CP even scalar H_0 and one CP odd scalar A_0 . The charged scalars of IDM are of great importance as they contribute significantly to the decays of SM Higgs into $\gamma\gamma$ and γZ . The signal strength of Higgs decay into diphoton $R_{\gamma\gamma}$ are measured by CMS and ATLAS experiments. CMS has reported Higgs to diphoton

signal strength $R_{\gamma\gamma}^{\text{CMS}} = 0.78_{-0.26}^{+0.28}$ while the same obtained by ATLAS experiment is $R_{\gamma\gamma}^{\text{ATLAS}} = 1.57_{-0.29}^{+0.33}$ [84]. The singlet scalar extended IDM is constrained by different theoretical and experimental bounds namely vacuum stability, unitarity, LEP II, DM relic density measured by PLANCK, Higgs to diphoton signal strength results at LHC (CMS and ATLAS), DM direct detection experimental bounds. The valid region (that satisfies all these constraints) of the model parameter space for the model is thus obtained. In order to compare the Higgs signal strength obtained from LHC, one of the CP even scalar in singlet extended IDM is treated as SM-like Higgs (h_1 with mass $m_1 = 125$ GeV) and the other scalar h_2 is the non-SM scalar which gives the results from new physics input in the scalar sector. Correlation between the signal strengths $R_{\gamma\gamma}$ and $R_{\gamma Z}$ is obtained for the valid range of model parameter space with different values of the additional non-SM scalar mass m_2 . Our calculation show that within the framework of present model, the constrained model parameter space cannot simultaneously satisfy the Higgs to diphoton signal strength results obtained from ATLAS and the direct detection limits on DM-nucleon scattering cross section given by XENON100 or LUX. However, the same model parameter space appears to explain the CMS predicted value of $R_{\gamma\gamma}^{\text{CMS}}$ and DM direct detection experimental observations simultaneously. Thus the proposed extension of the SM favours CMS data over the ATLAS results.

The model, thus justified and allowed parameter space obtained, the γ -ray flux from the annihilation of dark matter candidate in this model now calculated and compared with the observed γ -ray flux measured by Fermi-LAT [49] experiment from the direction of galactic centre or GC. Analysis of the Fermi-LAT data suggests that a 31-40 GeV dark matter annihilating into $b\bar{b}$ pair with annihilation cross-section $\langle\sigma v\rangle = 1.4 - 2.0 \times 10^{-26} \text{ cm}^3\text{s}^{-1}$ can explain the observed inner galaxy (inner 5° of GC) gamma ray results [59]. It is also shown that the dark matter candidate by extending the SM with an inert doublet model (IDM) only cannot explain the

observed GC gamma ray findings and a further extension of IDM is called for. As discussed earlier this model is then extended by including an additional singlet scalar. Inclusive study of the extended IDM with additional scalar singlet reveals that the model can provide suitable explanation for the GC γ -ray flux observation by Fermi-LAT. In this singlet extended inert doublet model a 31-40 GeV dark matter can fit the GC γ -ray results when the mass of the non-SM scalar in the model is about 70 GeV.

So far, all the dark matter models explored in the thesis, are similar in nature in the sense that the stability of DM candidate is ensured by assuming discrete Z_2 symmetry. On the other hand, SM of particle physics does not encourage any such discrete symmetry. Hence, the nature of DM candidate may not be that simple as the stabilisation of dark matter candidate by discrete symmetry is ad-hoc and dark matter may be obtained from a hidden sector which may sort out such discrepancy with SM. In the next work of the thesis therefore, a hidden sector dark matter model is proposed without invoking any discrete symmetry. In this model, the hidden sector (dark sector) follows a $SU(2)_H$ gauge theory and a doublet field similar to the SM Higgs doublet is assumed. The hidden sector fermions also have a global $U(1)_H$ symmetry which remains intact while the scalar in the dark sector is not charged under this $U(1)_H$. This $SU(2)_H$ gauge symmetry is broken spontaneously to generate masses of hidden sector particles (gauge bosons and fermions). The SM Higgs doublet mixes up with the dark Higgs doublet field resulting in two Higgs like scalar particles h_1 and h_2 which enriches the scalar sector with new physics as well. The hidden sector gauge bosons do not mix up with the SM gauge bosons due to the non-abelian nature of $SU(2)_H$ while the hidden fermions behave as a singlet under the SM sector. As the hidden sector is composed of only $SU(2)_H$ gauge, the gauge bosons in the dark sector are of equal mass. The lightest fermion in the dark sector can be treated as a potential candidate for dark matter. The dark sector fermion can

interact with SM sector only through the Higgs mediated channels as the SM Higgs doublet mixes with the dark Higgs doublet. The parameter space of the hidden dark matter scenario is constrained by several theoretical and experimental bounds and valid model parameter space is obtained. An updated study of GC gamma ray results has been done by Calore, Cholis and Weniger (CCW) [60]. The viability of the present model is further tested by comparing the GC gamma ray flux computed for the allowed model parameter space with this updated analysis of Fermi-LAT data of GC gamma ray. In addition, recently Fermi-LAT also investigated the gamma ray flux for 15 different dwarf galaxies [61]. From their observation of dwarf galaxies, Fermi-LAT provides bound on the γ -ray flux and also give limits on DM annihilation cross-sections for different DM mass. Similar studies for eight newly found dwarf galaxies are also given by Dark Energy Survey (DES) in collaboration with Fermi-LAT [62]. Moreover, detailed study of the gamma ray flux obtained for another dwarf galaxy Reticulum 2 (Ret2) by Geringer-Sameth et. al [133] reported an excess emission of gamma ray which can be a promising signature of dark matter as dwarf galaxies are supposed to be enriched with dark matter. Comprehensive study of this proposed $SU(2)_H$ fermionic dark matter is carried out thoroughly in order to compare the gamma ray flux obtained for dark matter annihilation calculation in this model with the dwarf galaxy gamma ray observations (including Ret2 observation as well). We show that the available model parameter space of hidden sector $SU(2)_H$ fermionic dark matter can indeed explain the updated GC gamma ray results from CCW, dwarf galaxy gamma ray flux results and the excess of γ ray obtained from Ret2.

The thesis is composed of eight chapters and these are as follows,

Chapter 1. Prelude to dark matter :

In this chapter the primary introduction dark matter problem will be addressed. Some astrophysical evidences for dark matter and nature of dark matter will be discussed also in this chapter.

Chapter 2. Standard Model :

In this chapter, a brief overview of Standard Model of particle physics will be presented and deficiencies of SM will be discussed.

Chapter 3. Physics of Dark Matter :

In this chapter detailed study thermal evolution of dark matter will be presented. Direct and indirect detection methods of dark matter candidate will also be discussed in this chapter.

Chapter 4. Fermionic dark matter in two Higgs doublet model :

Comprehensive study of particle physics model for fermionic dark matter in two Higgs doublet model will be explored in this chapter.

Chapter 5. Singlet scalar extension of inert doublet model (IDM) part-I :

In this chapter, detailed study of inert doublet model with additional scalar singlet will be addressed.

Chapter 6. Singlet scalar extension of inert doublet model (IDM) part-II :

In this chapter inclusive study of galactic centre gamma ray excess with a singlet scalar extended inert doublet dark matter model will be explored.

Chapter 7. Hidden sector Fermionic dark matter Model:

A model for hidden fermionic dark matter originating from a hidden $SU(2)_H$ will be presented in this chapter.

Chapter 8. Summary :

In this chapter the thesis will be summarised and the future directions will be addressed.

List of Figures

1.1	Rotation curve for the spiral galaxy NGC 6503 adopted from Ref. [1].	2
1.2	Gravitational lensing effect produced by Abell 2218 galaxy cluster. . .	3
1.3	Image of Bullet cluster 1E0657-56 observed by Chandra X-ray observatory [2].	5
2.1	Potential V plotted against the variation of scalar field Φ for $\mu^2 > 0$ and $\mu^2 < 0$	14
4.1	Allowed $\sin\alpha$ - $\tan\beta$ parameter space for type I THDM consistent with R_{CMS} within the framework of present DM model (Fig. 4.1a). Green and blue coloured regions are for $m_H = 150$ GeV and 200 GeV respectively. Similar plots for the case of type II THDM is shown in Fig. 4.1b. Valid parameter space in type II THDM satisfying R_{ATLAS} only is depicted in Fig. 4.1c. The computation for all the plots are performed with the constrained range of model parameter space values which produce required DM relic density consistent with PLANCK results. For all the plots the constrained $R'_{I,II}$ is respected.	54

4.2	Fig. 4.2a-b shows the $m_\chi - \sigma_{\text{SI}}$ parameter space for FDM in type I THDM is allowed by PLANCK relic density and collider bounds plotted using R_{CMS} for $m_H = 150$ and 200 GeV. Similar plots in $m_\chi - \sigma_{\text{SI}}$ plane with type II THDM are shown in Fig. 4.2c-d whereas the plots in Fig. 4.2e-f are in agreement with R_{ATLAS} and $R'_{I,II} \leq 0.2$. The red and blue lines are respective bounds on DM-nucleon scattering cross-section from XENON100 and LUX DM direct search experiments.	60
5.1	Variation of $R_{\gamma\gamma}$ with DM mass m_{H_0} satisfying DM relic density for $m_2 = 150$ and 300 GeV.	75
5.2	Correlation plots between $R_{\gamma\gamma}$ and $R_{\gamma Z}$ for two choices of h_2 mass (150 and 300 GeV).	76
5.3	Allowed regions in $m_{H_0} - \sigma_{\text{SI}}$ plane for $m_2 = 150$ and 300 GeV. . . .	78
5.4	Allowed regions in $R_{\gamma\gamma} - R'_{\gamma\gamma}$ plane for $m_2 = 150$ and 300 GeV. . . .	79
6.1	The left panel shows the $m_{H_0} - \sigma_{\text{SI}}$ space allowed by DM relic density obtained from PLANCK. The right panel presents the variation of invisible decay branching ratio Br_{inv} with DM mass m_{H_0} for the same.	91
6.2	The upper panel shows the valid $m_{H_0} - \sigma_{\text{SI}}$ plane obtained for $m_1 = 70$ GeV with $\cos \alpha = 0.9 \times 10^{-3}$ and 3.5×10^{-2} . The lower panel shows the variation of signal strength R_2 with σ_{SI} for $m_{H_0} = 35$ GeV for the same.	95
6.3	Allowed parameter space in $R_1 - \sin \alpha$ plane for $m_1 = 70$ GeV. Also shown in blue corresponds to the parameter space for $m_{H_0} = 35$ GeV.	96

6.4	γ -ray flux obtained from the benchmark points in Table 6.1 and compared with the results from [59] for two different mixing angles.	100
7.1	Feynman diagrams for dark matter annihilation into fermions (quarks and leptons), gauge bosons and scalars contributing to DM annihilation cross-section.	112
7.2	The allowed range of $m - \sigma_{\text{SI}}$ parameter space obtained for $m_2 = 100$ GeV (left panel) and $m_2 = 110$ GeV (right panel) plotted using the bounds from vacuum stability, LHC constraints on SM Higgs and relic abundance of DM obtained from PLANCK [3]. Limits on DM-nucleon cross-section from LUX [28] is also plotted (blue line) for comparison.	124
7.3	The valid model parameter space in $\lambda_3 - \alpha$ (in deg) plane obtained for the case of $m_2 = 100$ GeV (left panel) and $m_2 = 110$ GeV (right panel) satisfying the limits from vacuum stability, LHC findings, PLANCK DM relic abundance and direct detection limits on σ_{SI} from LUX experiment.	126
7.4	Comparison of the GC γ -ray flux data from [60] with those calculated for benchmark points in Table 7.1.	128
7.5	The allowed range of $m - \langle\sigma v\rangle$ space (for annihilation into $b\bar{b}$) along with the bounds on $\langle\sigma v\rangle$ (into $b\bar{b}$ channel only) obtained from GC γ ray search results CCW [60] and dwarf galaxies [61, 62] compared with the same obtained from benchmark points in Table 7.1.	130
7.6	Comparison of the observed upper bound on γ -ray flux for 8 DES dSphs with the calculated γ -ray flux from BP1 and BP2 tabulated in Table 7.1.	132

7.7	Benchmark points BP1 and BP2 compared with the allowed region of model parameter space shown in $m - J_{19}\langle\sigma\nu\rangle_{-26}$ plane obtained from [133]	133
-----	---	-----

List of Tables

1.1	Dark matter halo density functions and scaling parameters.	6
5.1	Benchmark points satisfying observed DM relic density obtained from PLANCK data and direct detection cross-section reported by LUX results for two different choices of h_2 mass.	82
6.1	Benchmark points of singlet extended IDM with DM mass $m_{H_0} = 35$ GeV.	99
7.1	Benchmark points obtained from the constrained model parameter space in agreement with the bounds from vacuum stability, SM Higgs signal strength from LHC, DM relic density from PLANCK and LUX DM search bounds on DM-nucleon scattering cross-section.	128

Chapter 1

Prelude to dark matter

One of the most astounding and unresolved puzzle in modern physics and cosmology in present era is dark matter (DM). Cosmological evidences from the study of cosmic microwave background radiation (CMBR) indicate that dark matter constitutes about 26% of our Universe while only 5% of the visible Universe is formed by baryonic matter. The rest 69% of the Universe is made up of mysterious energy known as dark energy. The visible Universe is mainly governed by four kind of forces (gravitation, weak, strong and electromagnetic) which can be well explained by Standard Model (SM) of particle physics. However, signatures of dark matter observed in the Universe is purely gravitational and nature of dark matter still remains unexplained. Although strong gravitational evidences in support of the presence of dark matter in Universe is found, the pattern of dark matter distribution in the Universe is not known. Besides, particle constituent of dark matter is also unknown and numerous particle physics models for dark matter candidate with mass ranging from few keV to hundreds of TeV are proposed. In this chapter we will discuss some preliminary topics related to basic concept in dark matter physics.

1.1 Astrophysical evidences for dark matter

- **Velocity distribution curves for spiral galaxies**

As mentioned, most compelling evidence for dark matter is gravitational in

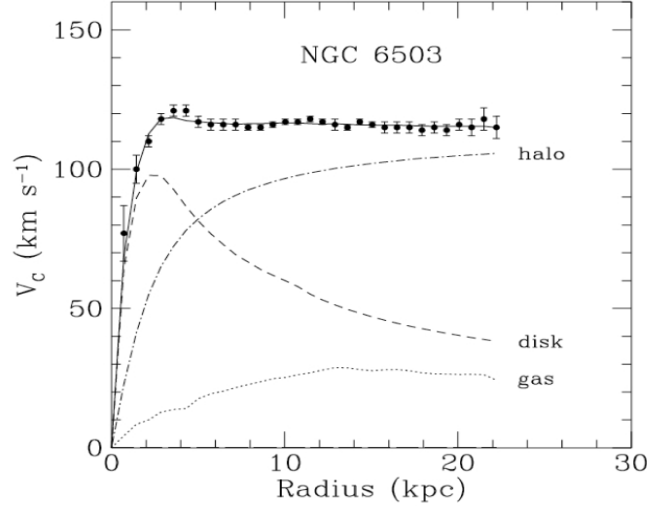


Figure 1.1: Rotation curve for the spiral galaxy NGC 6503 adopted from Ref. [1].

nature. One of the most prominent gravitational evidences for dark matter is related to observation of rotation curves of spiral galaxies. Galaxy rotation curves are basically the measure of rotational velocity $v(r)$ of a star or gas at a distance r from the galactic centre. According to Newtonian dynamics, velocity of a star at a distance r from galactic centre (GC) enclosing a mass $M(r) = \int_0^r \rho(r')r'^2 dr'$ will be

$$v(r) = \sqrt{\frac{GM(r)}{r}}, \quad (1.1)$$

where ρ denotes the density of matter within the central part of the galaxy. Hence, it is clear from Eq. 1.1 that in the inner core region of the galaxy, velocity of star will increase with distance $v(r) \propto r$. On the other hand for star or gas residing at the outer shell of the galaxy will fall gradually following

$v(r) \propto \frac{1}{\sqrt{r}}$ when mass of outer region of the galaxy is neglected where the mass density of visible mass is much less than that in the central region of the galaxy. Observation of velocity distribution curves for rotating star (or gas) around the galactic centre for different spiral galaxies shows that though the velocity of rotating matter within the central region of galaxy increases and obeys the relation $v(r) \propto r$ but for regions away from the dense central regime of the galaxy velocity distribution do not follow the predicted relation $v(r) \propto \frac{1}{\sqrt{r}}$ and remains constant. Instead, from these observations it can be concluded that there is considerable amount of mass present in the outer part of galaxy than expected. This indicates the presence of dark matter halo of a galaxy whose extent is far beyond the reaches of the galaxy and the galaxy is embedded in this dark matter halo. In Fig. 1.1 the observed rotation curve (velocity distribution plotted against radial distance) for NGC6503 spiral galaxy is shown as an example. The contribution to the velocity distribution from galactic disk, gas and dark matter halo are mentioned within the figure.

- **Gravitational lensing**

Gravitational lensing effect also provides strong evidence for the existence of

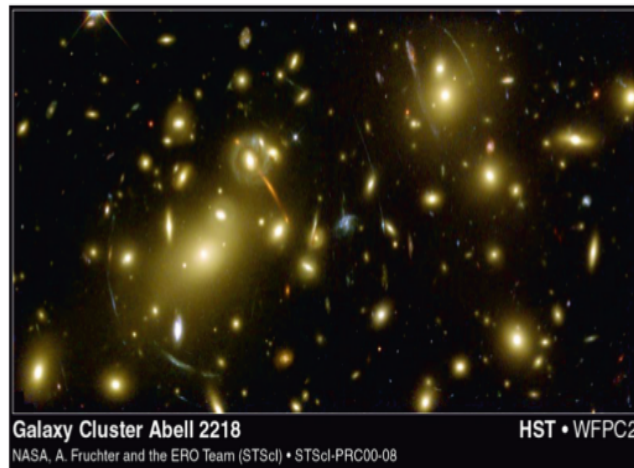


Figure 1.2: Gravitational lensing effect produced by Abell 2218 galaxy cluster.

invisible and unknown dark matter. Gravitational lensing is based on Einstein's general theory of relativity. Light rays originated from distant sources bend due to immense gravitational force exerted by massive astrophysical objects (such as galaxy clusters). As a result, multiple images of a distant object behind the galaxy cluster will be formed when seen through a telescope placed at the foreground of the cluster. Mass of a galaxy cluster can be estimated from the deflection angle of light from the background cluster. Such lensing observations of galaxy cluster provides an estimate of total mass present in the cluster. A comparison of this total mass with the estimated visible mass (mainly from X-ray emitting gas) shows that the total mass far exceeds the observed visible mass confirming the presence of huge amount of dark matter in galaxy cluster. This indicates the existence of dark matter halo surrounding the visible part of the cluster. Fig. 1.2 shows an example of gravitational lensing effect produced by Abell 2218 cluster. The images of a background galaxy or galaxy cluster lensed by the background Abell 2218 cluster forms a ring like at the left central region.

- **Bullet Cluster**

Existence of dark matter in the Universe is also confirmed by the study of colliding galaxies (also known as bullet cluster). Collision of galaxies produce hot X-ray emission due to interaction of baryonic matters within which is observed then by X-ray telescopes. Mass of the cluster is obtained from the study of gravitational lensing effects produced by the cluster. It is found that the lensing is weak near visible mass (region of X-ray emission which contains about 90% of the total visible matter within the cluster). Strong lensing region suggests presence of massive substructures situated afar from the visible region. Hence mass distribution (or gravitation potential) do not follow the baryonic mass distribution, is governed by dark matter distribution of the galaxy cluster.



Figure 1.3: Image of Bullet cluster 1E0657-56 observed by Chandra X-ray observatory [2].

This offset between the visible region and massive substructure confirms the presence of dark matter halos which do not interact with baryonic matter and passes through each other during the collision. In Fig. 1.3 an image of Bullet cluster 1E0657-56 observed by Chandra X-ray observatory is shown.

- **Cosmic Microwave Background Radiation**

An estimate of dark matter content of the Universe is given by observing and analysing the anisotropies in Cosmic Microwave Background Radiation (CMBR). The satellite borne experiment namely PLANCK [3] or WMAP [4] (Wilkinson Microwave Anisotropy Probe) look for anisotropies in CMBR. This microwave background radiation is basically the early photons that decoupled from the thermal bath of Universe in the recombination epoch. PLANCK (and earlier WMAP) measures the anisotropies in the temperature of Universe. This fluctuation in temperature can be expressed in the form of spherical harmonics and angular power spectrum is obtained. CMB angular spectrum data is then compared with different cosmological models to find out best fit values of model parameters (such as baryon density $\Omega_b h^2$, matter density $\Omega_m h^2$, cosmological

constant Λ etc.¹). Analysis of CMBR by PLANCK predicts $\Omega_b h^2 = 0.022$ and $\Omega_m h^2 = 0.1423 \pm 0.0029$ (68% C.L.) which ensures that most of the matter in the Universe is made up of dark matter.

1.2 Distribution of dark matter

Name of halo profile	Density distribution $\rho(r)$	r_s kpc	ρ_s GeV/cm ³	α
NFW [5]	$\rho_s \frac{r_s^3}{r(r+r_s)^2}$	20.0	0.259	-
Einasto [6]	$\rho_s \exp \left[-\frac{2}{\alpha} \left[\left(\frac{r}{r_s} \right)^\alpha - 1 \right] \right]$	20.0	0.061	0.17
Isothermal [7]	$\frac{\rho_s r_s^2}{(r+r_s)^2}$	3.5	2.069	-
Moore [8]	$\left(\frac{r_s}{r} \right)^{1.16} \left(1 + \frac{r}{r_s} \right)^{-1.84}$	30.28	0.108	-
Burkert [9]	$\frac{\rho_s}{(1+r/r_s)(1+(r/r_s)^2)}$	12.67	0.727	-

Table 1.1: Dark matter halo density functions and scaling parameters.

Presence of dark matter in the Universe is well established from both cosmological and astrophysical studies. However, dark matter distribution within the Universe is not well defined. Dark matter halo provides valuable information about dark matter density distribution $\rho(r)$ within massive astrophysical bodies (galaxies, galaxy clusters, dwarf galaxies etc.) where r usually denotes the distance from the centre of the observed body. Different theoretical models for dark matter halo is motivated from the observation of spiral galaxy rotation curves in galactic scale and numerical simulations. In general, dark matter halo profiles are assumed to be canonical in nature. In Table 1.1, we tabulate characteristic formulae of density distribution and respective parameters for different halo models for dark matter. Parameters r_s and ρ_s in Table 1.1 denote scale radius and scale density of the corresponding halo profile.

¹ $\Omega = \frac{\rho}{\rho_c}$, is the density ρ of a particular species normalised to the critical density ρ_c of the Universe. The dimensionless quantity h denotes the Hubble parameter at present epoch normalised to the value $100 \text{ kms}^{-1} \text{ MPc}^{-1}$.

Values of scale radius and scale density for different halo profiles tabulated in Table 1.1 are normalised in a manner such that it produce local dark matter density $\rho_{\odot} = 0.3$ GeV/cm³ at a distance $r = r_{\odot} = 8.5$ kpc from galactic centre. Apart from the Einasto halo profile mentioned in Table 1.1, a modified Einasto profile known as EinastoB [10] is also preferred when contribution from baryonic matter is taken into account. EinastoB halo profile is steeper than the usual Einasto profile having smaller value of $\alpha = 0.11$.

1.3 Candidates for dark matter

In previous section, we have discussed structural models for dark matter halos in the Universe. Although astrophysical observation suggests strong evidence in support of dark matter, particle nature of dark matter is still a mystery to be resolved. Also the interaction nature of dark matter with baryonic matter is not known. There are several particle physics models which provide a plausible candidate for dark matter. In this section we will briefly discuss particle physics candidates for dark matter. Depending on the constituent of dark matter, there are two different types of dark matter candidates namely baryonic and non-baryonic. Since Standard Model of particle physics can not account for dark matter candidates, dark matter particle would mostly follow from a theory beyond Standard Model. Besides baryon budget of Universe is small compared to dark matter density which indicates that dark matter is mostly non baryonic. Before we initiate discussion on particle candidates for dark matter, we must mention some general features of dark matter candidate,

- The dark matter candidate must be stable in nature with high decay lifetime (more than the age of Universe.)

- Dark matter must be very weakly interacting, almost having no interaction with normal matter such as baryons, leptons, photons etc.
- The self interaction between dark matter particles should be small otherwise halo evaporation will occur which is in contrast with the gravitational lensing effect.

Based on these characteristic features, theoretical models for non baryonic dark matter are proposed. Dark matter candidates obtained from these models are commonly assumed as Weakly Interacting Massive Particles or WIMPs [11]. Supersymmetry (SUSY) is one of the popular theories beyond Standard that provides WIMP like candidates for dark matter [1]. The lightest supersymmetric particle (LSP) appearing in supersymmetric models is considered to be a viable candidate for dark matter. Stability of LSP is ensured by R parity conservation of fermionic superpartners of gauge boson and Higgs boson are highly motivated candidates for dark matter in supersymmetric models. Axinos, gravitinos (superpartner of non SM particles such as Axions, graviton) are also treated as plausible dark matter candidate as well. Apart from supersymmetry based dark matter models there are also different non-SUSY dark matter models which may provide viable dark matter candidates. For example, particle physics models with sterile neutrino dark matter and Axion dark matter are pursued in literatures. Extra dimension models for dark matter are also explored where lightest Kaluza Klein particle (LKP) in Universal extra dimension (UED) serves as a potential candidate for dark matter [12]. Simple non-SUSY extension of the Standard Model Higgs sector with singlet scalar [13], inert scalar doublet [14] where a Z_2 symmetry is invoked in order to stabilise the lightest scalar particle (dark matter candidate) have also been explored as well. There are also proposals for fermion dark matter models [15], vector dark matter models [16] etc. in literatures.

In the above, we have mentioned different non baryonic dark matter candidates obtained from extension of Standard Model of particle physics. Based on the freeze out temperature of dark matter (for details see Chapter 3), non baryonic dark matter candidates can be classified into three categories.

- Cold dark matter (CDM) is the type of dark matter which is non relativistic in nature at the time of its decoupling (freeze out) from the rest of the Universe. The freeze out temperature (T_F) of these types of dark matter is such that $x_F \gg 3$, where $x_F = m/T_F$, m being the mass of dark matter particle. Sneutrino, neutralino, singlet scalar dark matter, inert doublet dark matter etc. in different particle physics models are the candidates of CDM.
- Hot dark matter (HDM) particles, are those for which freeze out occurs for $x_F \ll 3$ (i.e., at higher temperature than its mass) and hence for this case, dark matter particle is relativistic. Apart from SM neutrinos, axinos can also be potential hot dark matter candidate.
- Warm dark matter (WDM) corresponds to the case when dark matter is neither cold nor hot. Sterile neutrino, gravitino etc. are example of warm dark matter candidates.

Dark matter can further be distinguished into two sectors depending on the nature of its evolution in the Universe. If the dark matter candidate (produced at some early stage) remains in equilibrium with the expanding Universe and decouples from the thermal bath at some decoupling temperature (freeze out) then the dark matter component is known as thermal dark matter. On the other hand if dark matter component is initially absent at early stage of Universe and produced later from out of equilibrium decay of some long lived particles or scalar fields, then it is called non thermal dark matter. Dark matter candidates such as singlet scalar dark

matter, inert doublet dark matter etc. which are produced thermally and freezes out are common example of thermal dark matter whereas axion having a non thermal production mechanism is a plausible candidate for non thermal dark matter. Of late there is a proposal for another category of dark matter known as Feebly Interacting Massive Particles or FIMPs [17]-[18]. In this case some dark matter already present in the Universe at very early epoch are not in thermal equilibrium and the interaction is very weak (coupling strength $\sim 10^{-12}$). Such candidates grow and approaches chemical equilibrium. While for WIMP, the particles go away from equilibrium at freeze out, for FIMPs they approach towards equilibrium and suffer freeze in.

Chapter 2

Standard Model

In Chapter 1, we have mentioned that only 5% of the observable Universe is made up of visible matter. Leptons and quarks are fundamental constituents of visible sector. Apart from the gravitational force, interactions of visible sector particle is governed by three other forces namely strong, weak and electromagnetic force. Standard Model (SM) of particle physics is a gauge theory ($SU(3)_C \times SU(2)_L \times U(1)_Y$) that unifies the fundamental forces of strong, weak and electromagnetic interaction where subscript C defines colour, L corresponds to left chiral field and Y is the weak hypercharge. In SM, strong interaction between quarks is mediated via gluon while gauge bosons W^\pm , Z are responsible for weak interaction of quarks and leptons. Electromagnetic interaction of charged particles in SM is mediated by massless photon field. In this chapter we will discuss the unified gauge theory of weak and electromagnetic interaction developed by Sheldon Glashow [19], Abdus Salam [20] and Steven Weinberg [21] independently which is known as electroweak theory ($SU(2)_L \times U(1)_Y$) of SM. Despite the success of SM of particle physics, there are some drawbacks of the model. Deficiencies of SM of particle physics will also be addressed in this chapter to motivate theories beyond Standard Model (BSM).

Theory of strong interaction of quarks is known as quantum chromodynamics (QCD). QCD follows a non-abelian gauge theory of $SU(3)$ gauge group where all the quarks are denoted by a field ψ_i , ($i = 1 - 3$). Thus, quarks exist in three colours and the label i denotes the colour quantum number. Hence quarks transform as a triplet representation of colour $SU(3)$ ($SU(3)_C$). There are eight generators of $SU(3)_C$ in triplet representation resulting in eight massless gauge bosons known as gluons. These eight gauge bosons (gluons) are the force carriers and they mediate strong interactions. Since QCD is non-abelian, gluons have colour charge and they can have self-interaction. One of the most remarkable features of QCD is that the couplings of quarks and gluons (and gluon self-interaction) decrease as the energy increases. Hence at higher energy it is easy to perform perturbative calculations for strong interaction. Moreover, as the distance between quarks increases, the bonding between quarks increases making it impossible to isolate quarks or gluons. This is also a significant characteristic of QCD. However, we will not discuss strong interaction in this chapter and focus ourselves on the electroweak theory of SM.

2.1 Electroweak theory of Standard Model

In the Standard Model, local invariance of $SU(2)_L \times U(1)_Y$ gauge symmetry prohibits us from adding mass terms for the gauge and fermion fields. The vacuum of gauge symmetry is spontaneously broken via the Higgs mechanism, which generates mass for gauge bosons and fermions. Spontaneous symmetry breaking (SSB) of $SU(2)_L \times U(1)_Y$ symmetry can be initiated by introducing a scalar field invariant under $SU(2)_L \times U(1)_Y$ transformation. After SSB, the ground state of the scalar potential in the SM Lagrangian acquires a non-zero vacuum expectation value (VEV). This scalar field with non-zero VEV, having coupling with the gauge and fermion

sector of SM, generates gauge boson and fermion mass.

- **Scalar sector of SM**

The $SU(2)_L \times U(1)_Y$ invariant Lagrangian for the scalar field in SM is given as

$$\mathcal{L}_{scalar} = (D_\mu \Phi)^\dagger (D^\mu \Phi) - \mu^2 \Phi^\dagger \Phi - \lambda (\Phi^\dagger \Phi)^2, \quad (2.1)$$

where Φ is a complex scalar doublet written as

$$\Phi = \begin{pmatrix} \Phi^+ \\ \Phi^0 \end{pmatrix} \quad (2.2)$$

and is also known as Higgs doublet. In the above (Eq. 2.2) Φ^+ and $\Phi^0 = (h + i\eta)/\sqrt{2}$ are complex scalars with electric charge +1 and 0. The covariant derivative D_μ in Eq. 2.1 can be expressed as

$$D_\mu \Phi = \left(\partial_\mu + i \frac{g}{2} \sum_{a=1}^3 \tau_a W_\mu^a + i g' Y B_\mu \right) \Phi, \quad (2.3)$$

where $\tau_a, a = 1 - 3$ are generators of $SU(2)_L$ gauge transformation representing the weak isospin I and $Y (= \frac{1}{2})$ is the weak hypercharge associated with $U(1)_Y$ of Φ doublet. The couplings g and g' are interaction strengths of gauge fields W_μ^a and B_μ field. Spontaneous symmetry breaking will generate a non zero VEV for Φ^0 which then provides mass to the gauge fields (will be discussed later). The scalar potential in Eq. 2.1 can be rewritten as

$$V = \mu^2 \Phi^\dagger \Phi + \lambda (\Phi^\dagger \Phi)^2. \quad (2.4)$$

Hermiticity of the potential demands that the parameters μ^2 and λ must be real. Also the potential should be bounded from below which requires $\lambda > 0$. For

$\mu^2 < 0$, choice of particular ground state vacuum of Φ will spontaneously break the gauge symmetry. However the vacuum of Φ may still be invariant under a residual subgroup of the gauge group. Hence, the gauge field corresponding to this subgroup will remain massless. In SM $SU(2)_L \times U(1)_Y$ gauge symmetry gets spontaneously broken into $U(1)_{em}$ which is still a symmetry of the vacuum resulting a massless photon responsible for electromagnetic interaction.

- **Higgs mechanism of electroweak symmetry breaking**

In order to explain the SSB, we start with the Lagrangian for the scalar field

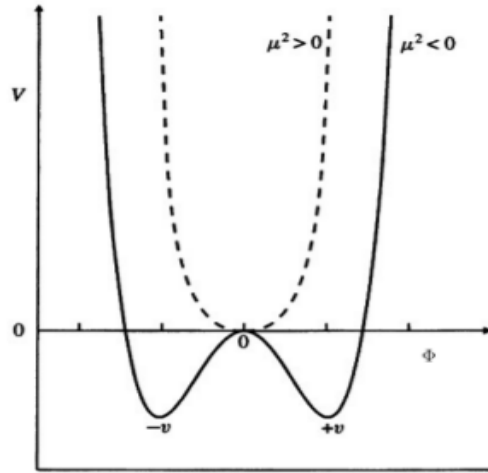


Figure 2.1: Potential V plotted against the variation of scalar field Φ for $\mu^2 > 0$ and $\mu^2 < 0$.

mentioned in Eq. 2.1. The Lagrangian expressed in Eq. 2.1 is locally invariant under $SU(2)_L \times U(1)_Y$ gauge symmetry. Behaviour of the scalar potential Eq. 2.4 at ground state depends on the parameters μ^2 and λ . As mentioned earlier, the potential must be bounded from below to achieve a stable vacuum $\lambda > 0$. The parameter μ^2 appearing in Eq. 2.4 can be either positive or negative. In Fig. 2.1, we plot the potential V_Φ as a function of Φ for both the cases with i) $\mu^2 > 0$ and ii) $\mu^2 < 0$. It can be observed from Fig. 2.1 that for $\mu^2 > 0$, the ground state of the potential occurs at $\langle \Phi \rangle = 0$ and the symmetry

is conserved where $\langle \Phi \rangle = 0$ denotes the expectation value of Φ at ground state or vacuum. Hence for $\mu^2 > 0$, both the fields Φ^0 and Φ^+ are degenerate with zero vacuum expectation value and the solution is trivial. However, for $\mu^2 < 0$ (see Fig. 2.1), the ground state is degenerate and minimum of the potential is obtained for non zero expectation values $\langle \Phi \rangle = \pm \sqrt{\frac{-\mu^2}{2\lambda}}$. Therefore, for the case when $\mu^2 < 0$, ground state of the potential can assume any one of the solutions for minima. Once the system jumps to a certain ground state minima and stabilises the internal symmetry of the potential is violated spontaneously. This phenomenon when the ground state does not protect the symmetry of the Lagrangian is known spontaneous symmetry breaking. In the present case, the gauge symmetry will be broken spontaneously.

Let us assume that the Higgs field breaks the gauge symmetry spontaneously at ground state with $\langle \Phi \rangle \equiv \begin{pmatrix} 0 \\ \frac{v}{\sqrt{2}} \end{pmatrix}$ where $v = \sqrt{\frac{-\mu^2}{\lambda}}$. Therefore the Higgs field about the minima can then be expressed as

$$\Phi = \begin{pmatrix} \Phi^+ \\ \frac{v+h+i\eta}{\sqrt{2}} \end{pmatrix}, \quad (2.5)$$

where the fields h and η have zero VEV. Substituting Eq. 2.5 in the Eq. 2.4 we obtain that the real scalar field acquires a mass $m_h = \sqrt{2\lambda}v$. This real scalar field is known as Higgs boson while other fields (Φ^\pm, η) remain massless. These massless modes (originated due to SSB) are known as Goldstone modes which are absorbed by massive gauge bosons.

- **Standard Model gauge bosons**

We will now explore the gauge sector of SM. The electroweak theory of SM preserves the $SU(2)_L \times U(1)_Y$ gauge symmetry resulting four gauge fields (three $SU(2)$ gauge field ($W_\mu^a, a = 1 - 3$) and one $U(1)$ gauge field B_μ). The gauge

invariant Lagrangian for the gauge fields in SM is

$$-\mathcal{L}_{gauge} = \frac{1}{4} W_{\mu\nu}^a W_a^{\mu\nu} + \frac{1}{4} B_{\mu\nu} B^{\mu\nu} , \quad (2.6)$$

are kinetic energy and self interaction terms of the W_μ gauge fields and kinetic term of B_μ field. The field strength tensor for W_μ and B_μ field can explicitly be written as

$$\begin{aligned} W_{\mu\nu}^a &= \partial_\mu W_\nu - \partial_\nu W_\mu - g\epsilon_{abc} W_\mu^b W_\nu^c , \\ B_{\mu\nu} &= \partial_\mu B_\nu - \partial_\nu B_\mu . \end{aligned} \quad (2.7)$$

The Lagrangian in Eq. 2.6 does not have any mass term for the gauge fields. Besides the gauge symmetry will be lost if one introduces mass terms for gauge fields explicitly. However, in order to explain weak interaction of particles, massive gauge fields are needed. In SM, masses of the gauge fields are generated via Higgs mechanism which breaks the $SU(2)_L \times U(1)_Y$ gauge symmetry spontaneously. Using the expression of Higgs field (Eq.2.5) and putting $Y = \frac{1}{2}$ in Eq. 2.3, the covariant derivative term of the Higgs field can be rewritten as

$$D_\mu \Phi = \left[\partial_\mu + \frac{i}{2} \begin{pmatrix} gW_\mu^3 + g'B_\mu & g(W_\mu^1 - iW_\mu^2) \\ g(W_\mu^1 + iW_\mu^2) & -gW_\mu^3 + g'B_\mu \end{pmatrix} \right] \begin{pmatrix} \Phi^+ \\ \frac{v+h+i\eta}{\sqrt{2}} \end{pmatrix} . \quad (2.8)$$

In Eq. 2.8, g and g' are the respective coupling strengths of the $SU(2)_L$ and $U(1)_Y$ gauge sector. Substituting Eq. 2.8 in Eq. 2.1 and replacing the Higgs field

only with its VEV, the effective kinetic term of the scalar Lagrangian becomes

$$\begin{aligned}
 (D_\mu \Phi)^\dagger (D^\mu \Phi) &= \frac{1}{8} \left| \left[\begin{pmatrix} gW_\mu^3 + g'B_\mu & g(W_\mu^1 - iW_\mu^2) \\ g(W_\mu^1 + iW_\mu^2) & -gW_\mu^3 + g'B_\mu \end{pmatrix} \right] \begin{pmatrix} 0 \\ v \end{pmatrix} \right|^2 \\
 &= \frac{1}{8} g^2 v^2 [(W_\mu^1)^2 + (W_\mu^2)^2] + \frac{1}{8} v^2 (-gW_\mu^3 + g'B_\mu)(-gW_\mu^3 + g'B_\mu) \\
 &= \frac{1}{4} g^2 v^2 W_\mu^+ W_\mu^- + \frac{1}{8} v^2 (W_\mu^3 \ B_\mu) \begin{pmatrix} g^2 & -gg' \\ -gg' & g'^2 \end{pmatrix} \begin{pmatrix} W_\mu^3 \\ B_\mu \end{pmatrix}, \tag{2.9}
 \end{aligned}$$

where we have redefined the gauge fields such that

$$W_\mu^\pm = \frac{(W_\mu^1 \mp iW_\mu^2)_\mu}{\sqrt{2}}. \tag{2.10}$$

First term in Eq. 2.9 corresponds to the mass of charged gauge bosons W^\pm with mass $M_W = \frac{1}{2}gv$ while the second term is off diagonal in W_μ^3 and B_μ . To obtain the physical gauge bosons we have to diagonalise the off diagonal mass matrix. Diagonalisation of the mass matrix leads to two normalised neutral bosons Z_μ and A_μ of the form

$$\begin{aligned}
 Z_\mu &= \frac{1}{\sqrt{g^2 + g'^2}} (gW_\mu^3 - g'B_\mu), \\
 A_\mu &= \frac{1}{\sqrt{g^2 + g'^2}} (g'W_\mu^3 + gB_\mu), \tag{2.11}
 \end{aligned}$$

which are mass eigenstates having eigen mass $M_Z = \frac{1}{2}\sqrt{g^2 + g'^2}$ and $M_A = 0$. Hence one of the physical gauge boson remains massless. From Eq. 2.11, it can be realised that diagonalisation of mass matrix is simply an orthonormal

transformation of the gauge fields such that

$$\begin{aligned} Z_\mu &= \cos \theta_W W_\mu^3 - \sin \theta_W B_\mu , \\ A_\mu &= \sin \theta_W W_\mu^3 + \cos \theta_W B_\mu , \end{aligned} \quad (2.12)$$

where θ_W is the weak mixing angle given by

$$\theta_W = \tan^{-1} \frac{g'}{g} . \quad (2.13)$$

Hence electroweak symmetry breaking triggered by Higgs mechanism in SM leads to three massive gauge fields W^\pm, Z and one massless field A_μ . The massless field respects the $U(1)_{em}$ (sub group of $SU(2)_L \times U(1)_Y$ gauge symmetry) symmetry of electromagnetic interaction and remains invariant. Hence, the charge corresponding to $U(1)_{em}$ symmetry, i.e., electric charge is conserved and information of any electromagnetic interaction is carried by A_μ , is the photon field itself.

- **Fermions in SM**

The fermion sector of SM is comprised of three generations of quark and three generations of leptons. Left handed fermion fields in SM are $SU(2)_L$ doublets while right handed partners transform as a singlet. Hence, the generalised Lagrangian for the fermions invariant under the $SU(2)_L \times U(1)_Y$ gauge symmetry in SM is

$$-\mathcal{L}_{fermion} = \bar{L}_i \left(\partial_\mu + i \frac{g}{2} \sum_{a=1}^3 \tau_a W_\mu^a + i g' Y B_\mu \right) L_i + \bar{R}_i (\partial_\mu + i g' Y B_\mu) R_i , \quad (2.14)$$

where L_i represents left handed fermion (quark or lepton) doublet field and R_i is right handed partner of the quark (lepton) field for i th generation which can

explicitly be written as

$$L_i = \begin{pmatrix} \nu^i \\ l^i \end{pmatrix}_L, \quad \begin{pmatrix} u^i \\ d^i \end{pmatrix}_L; \quad R_i = u_R^i, d_R^i, l_R^i, \quad (i = 1 - 3). \quad (2.15)$$

Expanding the Lagrangian expressed in Eq. 2.14, kinetic terms and interaction terms of fermion fields with gauge bosons and photon are obtained. From Eq. 2.15 it can be observed that right handed neutrino fields are absent in SM. This is due to the fact that till date there is no experimental evidence for the presence of right handed neutrinos. Since the Lagrangian in Eq. 2.14 preserves the gauge symmetry a fermionic mass term is not allowed as it will break the gauge symmetry. Fermion mass can be generated from the Yukawa interaction via Higgs mechanism when the gauge symmetry gets broken spontaneously. Gauge invariant scalar-fermion Yukawa interaction for a single generation fermion can be expressed as

$$-\mathcal{L}_{Yukawa} = y_1 \bar{L}_1 \Phi R_1 + h.c. , \quad (2.16)$$

where y_1 is the Yukawa coupling constant for the first generation fermion. After SSB the Higgs field Φ acquires a VEV v . If we write the scalar field Φ as $\Phi^T = (0 \ (v + h)/\sqrt{2})$ (T denotes transpose), for a single fermion generation (viz. electron) Eq. 2.16 takes the form

$$-\mathcal{L}_{Yukawa}^e = y_e \frac{v}{\sqrt{2}} (\bar{e}_L e_R + \bar{e}_R e_L) + y_e \frac{h}{\sqrt{2}} (\bar{e}_L e_R + \bar{e}_R e_L). \quad (2.17)$$

The first term appearing in Eq. 2.17 is electron mass term and the second term is the interaction term between the scalar Higgs field h and electron. Hence

electron mass in SM is

$$m_e = y_e \frac{v}{\sqrt{2}}. \quad (2.18)$$

Masses of other leptons and quarks can also be produced in similar manner from the idea of SSB. It is to be noted that Yukawa Lagrangian mentioned in Eq. 2.16 in principle can generate masses for down type quarks and charged leptons only. Since there is no right handed neutrino field, neutrinos in SM remains massless. In order to generate mass for up type quarks we must construct a new Higgs doublet

$$\Phi_c = i\tau_2 \Phi^* = \begin{pmatrix} -\bar{\Phi}^0 \\ \Phi^- \end{pmatrix}, \quad (2.19)$$

is the charge conjugate of scalar field Φ . Φ_c transforms identically as Φ under $SU(2)$ transformation but has weak hypercharge opposite to Φ . For example, Yukawa interaction term that generates mass of first generation up quark can be written as

$$-\mathcal{L}_{Yukawa}^u = (\bar{u} \quad \bar{d})_L \begin{pmatrix} -\bar{\Phi}^0 \\ \Phi^- \end{pmatrix} u_R + h.c. . \quad (2.20)$$

- **Neutrinos in SM**

As we have mentioned earlier, since there are no right chiral neutrinos in Standard Model, neutrinos remain massless. Though it is possible to add right handed Dirac neutrinos to SM and generate neutrino mass, however it also results in several problems (such as charged lepton mixing etc. discussed later in 2.2). Also experimental observations of neutrino helicity is found to be -1 and there is no evidence that neutrinos can be right handed. Hence, in order to comply with experimental results of absence of right handed neutrinos, right handed neutrinos has not been introduced in Standard Model. However, neutrino oscillation phenomena confirms that neutrinos are massive. Moreover, neutrinos being charge neutral which indicate that neutrinos can be both Dirac

type and Majorana type. In order to explain the lightness of neutrino mass a simple extension of SM is invoked where heavy right handed self conjugate Majorana fields are introduced. The Lagrangian for the neutrino sector is then

$$-\mathcal{L}_{neutrino} = (Y^\nu)_{ij} \bar{L}_i \tilde{\Phi} N_{Rj} + \frac{1}{2} M_{Rij} \bar{N}_{Ri}^c N_{Rj} + h.c.^1, \quad (i, j = 1 - 3), \quad (2.21)$$

where N_R denotes the right handed Majorana fields and M_R is the mass matrix for these heavy right handed neutrinos. In the above Eq. 2.21, Y_{ij}^ν are Yukawa coupling, which produce Dirac neutrino mass via spontaneous symmetry breaking

$$m_D = \frac{v}{\sqrt{2}} Y^\nu. \quad (2.22)$$

Light neutrino mass is then generated through see-saw mechanism at tree level,

$$M_\nu = -m_D M_R^{-1} m_D^T, \quad (2.23)$$

where M_ν is the neutrino mass matrix. The above mentioned mechanism for neutrino mass generation is known as type I see-saw. Apart from Type I see-saw there are also other mechanism of neutrino mass generation known as type II, type III, inverse see-saw which can also provide neutrino mass. However, we do not intend to discuss these topics in detail herein and can be found in literatures. In type I see-saw, smallness of neutrino mass is ensured by heaviness of right handed Majorana neutrinos along with smallness of Yukawa couplings respectively. Apart from successful generation of neutrino mass these right handed neutrinos can generate lepton asymmetry and baryon asymmetry which is also not a part of our discussion and hence skipped.

¹Here L represents lepton doublets only.

2.2 Shortcoming of Standard Model

Although Standard Model of particle physics proposed by Glashow , Weinberg and Salam (GWS) successfully unifies the weak and electromagnetic interaction, there are several shortcomings of the model which indicate that SM is only an effective theory and extension of SM is required. In this section we will briefly discuss some phenomenological problems unexplained by SM.

- **Gravitation**

The first and the foremost issue unresolved by SM is gravitation. Despite the fact that SM provides an unification of strong, weak and electromagnetic interaction, it does not explain gravitational interaction between particles. This is due to the fact that Standard Model of particle physics is based on the assumption that gravitational interaction is weak and negligible.

- **Divergence of Higgs mass**

Spontaneous breaking of $SU(2)_L \times U(1)_Y$, i.e., the electroweak breaking scale in SM is ~ 100 GeV. Mass of Higgs boson discovered by LHC is ~ 125 GeV. However radiative corrections to the mass of Higgs boson due to self-energy (contribution from fermionic one loop) is found to be quadratically divergent ($\sim \Lambda^2$, where Λ is a high energy cut-off scale). Such divergence of Higgs mass can be canceled by adding suitable counter term to the Lagrangian. Hence self energy terms of Higgs lead to unnatural cancellation (fine tuning) depending on the cut-off scale Λ_c . For example, if we consider the cut-off is at Planck scale then a fine tuning cancellation of order $\sim 10^{30}$ will be required in order to obtain the observed Higgs mass. Also this cancellation should appear at all perturbative orders to maintain the Higgs mass at electroweak scale. Such a huge cancellation at perturbative levels is quite unnatural. Moreover, contributions from other

Higgs self energy diagrams via gauge bosons or Higgs itself also diverges. Thus mass of Higgs boson is not protected by any symmetry in SM and a large mass term can appear from self energy correction even if we set Higgs mass to zero.

- **Fermion mass hierarchy**

Fermion mass in SM originates from Yukawa type interactions after spontaneous breaking of $SU(2)_L \times U(1)_Y$ gauge symmetry. However, there exists a large mass hierarchy between different fermion generations of SM. For instance, the lightest fermion mass in SM is ~ 0.5 MeV while the heaviest weighs about ~ 173 GeV (Since electroweak theory of SM do not have any mechanism to generate neutrino mass, neutrinos in SM are massless and as a result electron is the lightest fermion in SM). There is no feasible explanation to this mass hierarchy in SM.

- **Neutrino mass problem**

According to Standard Model of particle physics neutrinos are massless. However neutrino oscillation phenomena observed by Super-Kamiokande collaboration [22] and SNO [23] indicate that neutrinos are massive and there are finite mass differences between any two of the neutrino generations. It is found that neutrino mass eigenstates differ from neutrino flavour eigenstates which leads to oscillation of neutrinos from one flavour to another. Standard Model of particle physics contains both left chiral and right chiral fields for all fermions except neutrinos. However one may simply add neutral $SU(2)_L$ singlet right handed Dirac neutrinos to the model for each charged lepton doublets. This would then generate neutrino mass in the same way mass of quarks and leptons generated in SM. But oscillation of neutrinos indicate that the mass matrix for neutrinos in flavour basis is not diagonal and hence one have to diagonalise the neutrino mass matrix to find out the physical fields. However this leads to a serious

problem when we consider charge current interactions between gauge bosons and leptons. As we replace the neutrinos in flavour basis with their physical fields we find that lepton numbers L_e , L_μ , L_τ are not conserved and leads to lepton flavour violating processes which do not occur. Also such an assumption with right handed neutrinos do not explain the lightness of neutrinos or why the Yukawa couplings for neutrinos should be small. The origin of mass for the neutrinos therefore can not be explained within the framework of Standard Model of particle physics and one may need theories beyond Standard Model to explain how neutrinos acquire mass. Thus neutrinos provide us an window for new physics beyond Standard Model.

- **Dark Matter**

Existence of dark matter has been confirmed by various gravitational and cosmological evidences. Study of cosmic microwave background radiation by WMAP and PLANCK satellite experiment gives an exact measure of dark matter relic abundance suggesting that about 80% of material Universe is made up of dark matter². Standard model of particle physics is unable to provide a suitable explanation to the dark matter problem. Also SM can not account for a stable particle candidate for dark matter. Extension of Standard Model is apparent in order to explain particle nature of dark matter.

- **Baryogenesis**

Baryogenesis is one of the most astounding puzzle in the Universe that yet remains a mystery to be solved. According to the results from WMAP the ratio of baryon to photon density in the Universe is $\eta \sim 6.19 \times 10^{-10}$ [24], where η is expressed as

$$\eta = \frac{n_b - n_{\bar{b}}}{n_\gamma} . \tag{2.24}$$

²Here “dark matter” refers to cold dark matter only excluding neutrino dark matter, baryonic dark matter etc.

In the above Eq. 2.24, n_x , ($x = b, \bar{b}, \gamma$) denotes number density of baryon (b), anti baryon (\bar{b}) and photon (γ). Hence there exists a formidable amount of matter antimatter asymmetry in the Universe. Standard Model of particle physics can not produce the required amount of baryon to photon ratio. This suggests that in order to explain the process of baryogenesis, SM should be extended with new sources of CP violation.

The above mentioned problems (such as neutrino mass problem, dark matter etc.) can not be explained by Standard Model of particle physics itself and extension of SM required. Hence one can presume that SM is a theory which unifies strong, weak and electromagnetic interaction very well but fails to explain other aspects such as dark matter, baryogenesis etc. which requires new physics input (a new energy scale where SM cannot be treated as an exact theory) apart from SM. In this view it can be concluded that SM is a low energy theory (or effective theory) and basically is a subset of a higher gauge group which resolves all of the above mentioned problems leading to theories like Grand Unified Theory (GUT) or SUSY.

Chapter 3

Physics of Dark Matter

In this chapter the physics of dark matter will be discussed in brief which includes the study of thermal evolution of dark matter and prospects of direct and indirect detection of dark matter. Study of the dynamics of dark matter in thermal equilibrium is governed by the Boltzmann equation for the dark matter candidate. The relic density for the dark matter can be calculated by numerical solution of this Boltzmann equation. Detailed study of the relevant Boltzmann equation for thermal dark matter and its solution will also be discussed in this chapter. Apart from the physics of evolution of dark matter in early Universe, detection of dark matter (both direct and indirect) is also significant. The direct detection experiments provide upper bounds on dark matter nucleon scattering cross-section for different masses of dark matter particle, while the possible indirect signatures can provide limits on the pair production annihilation cross-section of dark matter. A brief account of both dark matter direct and indirect detection experiments will be presented in this chapter.

3.1 Thermal evolution of dark matter and relic density

We begin with the calculation of relic densities of dark matter by solving the Boltzmann equation. For simplicity, we consider a single component dark matter candidate χ . The Boltzmann equation for the evolution of a particle species χ can be obtained from the relation

$$L[f_\chi(p_\chi^\mu, x^\mu)] = C[f_\chi(p_\chi^\mu, x^\mu)] , \quad (3.1)$$

where $f_\chi(p_\chi^\mu, x^\mu)$ is the phase space distribution function of a particle species χ and p_χ^μ denotes four momentum of the particle species at any space time point x^μ . In Eq. 3.1, L and C are Liouville operator and collision operator respectively. Since Friedmann-Robertson-Walker (FRW) model of cosmology is based on the hypothesis that the phase space density is isotropic and homogeneous. Hence, the Liouville operator can be expressed as

$$L[f_\chi(E_\chi, t)] = E_\chi \frac{\partial f_\chi}{\partial t} - H |\vec{p}_\chi|^2 \frac{\partial f_\chi}{\partial E_\chi} , \quad (3.2)$$

where H denotes the Hubble parameter. Now the expression of number density is given by

$$n_\chi(t) = \frac{g_\chi}{(2\pi)^3} \int f_\chi(E_\chi, t) d^3p_\chi . \quad (3.3)$$

where g_χ denotes the internal degrees of freedom and f_χ is the distribution function for the species χ . Using Eqs. 3.1-3.3, the Boltzmann equation for the evolution of

density of χ takes the form

$$\frac{\partial n_\chi}{\partial t} + 3Hn_\chi = \frac{g_\chi}{2\pi^3} \int \frac{C[f_\chi(E_\chi, t)]}{E_\chi} d^3p_\chi. \quad (3.4)$$

For a $2 \leftrightarrow 2$ interaction process, the collision term appearing in the RHS of Eq. 3.4 can be expressed as

$$\begin{aligned} \frac{g_\chi}{2\pi^3} \int \frac{C[f_\chi(E_\chi, t)]}{E_\chi} d^3p_\chi &= - \sum_{\text{spin}} \int d\Pi_\chi d\Pi_\psi d\Pi_a d\Pi_b (2\pi)^4 \delta^4(p_\chi + p_\psi - p_a - p_b) \\ &\times \left[|M|_{\chi+\psi \rightarrow a+b}^2 f_\chi f_\psi (1 \pm f_a)(1 \pm f_b) \right. \\ &\left. - |M|_{a+b \rightarrow \chi+\psi}^2 f_a f_b (1 \pm f_\chi)(1 \pm f_\psi) \right], \quad (3.5) \end{aligned}$$

where f_χ, f_ψ, f_a, f_b are respective phase space densities of particles χ, ψ, a, b and

$$d\Pi_f = \frac{d^3p_f}{2E_f(2\pi)^3}.$$

In Eq. 3.5, $+(-)$ used in the factor $(1 \pm f_i), i = \chi, \psi, a, b$ denotes whether the species is a boson (fermion) particle. The square of matrix element for the forward process is $|M|_{\chi+\psi \rightarrow a+b}^2$ and the same for the backward process is $|M|_{a+b \rightarrow \chi+\psi}^2$, averaged over the initial spins of incoming particles and final spins of outgoing particles. Energy and momentum conservation for the process is ensured by delta function for four momentum. The collision term expressed in Eq. 3.5, can be simplified with well motivated assumptions. Firstly, we assume that the final particles produced in the $\chi + \psi \rightarrow a + b$ are in equilibrium with thermal bath. Hence the distribution functions for final particles f_a and f_b are replaced by f_a^{eq} and f_b^{eq} . Applying principle of detailed balance we get $f_a^{\text{eq}} f_b^{\text{eq}} = f_\chi^{\text{eq}} f_\psi^{\text{eq}}$. Secondly, since the annihilation process of the particles χ and ψ into a and b is CP invariant, square of the matrix elements for both

forward and backward reaction are same, i.e.,

$$|M|_{a+b \rightarrow \chi+\psi}^2 = |M|_{\chi+\psi \rightarrow a+b}^2 . \quad (3.6)$$

In order to solve the Boltzmann equation, a final assumption has been made in which we consider that the phase space distribution functions for all the initial particles and final particles appearing in the process follow classical statistics governed by Maxwell-Boltzmann statistics. Using these assumptions mentioned above, the collision term given by Eq. (3.5) can eventually be written as

$$\frac{g_\chi}{2\pi^3} \int \frac{C[f_\chi(E_\chi, t)]}{E_\chi} d^3 p_\chi = -\langle \sigma_{\chi+\psi \rightarrow a+b} v \rangle (n_\chi n_\psi - n_a^{\text{eq}} n_b^{\text{eq}}) , \quad (3.7)$$

where $\langle \sigma_{\chi+\psi \rightarrow a+b} v \rangle$ denotes the thermally averaged cross-section times relative velocity for the process $\chi + \psi \rightarrow a + b$. When the initial particles are identical or antiparticle to each other the term $\langle \sigma_{\chi+\psi \rightarrow a+b} v \rangle$ in Eq. 3.7 can be expressed as follows [25]

$$\langle \sigma_{\chi+\psi \rightarrow a+b} v \rangle = \frac{1}{8m^4 T K_2^2\left(\frac{m}{T}\right)} \int_{4m^2}^{\infty} \sigma_{\chi+\psi \rightarrow a+b}(s - 4m^2) \sqrt{s} K_1\left(\frac{\sqrt{s}}{T}\right) ds \quad (3.8)$$

where

$$\sigma_{\chi+\psi \rightarrow a+b} = \frac{1}{4 E_\chi E_\psi g_\chi g_\psi v} \sum_{\text{spin}} \int d\Pi_a d\Pi_b (2\pi)^4 \delta^4(p_\chi + p_\psi - p_a - p_b) |M|_{\chi+\psi \rightarrow a+b}^2 , \quad (3.9)$$

is the cross-section for the process $\chi + \psi \rightarrow a + b$ and the relative velocity between two initial state particles is v . In Eq. 3.8, T denotes the temperature of thermal bath, m is the mass of particle χ and s is the centre of momentum energy for the

process. The factors K_i , $i = 1, 2$ are the modified Bessel functions of order i . Using the expression of collision term obtained in Eq. 3.7, the Boltzmann equation becomes

$$\frac{\partial n_\chi}{\partial t} + 3H n_\chi = -\langle \sigma_{\chi+\psi \rightarrow a+b} v \rangle (n_\chi n_\psi - n_\chi^{\text{eq}} n_\psi^{\text{eq}}) . \quad (3.10)$$

It is to be noted that the process $\chi + \psi \rightarrow a + b$ can occur through different channels depending on the interaction between these particles. Since Boltzmann equation solves for the number density of the particle species, all the channels that produce a and b from initial particles χ and ψ must be taken into account. Moreover all the processes which result change in modifying the number density of dark matter particles (apart from producing a and b) are also to be included. Thus, the modified Boltzmann equation involving all possible interaction channels is written as

$$\frac{\partial n_\chi}{\partial t} + 3H n_\chi = -\langle \sigma v \rangle (n_\chi n_\psi - n_\chi^{\text{eq}} n_\psi^{\text{eq}}) , \quad (3.11)$$

where σ defines the total cross-section attributed from all possible interaction modes. Now we investigate the case for which the initial particles χ and ψ are identical. In this case therefore $n_\chi = n_\psi$ and $n_\chi^{\text{eq}} = n_\psi^{\text{eq}}$. Hence, the Boltzmann equation for the case of interaction of identical particles takes the form (dropping the subscripts appearing in number density)

$$\frac{\partial n}{\partial t} + 3H n = -\langle \sigma v \rangle (n^2 - n_{\text{eq}}^2) . \quad (3.12)$$

However, if χ is antiparticle of ψ or vice versa, a factor of $\frac{1}{2}$ is to be multiplied on the right hand side of Eq. 3.12 to avoid double counting of the total number density of the species ($n = n_\chi + n_\psi = 2n_\chi$). Before we solve the Boltzmann equation for a certain particle species we introduce a characteristic temperature T_F , known as freeze out temperature of the particle species. Freeze out temperature T_F for a particle

species χ (initially in thermal equilibrium) is defined as the temperature at which it decouples from the thermal bath and cannot sustain the equilibrium between forward and backward processes. The criterion that determines whether a particle species will remain coupled or be decoupled from the thermal bath of Universe depends on its interaction rate Γ and expansion rate of universe H . If $\Gamma < H$ (i.e., the interaction rate becomes smaller than the expansion rate of Universe), self annihilation process of the particle species producing different particles will be restricted. Therefore, if the particle is long lived, as the Universe expands the interaction of the particle freezes out (for $\Gamma < H$) and becomes relic having significant relic abundance at present. Depending on the size of the smallest dark matter halo it can form in early Universe, dark matter, can be distinguished into two categories namely cold dark matter (CDM) and hot dark matter (HDM). The dark matter halo is assumed to be formed by accumulation of considerable amount of dark matter particles. Halo formation depends on the free streaming length of constituent particles and also the kinetic decoupling temperature (i.e., freeze out temperature) of these relic particles. It is found that if the particles are relativistic at the time of decoupling then dark matter is hot whereas if particles in the halo are non-relativistic then dark matter is cold. Hence, for simplicity one can distinguish the nature of dark matter (cold or hot) depending on freeze out temperature assuming dark matter is either cold for $x_F > 3$ and hot relic for $x_F < 3$, where $x_F = m/T_F$, is the ratio of mass of the particle and freeze out temperature T_F of the dark matter particle. In this chapter thermal evolution of the cold relic particles will be addressed. In order to study the evolution of cold relic particles, we start initially from the expression of Boltzmann equation (Eq. 3.12) for identical particles. For simplicity we define a dimensionless quantity $Y = n/s$ where s is the entropy density of the Universe. We also define a dimensionless quantity $x = m/T$ (T being the temperature). In terms of these

quantities (Y and x) Eq. 3.12 can be written in the form [26]

$$\frac{dY}{dx} = -\frac{ds}{dx}\langle\sigma v\rangle\frac{Y^2 - Y_{eq}^2}{3H} \quad (3.13)$$

In the above equation the Hubble parameter is $H = (8\pi G\rho/3)^{1/2}$.

The total energy density ρ and total entropy density s are defined by

$$\rho = g_{eff}(T)\pi^2T^4/30 \quad (3.14)$$

$$s = h_{eff}(T)2\pi^2T^3/45 \quad (3.15)$$

where $g_{eff}(T)$ and $h_{eff}(T)$ are effective degrees of freedom for energy and entropy respectively. Using Eq. 3.15, Eq. 3.13 can be expressed as [25]

$$\frac{dY}{dx} = -(45G/\pi)^{-1/2}g_*^{1/2}m\langle\sigma v\rangle\frac{Y^2 - Y_{eq}^2}{x^2} \quad (3.16)$$

where

$$g_*^{1/2} = \left(1 + \frac{T}{3h_{eff}}\frac{dh_{eff}}{dT}\frac{h_{eff}}{\sqrt{g_{eff}}}\right). \quad (3.17)$$

Integrating Eq. 3.16 from $x = 0$ to $x = x_0$ where $x_0 = m/T_0$, T_0 being the present photon temperature, one obtains Y_0 at T_0 . The relic density for the species χ is then given by

$$\Omega_{DM} = \rho_{DM}/\rho_c = m_{DM}s_0Y_0/\rho_c \quad (3.18)$$

where ρ_c is the critical density of the Universe and $T_0 = 2.73\text{K}$, the CMB radiation temperature. Substituting the numerical value of ρ_c in Eq. 3.18 one obtains [25, 26]

$$\Omega_{DM}h^2 = 2.755 \times 10^8 Y_0 \frac{m_{DM}}{\text{GeV}}, \quad (3.19)$$

where we redefine Hubble parameter as $h = H/(100 \text{ kms}^{-1}\text{Mpc}^{-1})$. Now in order

to calculate Y_0 we have to solve Eq. 3.16 at freeze out temperature T_F . When temperature of Universe is $\sim T_F$, we define a quantity $\Delta = Y - Y_{eq}$. Substituting Δ in Eq. 3.16 we obtain

$$\frac{d\Delta}{dx} = - \left(\frac{45}{\pi} G \right)^{-1/2} \frac{g_*^{1/2} m}{x^2} \langle \sigma v \rangle \Delta (\Delta + 2Y_{eq}) - \frac{dY_{eq}}{dx}, \quad (3.20)$$

where Y_{eq} is the equilibrium density and takes the form (for the case of cold relic)

$$\frac{45g}{4\pi^4} \frac{x^2 K_2(x)}{h_{\text{eff}}(m/x)}, \quad x \gg 3. \quad (3.21)$$

In Eq. 3.21, g denotes the number of internal degrees of freedom. Since Y approaches equilibrium number density Y_{eq} , the quantity $\frac{d\Delta}{dx}$ in Eq. 3.20 can be neglected. We further assume that at freeze out temperature T_F , $\Delta = \delta Y_{eq}$ (δ is a chosen number). Substituting the value of Y_{eq} and using the expression for Δ , Eq. 3.20 can be rewritten as

$$\left(\frac{45}{\pi} G \right)^{-1/2} \frac{45g}{4\pi^4} \frac{K_2(x)}{h_{\text{eff}}(T)} g_*^{1/2} m \langle \sigma v \rangle \delta (\delta + 2) = \frac{K_1(x)}{K_2(x)} - \frac{1}{x} \frac{d \ln h_c(T)}{d \ln T}. \quad (3.22)$$

In the above $K_n(x)$ are modified Bessel functions of order n and $h_c(T)$ is the contribution to the degrees of freedom for entropy density from other coupled species at T . Eq. 3.22 is solved numerically and self consistently to obtain the freeze out temperature T_F . The quantity Y_0 can now be calculated by integrating Eq. 3.20 from T_0 to T_F which yields

$$\frac{1}{Y_0} = (45G/\pi)^{-1/2} \int_{T_0}^{T_F} g_*^{1/2} m \langle \sigma v \rangle dT. \quad (3.23)$$

In Eq. 3.23, Y at freeze out temperature is not taken into account as the value of Y_F

is negligibly small compared to other terms in the equation. Using the above value of Y_0 , relic density can now be computed for the cold relic particles.

3.2 Dark matter direct detection

Dark matter candidate (also known as WIMP) may interact with the normal baryonic matter when it experiences a scattering phenomenon with the constituents of matter (quarks) through a mediator. Local dark matter particles in the vicinity of solar system move with a velocity about 200 kms^{-1} . Thus dark matter particles in the process of possible scattering with the baryonic matter can transfer a part of its momentum to the nuclei of target material. A measure of the recoil energy of the target nucleus due to the momentum transfer can provide an estimate of dark matter nucleon scattering cross-section. A direct dark matter detection experiment is designed to measure the recoil energy of a target nucleus, a rare event, when a dark matter particle scatters off the target nucleus of the detector material. Since the recoil energy for DM-nucleon elastic scattering is very small $\sim \text{keV}$, a detector with sufficiently low background and low threshold is required for direct detection. Depending on the nature of interaction, the elastic scattering of dark matter with the nucleus is classified into two categories namely spin independent (SI) and spin dependent (SD) cross-section. The scalar mediated interaction of dark matter and nucleon is known as spin independent (SI) elastic scattering. Interaction Lagrangian for such a process is given as $L \sim \bar{\chi}\chi\bar{q}q$, where χ represents the dark matter candidate (WIMP). On the other hand, when the interaction between dark matter and quark takes place via an axial process ($L \sim \bar{\chi}\gamma^\mu\gamma_5\chi\bar{q}\gamma_\mu\gamma_5q$), the interaction will become spin dependent ¹. Such type of spin dependent interaction is valid only for nuclei with non

¹It is to be noted that apart from the above mentioned scalar and axial current interactions, WIMP can also have other type interactions with quarks such as neutral current interaction mediated

zero ground state spin. Both spin independent and spin dependent interactions are t -channel processes. Cross-section for spin independent elastic scattering varies with the square of atomic mass number A of the detector nucleus. The cross-section for spin dependent scattering of dark matter with nucleus is proportional to a factor $(J+1)/J$, where J is the initial spin of the detector nucleus at ground state. Different direct dark matter experiments like XENON100 [27], LUX [28], CDMS [29], SuperCDMS [30], CoGeNT [31], DAMA [32]-[34], EDELWEISS-II [35], CRESST [36] search for dark matter direct detection events via spin independent scattering of dark matter and nucleon. Study of spin dependent dark matter search is also performed by experiments like PICASSO [37], PICO [38] etc. Till date none of the dark matter direct detection experiments mentioned, have detected any event or signal of dark matter-nucleon scattering. From the null results, the direct dark matter search experiments provide exclusion limits for dark matter-nucleon scattering cross-sections with dark matter mass. These exclusion plots given by different direct dark matter detection experiments are treated as upper bounds on dark matter-nucleon elastic scattering cross-section. Strongest bound of spin dependent DM-nucleon interaction cross-section have been reported by LUX [28] while the most stringent bound on spin dependent scattering cross-section of dark matter off the nucleus is given by PICO [38] experiment.

3.3 Dark matter indirect detection

Indirect detection of dark matter is based on the search for excess gamma ray, positron, anti-proton, neutrino fluxes from astrophysical objects such as the galactic centre, galactic halo, Sun etc. These excess could be produced by annihilation of dark matter. Dark matter can be captured by the influence of enormous gravitational force via Z or Z' boson. Such an interaction is vector type spin independent interaction $\sim \bar{\chi}\gamma_\mu\chi\gamma^\mu\bar{q}q$.

of massive heavenly bodies such as galactic centre, dwarf galaxies core of Sun etc. when velocity of dark matter is less than the escape velocity required to overcome the gravitational influences of those massive objects. When accumulated in considerable amount over a long period, these astrophysical sites become rich in dark matter. These astrophysical bodies are probes to dark matter indirect detection. Trapped dark matter particles in these sites may then annihilate to produce excess energetic gamma rays or neutrinos than what is expected from known astrophysical processes. Ground based telescopes like HESS [39], MAGIC [40], VERITAS [41] and satellite borne telescope Fermi-LAT [42] look for high energy gamma rays from galactic centre and other astrophysical sites. Earth based neutrino telescopes such as ANTARES [43], ICECUBE [44] are designed to observe the high energy cosmic neutrino flux obtained from different galactic and extragalactic sources. Dark matter can also pair annihilate into pair of fermions and produce excess in positron (e^+) and anti-proton (\bar{p}) flux. Satellite borne experiments like AMS [45] and PAMELA [46] can detect such excesses in positron flux. In a recent work, AMS-02 [47] has reported their first measurement of anti-proton flux.

In the last few years, the analyses of Fermi-LAT publicly available data [48, 49] by several groups [50]- [56] have confirmed the existence of a low energy (few GeV range) γ -ray excess which appears to be emerging from the regions close to the centre of our Milky way galaxy. It is to be noted that apart from dark matter, non-DM sources such as millisecond pulsars may provide a feasible explanation to the excess of γ -ray observed at GC [57]. Study of unresolved point sources near GC by Lee et. al [58] suggests that point sources also contribute significantly to the gamma ray excess. However, in this work, we will consider DM as the origin of the observed excess in GC gamma ray to explore the phenomenology of dark matter. The analysis of Fermi-LAT data [49] by Daylan et. al. [59] shows that the the γ -ray excess from the GC can be well explained by the annihilating dark matter scenario. They have

also excluded all the known astrophysical processes which can act as the possible origin of this phenomenon. In Ref. [59] it is shown that the observed γ -ray spectrum from the GC can be well fitted by annihilating dark matter scenario with dark matter mass in the range $\sim 30 - 40$ GeV which pair annihilates into $b\bar{b}$ final state with an annihilation cross section $\langle\sigma v_{b\bar{b}}\rangle \sim (1.4 - 2.0) \times 10^{-26} \text{cm}^3/\text{s}$ with local dark matter density $\rho_{\odot} = 0.3 \text{ GeV}/\text{cm}^3$. In this work the authors have taken an angular region of 5° around the centre of our galaxy as their region of interest (ROI) and used Navarro, Frenk and White (NFW) halo profile with $\gamma = 1.26$ for the computation of γ -ray flux. However more recently, the authors Calore, Cholis and Weniger (CCW) of Ref. [60] have claimed to perform a detailed analysis of Fermi-LAT data for 60 galactic diffusion excess (GDE) models. Study of CCW shows that the observed excess in gamma ray is best fitted with a dark matter of mass $49_{-5.4}^{+6.4}$ GeV that annihilates into $b\bar{b}$ final state having annihilation cross-section $\langle\sigma v\rangle_{b\bar{b}} = 1.76_{-0.27}^{+0.28} \times 10^{-26} \text{ cm}^3\text{s}^{-1}$. The analysis of CCW assumes an NFW profile with $\gamma = 1.2$ for dark matter density distribution and a different region of interest (ROI) with galactic latitude $|l| \leq 20^{\circ}$ and longitude $|b| \leq 20^{\circ}$ masking out the inner region corresponding to $|b| \leq 2^{\circ}$.

Besides the GC, the dwarf galaxies may also be rich in dark matter. The dwarf galaxies are a class of faint and small satellite galaxies of our Milky Way galaxy. The huge amount of DM content within these dwarf spheroidal galaxies (dsphs) is inferred from their mass to luminosity ratio ($\frac{M}{L}$). The $\frac{M}{L}$ ratio for these galaxies are found to be much higher than what is expected from the estimation of their visible mass. The dark matter rich dsphs can also emit excess γ -rays due to the pair annihilation of dark matter. Nine such dwarf galaxies have recently been discovered in addition to the previously discovered 15 dwarf satellite galaxies of Milky way. Study of γ -rays from previously known 15 different dwarf galaxies by Fermi-LAT [61] and eight newly discovered dwarf galaxies by Fermi-LAT with DES collaboration [62] provide bound on DM mass and corresponding $\langle\sigma v\rangle$ for different annihilation channels.

3.4 Collider searches of dark matter

Particle accelerators like large hadron collider (LHC) also looks for dark matter particle within the accelerator. If dark matter is produced in particle collider it would remain undetected (since dark matter is weakly interacting and stable) and a missing energy signature will be obtained when momentum is reconstructed for the event. Observation of such missing energy can help to determine any signal of dark matter. Proposed accelerator experiment International Linear Collider (ILC) may also uncover the nature of dark matter and enlighten the physics of dark matter. ILC will probe high energy particles produced in TeV scale. In ILC direct collision of energetic leptons will be observed. Hence, it is possible that dark matter can be produced directly from the collision and valuable information such as spin, mass, coupling etc. of dark matter candidate can be measured. Moreover, dark matter can also be produced at collider from invisible decay of Higgs boson or Z boson. Invisible decay branchings of Higgs or Z boson is constrained by experiments at LHC, LEP which is then used to put further bound on invisible decay (such as couplings) of these bosons into dark matter.

Chapter 4

Fermionic dark matter in two Higgs doublet model

4.1 Introduction

The satellite borne experiments like Planck, WMAP etc. which study the anisotropies of cosmic microwave background radiation (CMBR) predict that more than a quarter of the constituents of the Universe is made of unknown dark matter. The recent Planck data obtained from the observation of CMBR suggest that the relic abundance for dark matter is within the range $\Omega_{\text{DM}}h^2 = 0.1199 \pm 0.0027$ [3], where h is the Hubble parameter normalised to $100 \text{ km s}^{-1} \text{ Mpc}^{-1}$. Although the dark matter (DM) searches are being vigorously pursued, the particle constituent of dark matter is not known at all. In the Chapter we consider an extension of Standard Model (SM) where a second Higgs doublet is introduced in addition to the SM Higgs doublet. Though the recent findings of CMS [63] and ATLAS [64] have confirmed the existence of a SM like scalar with mass 125 GeV, possibility of having

a second Higgs doublet accompanied by the SM sector Higgs doublet is not ruled out. Such an extension of SM sector including a second Higgs doublet is preferably known as two Higgs doublet model or THDM [65]. The two Higgs doublet model is the most general non supersymmetric extension of Standard Model (SM) when another complex doublet of same hypercharge is added to the SM. Also a discrete symmetry is introduced between the Higgs doublets of THDM to avoid flavour changing neutral current (FCNC) processes [66]. In this work, we consider a singlet fermionic dark matter candidate in THDM framework. Possibility of a singlet scalar appearing in THDM to provide a feasible DM candidate has been studied extensively in Refs. [67]-[74]. The case of low mass scalar DM in the framework of THDM has been presented in a recent work by [72]. Thus, the dark matter candidate is the singlet fermion in our model. We then explore the viability of this singlet fermion for being a candidate of cold dark matter in the framework of THDM. In a previous work [15], a minimal model of singlet fermionic dark matter is proposed which is formulated by adding a Lagrangian for the fermion to Standard Model Lagrangian. The fermionic dark matter particle in this minimal model couples with the SM Higgs doublet through a dimension five interaction term and a new physics scale Λ is introduced. However this minimal model of fermionic dark matter requires UV completion which can be achieved by adding a singlet scalar to the minimal model. Phenomenology of such renormalisable singlet fermionic dark matter models with additional singlet scalar are explored in literatures [75, 76]. In the present work, however, we consider a THDM with an additional singlet fermion which is treated as the DM candidate. Previous work including fermionic dark matter in THDM Ref. [69], is based on an ad-hoc assumption that the singlet dark matter couples to the SM Higgs (h) and does not couple to the other scalar H involved in THDM. Based on this simple assumption the work by Cai and Li [69] only explores the low mass dark matter region ($m_{\text{DM}} \leq 40$ GeV). But in our case, the singlet fermion, which is the DM candidate in the present

model, couples to both the Higgs doublets through a dimension five coupling when a new physics scale Λ is introduced. Hence, DM candidate in present scenario couples to both the scalar bosons h and H of THDM. The stability of such a dark matter is ensured either by assigning a discrete Z'_2 symmetry under which the singlet fermion is odd and the THDM sector is even or by assigning the baryon and lepton charge of the singlet fermion to be zero as taken in Ref. [15, 77]. In this work we explore the possibility that within the framework of this model, the fermion (added to the THDM) is a viable candidate for cold dark matter.

4.2 The Model

In the present work we add a singlet fermion χ with two Higgs doublet model. The singlet fermion χ in the resulting model, is the dark matter candidate. The Lagrangian for χ can be written as

$$\mathcal{L}_\chi = \bar{\chi}i\gamma^\mu\partial_\mu\chi - m_0\bar{\chi}\chi . \quad (4.1)$$

As mentioned earlier, the stability of χ can be confirmed either by assigning zero lepton number and zero baryon number to the singlet fermion [15] or by assuming a Z'_2 symmetry under which χ is odd and the SM sector is even. The total Lagrangian of the model in THDM framework can be written as

$$\mathcal{L} = \mathcal{L}_{\text{THDM}} + \mathcal{L}_\chi + \mathcal{L}_{\text{int}} , \quad (4.2)$$

where \mathcal{L}_{int} denotes the interaction Lagrangian. The two Higgs doublet model potential is expressed as

$$\begin{aligned}
 V(\Phi_1, \Phi_2) = & m_1^2 \Phi_1^\dagger \Phi_1 + m_2^2 \Phi_2^\dagger \Phi_2 + (m_{12}^2 \Phi_1^\dagger \Phi_2 + \text{h.c.}) + \frac{1}{2} \lambda_1 (\Phi_1^\dagger \Phi_1)^2 + \frac{1}{2} \lambda_2 (\Phi_2^\dagger \Phi_2)^2 \\
 & + \lambda_3 (\Phi_1^\dagger \Phi_1) (\Phi_2^\dagger \Phi_2) + \lambda_4 (\Phi_1^\dagger \Phi_2) (\Phi_2^\dagger \Phi_1) + \frac{1}{2} \lambda_5 [(\Phi_1^\dagger \Phi_2)^2 + \text{h.c.}] , \quad (4.3)
 \end{aligned}$$

where both the doublet Higgs fields Φ_1 and Φ_2 have non zero vacuum expectation values and a discrete symmetry (Z_2) is imposed in between the doublet fields in order to avoid FCNC processes. We consider a CP conserving two Higgs doublet model potential where all the parameters expressed in Eq. 4.3 are assumed to be real. In addition, the imposed discrete symmetry Z_2 will result in mainly four types of THDM namely type I, type II, lepton specific and flipped THDM according to the nature of the coupling of fermions with the doublet fields. In the present work we consider type I and type II THDM and construct the model. Thus the two scenarios we consider in this work are type I THDM + one singlet fermion and type II THDM + one singlet fermion. Both the scenarios will give rise to charged Higgs pair (H^\pm), two CP even scalar fields (h, H), one CP odd scalar (A) and Goldstone bosons (G^\pm, G). The Higgs doublets Φ_1 and Φ_2 expressed in terms of physical states of the particles are written as [78],

$$\Phi_1 = \begin{pmatrix} c_\beta G^+ - s_\beta H^+ \\ \frac{1}{\sqrt{2}}(v_1 + c_\alpha H - s_\alpha h + i c_\beta G - i s_\beta A) \end{pmatrix} , \quad (4.4)$$

$$\Phi_2 = \begin{pmatrix} s_\beta G^+ + c_\beta H^+ \\ \frac{1}{\sqrt{2}}(v_2 + s_\alpha H + c_\alpha h + i s_\beta G + i c_\beta A) \end{pmatrix} , \quad (4.5)$$

where $\tan \beta (= \frac{v_2}{v_1})$, is the ratio of the vacuum expectation values v_2 and v_1 of the doublets Φ_1 and Φ_2 and α is the measure of mixing between two CP even scalars. The terms c_x and s_x ($x = \alpha, \beta$) denote $\cos x$ and $\sin x$ respectively. The scalar potential for the THDM as expressed in Eq. 4.3 must be bounded from below for the stability of vacuum. The Conditions for a stable vacuum for THDM are

$$\lambda_1, \lambda_2 > 0, \quad \lambda_3 + 2\sqrt{\lambda_1\lambda_2} > 0, \quad \lambda_3 + \lambda_4 - |\lambda_5| + 2\sqrt{\lambda_1\lambda_2} > 0 .$$

Perturbative unitarity constraints for the THDM are also taken into account. Bounds from the unitarity limits on THDM parameters are adopted from [65].

The interaction Lagrangian, \mathcal{L}_{int} of dark matter fermion (Eq. 4.2) with Φ_1 and Φ_2 doublet fields is given by

$$\mathcal{L}_{\text{int}} = -\frac{g_1}{\Lambda}(\Phi_1^\dagger\Phi_1)\bar{\chi}\chi - \frac{g_2}{\Lambda}(\Phi_2^\dagger\Phi_2)\bar{\chi}\chi , \quad (4.6)$$

where Λ is a high energy scale and $g_{1,2}$ are dimensionless couplings with the doublet fields $\Phi_{1,2}$. Interaction of THDM sector with the DM candidate can now be obtained easily from Eqs. 4.2-4.6. Dark matter fermion couples to both the physical Higgs particles h and H which are given by

$$\begin{aligned} g_{\bar{\chi}\chi h} &= \frac{v}{\Lambda}(-g_1 \sin \alpha \cos \beta + g_2 \cos \alpha \sin \beta) , \\ g_{\bar{\chi}\chi H} &= \frac{v}{\Lambda}(g_2 \cos \alpha \cos \beta + g_1 \sin \alpha \sin \beta) , \end{aligned} \quad (4.7)$$

where Λ being a very large scale with respect to v . Hence the couplings $g_{\bar{\chi}\chi h}$ and $g_{\bar{\chi}\chi H}$ are expected to be small. Using Eqs. 4.1-4.7, mass of the singlet is expressed as

$$m_\chi = m_0 + v^2 \left(\frac{g_1}{2\Lambda} \cos^2 \alpha + \frac{g_2}{2\Lambda} \sin^2 \alpha \right) ,$$

where $v(= \sqrt{v_1^2 + v_2^2})$, is 246 GeV. Note that the new physics scale Λ determines the coupling of DM particle to THDM sector and contributes significantly to the singlet fermion mass. As mentioned earlier, the discrete Z_2 symmetry imposed between the Higgs doublets will result in four different types of THDM. In this work we consider THDM of type I and type II. In type I THDM, only one scalar doublet (say Φ_2) couples to the SM particles whereas in type II THDM, up type quarks couple to one Higgs doublet and down type quarks and leptons couple to the other. Hence type I THDM can be implemented with discrete symmetry $\Phi_1 \rightarrow -\Phi_1$. On the other hand type II THDM is the case when $\Phi_1 \rightarrow -\Phi_1$ and $d_R^i \rightarrow -d_R^i$ (d_R^i , $i = 1 - 3$ represents down type quarks) is satisfied. Also it is assumed that right handed leptons follows the same discrete symmetry as the down type quarks. Higgs couplings to up type quarks, down type quarks and leptons in case of type I THDM are given as [66]

$$g_{\bar{f}fh} = -i \frac{gm_f \cos \alpha}{2M_W \sin \beta}, \quad g_{\bar{f}fH} = -i \frac{gm_f \sin \alpha}{2M_W \sin \beta}, \quad (4.8)$$

where f denotes all SM fermions (up quarks, down quarks and leptons) respectively. In case of type II THDM, Yukawa couplings are

$$\begin{aligned} g_{\bar{u}uh} &= -i \frac{gm_u \cos \alpha}{2M_W \sin \beta}, & g_{\bar{u}uH} &= -i \frac{gm_u \sin \alpha}{2M_W \sin \beta}, \\ g_{\bar{d}dh} &= -i \frac{gm_d - \sin \alpha}{2M_W \cos \beta}, & g_{\bar{d}dH} &= -i \frac{gm_d \cos \alpha}{2M_W \cos \beta}, \\ g_{\bar{l}lh} &= -i \frac{gm_l - \sin \alpha}{2M_W \cos \beta}, & g_{\bar{l}lH} &= -i \frac{gm_l \cos \alpha}{2M_W \cos \beta}. \end{aligned} \quad (4.9)$$

In the above, u corresponds to up type quarks (u, c, t), d corresponds to down type quarks (d, s, b) and l represents three families of leptons (e, μ, τ) respectively. Couplings to the gauge bosons ($V = W, Z$) for THDM I and THDM II are same and

given by [66]

$$\begin{aligned}
 g_{WW h} &= igM_W \sin(\beta - \alpha)g^{\mu\nu} , & g_{WW H} &= igM_W \cos(\beta - \alpha)g^{\mu\nu} , \\
 g_{ZZ h} &= ig\frac{M_Z}{\cos\theta_W} \sin(\beta - \alpha)g^{\mu\nu} , & g_{ZZ H} &= ig\frac{M_Z}{\cos\theta_W} \cos(\beta - \alpha)g^{\mu\nu} .
 \end{aligned} \quad (4.10)$$

In Eqs. 4.8-4.10, m_x ($x = u, d, l$ etc) represents the mass of quarks or leptons and M_W and M_Z denote the masses of W and Z bosons respectively. In the present framework with type I and type II THDM, we consider h to be SM-like Higgs boson with mass $m_h = 125$ GeV and H as the non-SM Higgs with mass m_H .

It is to be noted that a term $\sim \frac{1}{\Lambda}\Phi_1^\dagger\Phi_2\bar{\chi}\chi + h.c.$ can also be added to the interaction Lagrangian (Eq. 4.6). Such a term would result in an additional mass term $\sim v_1v_2$ for the dark matter candidate χ in the present model. Moreover, this term will also be responsible for interaction $\bar{\chi}\chi \rightarrow hH$. However, we have followed the formalism of Cai and Li [69] where such an interaction term is not taken into account. In this work we show that as we drop the ad-hoc assumption of $g_{\bar{\chi}\chi h} = 0$ or $g_{\bar{\chi}\chi H} = 0$ taken in [69], the results would be different and the allowed low mass region for dark matter $m_\chi \leq 40$ GeV will disappear.

4.3 Collider physics phenomenology

The existence of a scalar boson of mass 125 GeV has been confirmed by Large Hadron Collider (LHC) [63, 64]. In this work we treat the new found scalar boson to be equivalent to one of the CP even scalars (h) appearing in THDMs. We further extend the model by including a possible fermionic dark matter (FDM) candidate. This may necessarily affect the phenomenology of collider physics. If the dark matter mass is small ($m_\chi \leq m_h/2$) then one would expect an invisible decay of SM-like Higgs

boson (h) and the total decay width will change depending on the coupling constant $g_{\bar{\chi}\chi h}$ and other THDM parameters α, β . Since both the scalar bosons in THDM couple with the DM fermion in the present framework, it may change the standard bounds on THDM sector. The signal strength of SM like Higgs boson (h) to a specific channel for type I and type II THDM are given by

$$R_I = \frac{\sigma_h^I}{\sigma^{\text{SM}}} \frac{\text{BR}^I}{\text{BR}^{\text{SM}}}, \quad R_{II} = \frac{\sigma_h^{II}}{\sigma^{\text{SM}}} \frac{\text{BR}^{II}}{\text{BR}^{\text{SM}}}, \quad (4.11)$$

where $\frac{\sigma_h^{I,II}}{\sigma^{\text{SM}}}$ represents the ratio of Higgs production cross-section in type I as also in type II THDM with respect to that for SM (σ^{SM} , is the SM Higgs production cross-section). The branching ratio (BR) to any specific channel for the chosen model and for SM are given by BR^X , $X = I, II$ and BR^{SM} . The ratio $\frac{\sigma_h^X}{\sigma^{\text{SM}}}$ ($X = I, II$) in Eq. 4.11 for 125 GeV Higgs boson can be expressed as

$$\frac{\sigma_h^X}{\sigma^{\text{SM}}} = \frac{\sigma_{tt}f_t^2 + \sigma_{bb}f_b^2 + \sigma_{tb}f_t f_b}{\sigma^{\text{SM}}}, \quad (4.12)$$

where σ_{tt} , σ_{bb} are the Higgs production cross-sections from top and bottom quarks respectively and σ_{tb} is the contribution from top-bottom interference. For the calculation of SM Higgs signal strength, we have adopted the leading order (LO) production cross-sections obtained from [79]. The factors f_t, f_b in Eq. 4.11 are the Yukawa couplings of SM-like Higgs (h) with top and bottom quarks for the specific model normalised with respect to SM. For type I THDM, $f_t = f_b = \frac{\cos\alpha}{\sin\beta}$ and for type II THDM these factors are given as $f_t = \frac{\cos\alpha}{\sin\beta}$ and $f_b = \frac{-\sin\alpha}{\cos\beta}$. As defined earlier, α is the mixing angle between the CP even scalars h and H and β is given by the ratio of the VEVs v_2 and v_1 of Higgs doublets Φ_2 and Φ_1 respectively ($\tan\beta = \frac{v_2}{v_1}$). ATLAS and CMS experiments have measured the signal strengths of SM Higgs (h) boson to different production channels such as $b\bar{b}, \tau\bar{\tau}, \gamma\gamma, WW^*, ZZ^*$. The mean signal strengths of SM Higgs to these channels measured by ATLAS and the best

fit value of combined signal strength of h given by CMS experiment are found to be [80, 81]

$$R_{\text{ATLAS}} = 1.23 \pm 0.18, \quad R_{\text{CMS}} = 0.8 \pm 0.14. \quad (4.13)$$

In the present scenario with THDM, we have a non-SM Higgs (H) in addition to the SM scalar h . The signal strengths of non-SM Higgs boson for type I and type II THDM are given as

$$R'_I = \frac{\sigma_H^I}{\sigma'^{\text{SM}}} \frac{\text{BR}^I}{\text{BR}'^{\text{SM}}} \quad \text{and} \quad R'_{II} = \frac{\sigma_H^{\text{II}}}{\sigma'^{\text{SM}}} \frac{\text{BR}^{\text{II}}}{\text{BR}'^{\text{SM}}} \quad (4.14)$$

respectively, where σ_H^X ($X = \text{I}, \text{II}$ depending on the nature of THDM considered) is the non-SM Higgs production cross-section and BR'^X is the branching ratio of H to any specific channel. In Eq. 4.14, σ'^{SM} and BR'^{SM} represent the production cross-section and branching ratio of the non-SM Higgs boson (H) with mass m_H . The modified non-SM Higgs production cross-section ratio can be given as

$$\frac{\sigma_H^X}{\sigma'^{\text{SM}}} = \frac{\sigma'_{tt} f_t'^2 + \sigma'_{bb} f_b'^2 + \sigma'_{tb} f_t' f_b'}{\sigma'^{\text{SM}}}. \quad (4.15)$$

Similar to Eq. 4.11, in Eq. 4.15 also, the factors f'_t , f'_b are the SM normasiled Yukawa couplings of non-SM Higgs H with top and bottom quarks. For the case of type I THDM, $f'_t = f'_b = \frac{\sin \alpha}{\sin \beta}$, whereas those for type II THDM are $f'_t = \frac{\sin \alpha}{\sin \beta}$ and $f'_b = \frac{\cos \alpha}{\cos \beta}$. In the present work we consider two values of non-SM Higgs mass and they are chosen as $m_H = 150$ GeV and 200 GeV. The calculations are performed for each of these chosen masses. We use the leading order production cross-section (σ'_{tt} , σ'_{bb} , σ'_{tb} and σ'^{SM}) obtained from Ref. [79] for the chosen m_H values in the work. Invisible decay of the non-SM Higgs (for $m_\chi \leq m_H/2$) has also been taken into account. Since no signature of additional Higgs has been reported by ATLAS and CMS experiment, it is likely to assume that the non-SM Higgs signal strength is negligibly small compared

to that of SM Higgs. Hence, throughout the work, we restrict the signal strength for non-SM scalar satisfying the condition $R'_X \leq 0.2$ ($X = I, II$). SM branching ratios for specific decay modes of SM Higgs (BR^{SM} with mass $m_h = 125$ GeV) and non-SM Higgs (BR^{SM} for $m_H = 150$ and 200 GeV) are adopted from Ref. [82]. It is to be mentioned that in this work we do not consider any ad-hoc condition, e.g. by setting $g_{\bar{\chi}\chi h} = 0$ or $g_{\bar{\chi}\chi H} = 0$ [69] for the SM-like scalar (assuming $\sin(\beta - \alpha) = \pm 1$ when h is SM-like or $\sin(\beta - \alpha) = 0$ when H is SM-like). In the present formalism we consider the total allowed range of available parameter space independent of these conditions and restrict them by using limits on SM Higgs signal strength from CMS and ATLAS (Eq. 4.13).

4.4 DM annihilation and relic density

In order to evaluate the relic density of the fermionic dark matter candidate proposed in this work one requires to solve the Boltzmann equation [26]

$$\frac{dn}{dt} + 3Hn = -\langle\sigma v\rangle(n^2 - n_{eq}^2) \quad (4.16)$$

where n is the actual number density of the particle species, H is the Hubble parameter and n_{eq} is the number density at thermal equilibrium. An approximate expression for relic density Ω or Ωh^2 ($h = H/(100 \text{ kms}^{-1} \text{ Mpc}^{-1})$) that can be obtained from Eq. 4.16 is given by

$$\Omega_{\text{DM}} h^2 = \frac{1.07 \times 10^9 x_F}{\sqrt{g_*} M_{\text{Pl}} \langle\sigma v\rangle} \quad (4.17)$$

where $x_F = m_\chi/T_F$, g_* is the effective degrees of freedom and $M_{\text{Pl}} = 1.22 \times 10^{19}$ is the Planck mass. The particle physics input to Eqs. 4.16-4.17 is the thermal averaged

annihilation cross-section $\langle\sigma v\rangle$ and one needs to calculate this quantity for the present fermionic dark matter candidate in our model. The freeze out temperature T_F (or x_F) in Eq. 4.17 can be computed by iteratively solving the equation

$$x_F = \ln \left(\frac{m_\chi}{2\pi^3} \sqrt{\frac{45M_{Pl}^2}{2g_*x_F}} \langle\sigma v\rangle \right). \quad (4.18)$$

The freeze out temperature thus obtained is then used to evaluate the relic density of the dark matter candidate χ in our model. In order to solve for the freeze out temperature, it is therefore essential to calculate the annihilation cross-section of the dark matter candidate. Dark matter candidates in the present model annihilate to SM particles through h or H mediated s-channel processes. The total annihilation cross-section σv can be expressed as a sum of the three terms

$$\begin{aligned} \sigma v = & (s - 4m_\chi^2) \left[A \frac{1}{(s - m_h^2)^2 + m_h^2 \Gamma_h^2} + B \frac{1}{(s - m_H^2)^2 + m_H^2 \Gamma_H^2} \right. \\ & \left. + C \frac{2(s - m_h^2)(s - m_H^2) + 2m_h m_H \Gamma_h \Gamma_H}{[(s - m_h^2)^2 + m_h^2 \Gamma_h^2][(s - m_H^2)^2 + m_H^2 \Gamma_H^2]} \right]. \end{aligned} \quad (4.19)$$

In Eq. 4.19, Γ_h and Γ_H are decay widths of light Higgs (h) and heavy Higgs particle (H) respectively. We set the light Higgs mass m_h to be 125 GeV and consider each of the two values of non-SM Higgs mass $m_H = 150$ GeV and 200 GeV. Thus we assume $m_H > m_h$ in the present work. The terms A , B and C in the expression for σv (Eq. 4.19) in case of THDM I are given as (with summation convention imposed on quarks and leptons)

$$\begin{aligned} A = & g_{\chi\chi h}^2 \frac{G_F}{4\pi\sqrt{2}} \left[\frac{c_\alpha^2}{s_\beta^2} (N_c m_{u_i}^2 \gamma_{u_i}^3 + N_c m_{d_i}^2 \gamma_{d_i}^3 + m_{l_i}^2 \gamma_{l_i}^3) \right. \\ & \left. + \frac{1}{2} s_{\beta-\alpha}^2 s (1 - x_W + \frac{3}{4} x_W^2) \gamma_W + \frac{1}{4} s_{\beta-\alpha}^2 s (1 - x_Z + \frac{3}{4} x_Z^2) \gamma_Z \right], \end{aligned} \quad (4.20)$$

$$\begin{aligned}
 B = & g_{\bar{\chi}\chi H}^2 \frac{G_F}{4\pi\sqrt{2}} \left[\frac{s_\alpha^2}{s_\beta^2} (N_c m_{u_i}^2 \gamma_{u_i}^3 + N_c m_{d_i}^2 \gamma_{d_i}^3 + m_{l_i}^2 \gamma_{l_i}^3) \right. \\
 & \left. + \frac{1}{2} c_{\beta-\alpha}^2 s(1-x_W + \frac{3}{4}x_W^2)\gamma_W + \frac{1}{4} c_{\beta-\alpha}^2 s(1-x_Z + \frac{3}{4}x_Z^2)\gamma_Z \right], \quad (4.21)
 \end{aligned}$$

and

$$\begin{aligned}
 C = & g_{\bar{\chi}\chi h} g_{\bar{\chi}\chi H} \frac{G_F}{4\pi\sqrt{2}} \left[\frac{c_\alpha s_\alpha}{s_\beta^2} (N_c m_{u_i}^2 \gamma_{u_i}^3 + N_c m_{d_i}^2 \gamma_{d_i}^3 + m_{l_i}^2 \gamma_{l_i}^3) \right. \\
 & \left. + \frac{1}{2} s_{\beta-\alpha} c_{\beta-\alpha} s(1-x_W + \frac{3}{4}x_W^2)\gamma_W + \frac{1}{4} s_{\beta-\alpha} c_{\beta-\alpha} s(1-x_Z + \frac{3}{4}x_Z^2)\gamma_Z \right]. \quad (4.22)
 \end{aligned}$$

For type II THDM, the expressions for A , B and C are

$$\begin{aligned}
 A = & g_{\bar{\chi}\chi h}^2 \frac{G_F}{4\pi\sqrt{2}} \left[N_c m_{u_i}^2 \frac{c_\alpha^2}{s_\beta^2} \gamma_{u_i}^3 + N_c m_{d_i}^2 \frac{s_\alpha^2}{c_\beta^2} \gamma_{d_i}^3 + m_{l_i}^2 \frac{s_\alpha^2}{c_\beta^2} \gamma_{l_i}^3 \right. \\
 & \left. + \frac{1}{2} s_{\beta-\alpha}^2 s(1-x_W + \frac{3}{4}x_W^2)\gamma_W + \frac{1}{4} s_{\beta-\alpha}^2 s(1-x_Z + \frac{3}{4}x_Z^2)\gamma_Z \right], \quad (4.23)
 \end{aligned}$$

$$\begin{aligned}
 B = & g_{\bar{\chi}\chi H}^2 \frac{G_F}{4\pi\sqrt{2}} \left[N_c m_{u_i}^2 \frac{s_\alpha^2}{s_\beta^2} \gamma_{u_i}^3 + N_c m_{d_i}^2 \frac{c_\alpha^2}{c_\beta^2} \gamma_{d_i}^3 + m_{l_i}^2 \frac{c_\alpha^2}{c_\beta^2} \gamma_{l_i}^3 \right. \\
 & \left. + \frac{1}{2} c_{\beta-\alpha}^2 s(1-x_W + \frac{3}{4}x_W^2)\gamma_W + \frac{1}{4} c_{\beta-\alpha}^2 s(1-x_Z + \frac{3}{4}x_Z^2)\gamma_Z \right], \quad (4.24)
 \end{aligned}$$

$$\begin{aligned}
 C = & g_{\bar{\chi}\chi h} g_{\bar{\chi}\chi H} \frac{G_F}{4\pi\sqrt{2}} \left[N_c m_{u_i}^2 \frac{s_\alpha c_\alpha}{s_\beta s_\beta} \gamma_{u_i}^3 - N_c m_{d_i}^2 \frac{c_\alpha s_\alpha}{c_\beta c_\beta} \gamma_{d_i}^3 - m_{l_i}^2 \frac{c_\alpha s_\alpha}{c_\beta c_\beta} \gamma_{l_i}^3 \right. \\
 & \left. + \frac{1}{2} c_{\beta-\alpha} s_{\beta-\alpha} s(1-x_W + \frac{3}{4}x_W^2)\gamma_W + \frac{1}{4} c_{\beta-\alpha} s_{\beta-\alpha} s(1-x_Z + \frac{3}{4}x_Z^2)\gamma_Z \right]. \quad (4.25)
 \end{aligned}$$

In all the above expressions (Eqs. 4.20-4.25) $\gamma_a = (1 - \frac{4m_a^2}{s})^{\frac{1}{2}}$ ($a = u, d, l, W, Z$), $x_B = \frac{4m_B^2}{s}$ and $N_c = 3$ for quarks. Thermal average of pair annihilation cross-section

of DM to SM particles is given by

$$\langle\sigma v\rangle = \frac{1}{8m_\chi^4 T_F K_2^2(m_\chi/T_F)} \int_{4m_\chi^2}^{\infty} ds \sigma(s) (s - 4m_\chi^2) \sqrt{s} K_1(\sqrt{s}/T_F), \quad (4.26)$$

where K_1 and K_2 are modified Bessel function. Using Eqs. 4.19-4.26, the annihilation cross-section $\langle\sigma v\rangle$ of DM candidate into SM particles is evaluated for both type I and type II THDM. We first solve for the freeze out temperature T_F using Eq. 4.18. The relic density $\Omega_{\text{DM}} h^2$ of dark matter is obtained by solving Eq. 4.17 in order to satisfy dark matter relic density obtained from PLANCK experimental value $\Omega_{\text{DM}} h^2 = 0.1199 \pm 0.0027$ [3]. The DM relic density is computed with the chosen model parameters such that ¹

$$\begin{aligned} m_\chi &\leq 300 \text{ GeV} , \\ 10^{-4} &\leq |g_{\bar{\chi}\chi h}| \leq 0.1 , \\ 10^{-4} &\leq |g_{\bar{\chi}\chi H}| \leq 0.1 , \\ -\pi/2 &\leq \alpha \leq \pi/2 , \\ 1 &\leq \tan \beta < 30 . \end{aligned} \quad (4.27)$$

As mentioned earlier, the calculation of dark matter relic density is performed for two values of non-SM scalar mass m_H taken to be 150 GeV and 200 GeV. We further constrain the model parameter space using the bounds for SM Higgs signal strength as obtained from ATLAS and CMS experiments (Section 4.3) as also using the bounds on the signal strength of H ($R'_{I,II} \leq 0.2$).

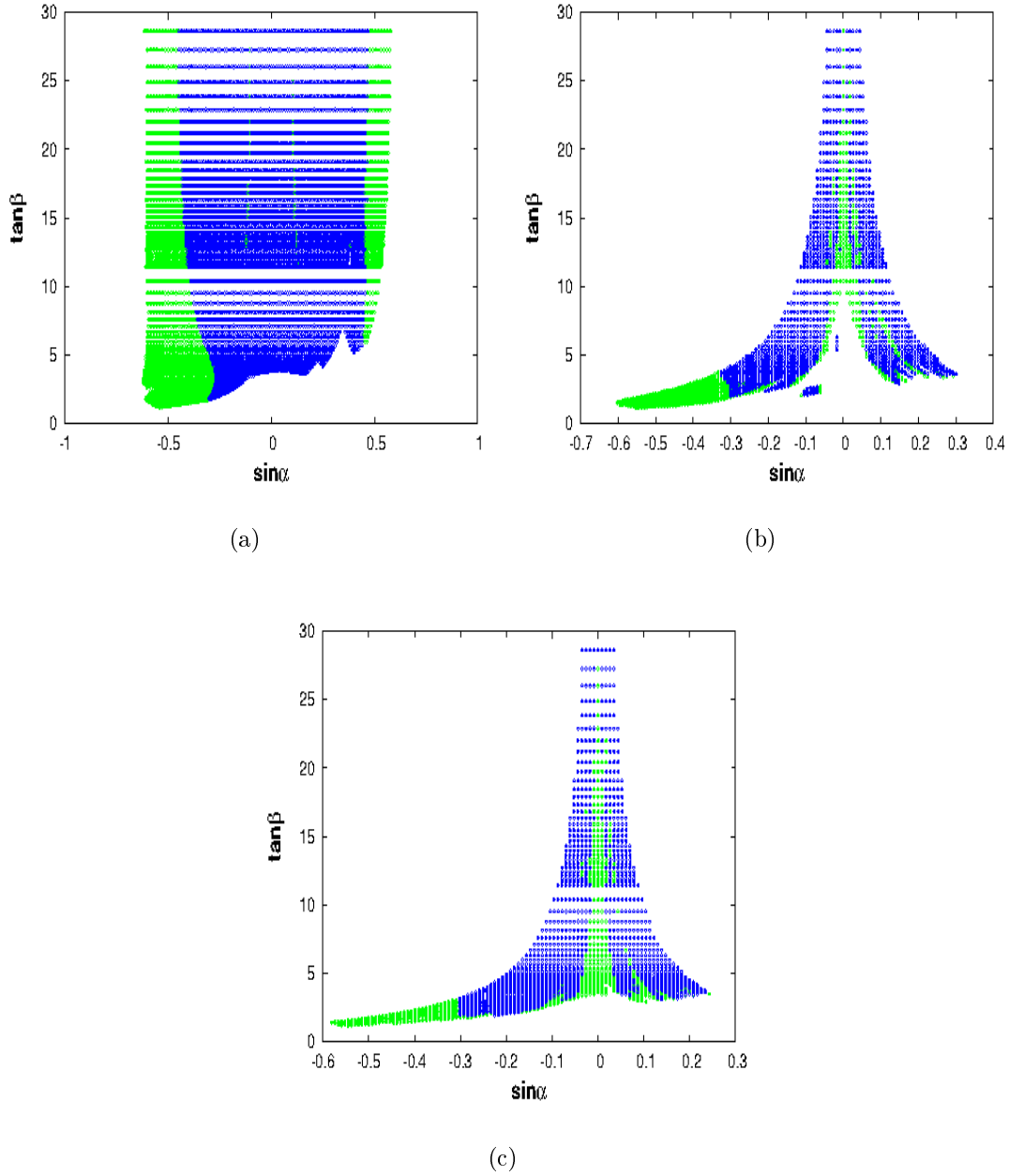


Figure 4.1: Allowed $\sin\alpha$ - $\tan\beta$ parameter space for type I THDM consistent with R_{CMS} within the framework of present DM model (Fig. 4.1a). Green and blue coloured regions are for $m_H = 150$ GeV and 200 GeV respectively. Similar plots for the case of type II THDM is shown in Fig. 4.1b. Valid parameter space in type II THDM satisfying R_{ATLAS} only is depicted in Fig. 4.1c. The computation for all the plots are performed with the constrained range of model parameter space values which produce required DM relic density consistent with PLANCK results. For all the plots the constrained $R'_{I,II}$ is respected.

4.5 Results

In this section we present the results for our fermionic dark matter in type I and type II THDM. We first obtain the relic density of the DM candidate by solving the Boltzmann equation (Eq. 4.16). The Boltzmann equation is solved by using the range of parameter space given in Eq. 4.27 and the relic density of the fermionic dark matter in the present model is then calculated. The comparison with the PLANCK's result for DM relic density, constraints the parameter space of the model considered in this work. The signal strength R_X ($X = I, II$; I, II corresponds to type I and type II THDM respectively) for the SM Higgs h is computed with the parameter space restricted by PLANCK results. As mentioned earlier, we also compute the signal strength R'_X , the signal strength of the other Higgs H and its value is kept in the limit $R'_X \leq 0.2$. The calculated values of both R_I and R_{II} are compared with the CMS and ATLAS limits for the SM signal strength. Thus the parameter space is further constrained by the CMS and ATLAS results. In Fig. 4.1a-c we show the allowed parameter space in $\sin\alpha$ - $\tan\beta$ plane for fermionic dark matter for each of type I and type II THDM scenarios extended with FDM. The plots in Fig. 4.1 are obtained for two values of H mass namely $m_H = 150$ and 200 GeV. In Fig. 4.1a the variations of $\sin\alpha$ with $\tan\beta$ for FDM extended type I THDM are shown. We found that for type I THDM along with FDM fails to satisfy the combined signal strength as predicted by ATLAS (R_{ATLAS}). Hence in Fig. 4.1a, only the constraints from CMS experimental results (for signal strength, i.e. R_{CMS}) are imposed. The blue and green scattered regions in Fig. 4.1a-4.1c represent the respective allowed parameter space when m_H is chosen to be 150 GeV and 200 GeV respectively. It can also be observed from Fig. 4.1a that increase in the mass of the other scalar H associated with the model results in considerable reduction in the overall allowed

¹We have checked that in order to satisfy the PLANCK results, these ranges of the parameters suffice.

THDM parameter space. In Fig. 4.1b we plot the available region of $\sin\alpha$ - $\tan\beta$ plane for the case of fermionic dark matter in type II THDM consistent with the PLANCK relic density as also SM Higgs signal strength R_{CMS} given in Eq. 4.13 with $R'_{II} \leq 0.2$. Similar allowed regions but R_{CMS} replaced with R_{ATLAS} (ATLAS bound) are shown in Fig. 4.1c for type II THDM scenario. For type II THDM, we use the same colour convention as used in the case of type I THDM (Fig. 4.1a) to show the valid region of parameter space for $m_H = 150$ and 200 GeV. Comparison of the plots in Fig. 4.1b-c with the type I THDM case (Fig. 4.1a) clearly shows that there is less allowed parameter space available for type II THDM. It is to be noted that for type II THDM involving FDM is in agreement with both the combined (for all five channels namely $b\bar{b}, \tau\bar{\tau}, \gamma\gamma, WW^*, ZZ^*$) signal strengths R_{CMS} and R_{ATLAS} as predicted independently by CMS and ATLAS experimental results. Note that, for the case of type II THDM shown in Fig. 4.1b-c too, the available region of $\sin\alpha$ - $\tan\beta$ plane decreases with increase of the mass of H which is similar to the trend observed for type I THDM formalism (Fig. 4.1a).

4.5.1 Direct detection measurements

We further restrict the allowed parameter space of our model with the direct detection experimental bounds on DM-nucleon scattering cross-section. Direct detection of dark matter utilises the phenomenon of a possible elastic scattering off a nucleus of detecting material. In order to enable a uniform comparison of experimental results from different dark matter experiments with different detecting materials, the experimentally obtained DM-nucleus elastic scattering cross-section (σ_{scat}) is reduced to DM-nucleon scattering cross-section. The experimental results are then expressed as the allowed region in $m_\chi - \sigma_{\text{scat}}^{\text{nucleon}}$ plane. This elastic scattering cross-section can be spin independent (SI) or spin dependent (SD), depending on

the ground state spin of detector nucleus. The elastic scattering of the dark matter particle off the target causes the recoil of the target nucleus. This recoil energy is measured in the experiment and allowed region in the plane of scattering cross-section and dark matter mass is then obtained. The spin independent dark matter-nucleon elastic scattering cross-section in the present model is given as

$$\sigma_{\text{SI}} \simeq \frac{m_r^2}{\pi} \left(\frac{g_{\bar{\chi}\chi h} g_{NNh}}{m_h^2} + \frac{g_{\bar{\chi}\chi H} g_{NNH}}{m_H^2} \right)^2. \quad (4.28)$$

In the above, m_r is the reduced mass $= \frac{m_\chi m_N}{m_\chi + m_N}$, where m_N is the mass of the scattering nucleon (proton or neutron) and g_{NNx} ($x = h$ or H) denotes the effective Higgs nucleon couplings expressed as [83]

$$g_{NNh} \simeq (1.217k_d^h + 0.493k_u^h) \times 10^{-3}, \quad g_{NNH} \simeq (1.217k_d^H + 0.493k_u^H) \times 10^{-3}. \quad (4.29)$$

For the case of THDM I, parameters k_u^h and k_d^h in Eq. 4.29 are given as

$$k_u^h = k_d^h = \frac{\cos \alpha}{\sin \beta}, \quad k_u^H = k_d^H = \frac{\sin \alpha}{\sin \beta}. \quad (4.30)$$

and for the case of THDM II these parameters are

$$k_u^h = \frac{\cos \alpha}{\sin \beta}, \quad k_d^h = -\frac{\sin \alpha}{\cos \beta}, \quad k_u^H = \frac{\sin \alpha}{\sin \beta}, \quad k_d^H = \frac{\cos \alpha}{\cos \beta}. \quad (4.31)$$

Using Eqs. 4.28-4.31, we compute σ_{SI} for the DM candidate within the framework of our chosen specific model in this work and compare them with the latest limits for σ_{SI} and m_χ (in $\sigma_{\text{SI}} - m_\chi$ plane) given by recent dark matter direct detection experiments namely XENON100 [27] and LUX [28]². In Fig. 4.2a-f we plot the variation of DM-nucleon scattering cross-section σ_{SI} with DM mass (m_χ) for the

²Both the experiments use liquid Xenon as detection material.

cases of both type I and type II THDM. The red and blue lines shown in Fig. 4.2a-f are the limits on DM-nucleon cross-section obtained from XENON100 and LUX. The calculations are performed with the parameter space (such as couplings etc.) of the present model which has already been constrained by PLANCK results and collider bounds (Fig. 4.1a-c). Thus the resulting $m_\chi - \sigma_{\text{SI}}$ parameter space is in agreement with the bounds from Higgs signal strength ($R_{\text{CMS,ATLAS}}$), limits on the signal strength on extra Higgs scalar of THDM ($R'_{I,II} \leq 0.2$) and also satisfies DM relic density predicted by PLANCK. Shown in Fig. 4.2a and Fig. 4.2b are the $m_\chi - \sigma_{\text{SI}}$ parameter space of DM candidate in type I THDM framework for $m_H = 150$ and 200 GeV respectively. Needless to mention, parameters used in these two plots are restricted by R_{CMS} , R'_I and PLANCK. It is to be noted from Fig. 4.1a that observational results of Higgs signal strength (Fig. 4.1a) indicate that there is no valid parameter space in type I THDM associated with our fermionic dark matter that corresponds to R_{ATLAS} . It is clear from Fig. 4.2a-b that due to the presence of an extra scalar in the model along with SM Higgs, an extra pole is likely to appear in the mass range $m_\chi \sim m_H/2$ with the normal SM Higgs pole occurring near $m_\chi \sim m_h/2$. This scenario also holds for the case of type II THDM as well. Study of the plots in Fig. 4.2a-b reveals that the fermionic DM particle χ in type I THDM can serve as a viable candidate of dark matter with a sufficient allowed parameter space that is in agreement with latest DM direct detection experimental results of XENON100 and LUX. Similarly using the allowed parameter space obtained in Fig. 4.1b-c (constrained by DM relic density, combined Higgs signal strength ($R_{\text{CMS,ATLAS}}$) and bound on additional Higgs signal (R'_{II})), we plot the viable parameter space in $m_\chi - \sigma_{\text{SI}}$ plane for DM in type II THDM (Fig. 4.2c-f). In Fig. 4.2c-d, the available $m_\chi - \sigma_{\text{SI}}$ spaces for two values of the scalar mass H , $m_H = 150$ GeV and 200 GeV respectively are shown. Each of these plots satisfies the model parameter space constrained by PLANCK, R_{CMS} and R'_{II} . Analogous plots are obtained in Fig. 4.2e-f but here only R_{ATLAS} is taken into

account instead of R_{CMS} . It is obvious from Fig. 4.2c-f, that the region of allowed $m_\chi - \sigma_{\text{SI}}$ space depends on the mass of the additional scalar H . Fig. 4.2c-f also shows that a considerable portion of DM-nucleon scattering cross-section σ_{SI} of the DM candidate χ in type II THDM lies in the allowed region set by XENON100 and LUX direct detection experiments. Hence, fermionic dark matter χ appearing in type II THDM can be treated as a potential candidate for dark matter. It is also seen from Figs. 4.2a-f that the low mass region of dark matter appearing in [69] ($m_\chi \leq 40$ GeV) is excluded when the condition $g_{\bar{\chi}\chi h} = 0$ or $g_{\bar{\chi}\chi H} = 0$ is relaxed.

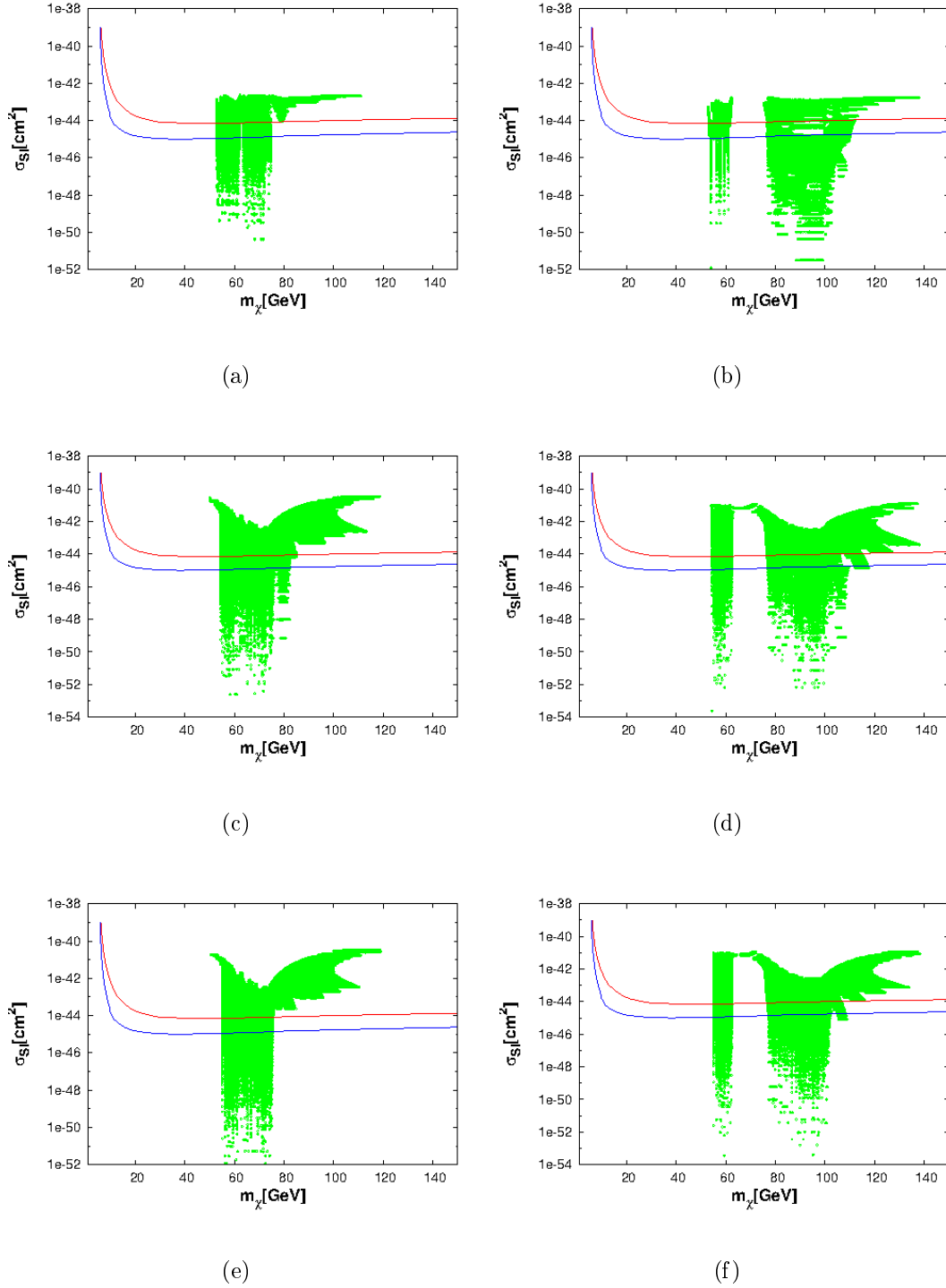


Figure 4.2: Fig. 4.2a-b shows the $m_\chi - \sigma_{SI}$ parameter space for FDM in type I THDM is allowed by PLANCK relic density and collider bounds plotted using R_{CMS} for $m_H = 150$ and 200 GeV. Similar plots in $m_\chi - \sigma_{SI}$ plane with type II THDM are shown in Fig. 4.2c-d whereas the plots in Fig. 4.2e-f are in agreement with R_{ATLAS} and $R'_{I,II} \leq 0.2$. The red and blue lines are respective bounds on DM-nucleon scattering cross-section from XENON100 and LUX DM direct search experiments.

4.6 Discussion

In this chapter we have explored a singlet fermion dark matter in a framework of two Higgs doublet model. We have explored the viability of such a fermionic dark matter in two different types of THDMs namely THDM I and THDM II and assumed that the new found scalar boson at LHC is one of the two CP even Higgs appearing in THDM. The fermionic dark matter candidate χ in our model couples to the CP even Higgs-scalars appearing in THDM with a non-renormalisable dimension five interaction. Hence, DM in the present model can undergo the process of annihilation into SM particles through Higgs mediated channels. We solve the Boltzmann equation for the DM candidate χ to calculate the DM relic density for the case of type I and type II THDM. We have constrained the model parameter space by PLANCK relic density criterion for dark matter, bounds on the SM Higgs signal strength obtained from LHC experiments (CMS and ATLAS) and latest direct detection limits on DM-nucleon scattering cross-section from XENON100 and LUX results. Since both the models (type I and type II THDM) involve an extra Higgs boson (H), additional bounds on the signal strength of non-SM scalar due to its non-observance are also taken into account. Study of the model parameters reveals that an increase in the mass of H (m_H) will result in a decrease in the valid parameter space for both the THDM's considered. The present analysis indicates that the fermionic DM χ in THDM I and II framework (as considered in the work) can be treated as a possible dark matter candidate satisfying the bounds on DM relic density, direct detection and Higgs signal strength results from CMS and ATLAS. The present framework of THDM excludes the low mass regime explored in the work [69] when the ad-hoc assumption on the DM-Higgs coupling is relaxed. This also holds for the case of scalar or vector dark matter candidate explored in the work [69].

It is to be noted that the present model is based on an effective theory

approach of dark matter in THDM framework assuming a dimension five non-renormalisable interaction of DM candidate χ with the THDM scalar doublets. This non renormalisable interaction invokes a new physics scale Λ similar to the case of minimal fermionic dark matter model [15]. Hence, the present model is not UV complete. UV completion of this model can simply be obtained by removing the dimension five couplings within the model and introducing a singlet scalar making the theory renormalisable (as illustrated in literatures [75, 76]). However, adding a singlet scalar to the THDM will change the scalar potential of the model. This new model of THDM with scalar singlet and fermionic dark matter will provide three Higgs like particles and also an extra resonance region apart from the THDM scalar resonances for the DM candidate. Direct detection of DM candidate in this model will also include all three Higgs like states and will be modified accordingly. Integrating out the newly introduced scalar field is inconvenient as the information about the scalar resonance region will be lost and direct detection results of DM-nucleon scattering will change. Hence the study of fermionic dark matter in THDM with additional singlet scalar will lead to a different Higgs and DM phenomenology compared to the present framework (fermionic DM in THDM) is not considered in this work. Detailed study of the model (THDM with singlet scalar and fermionic dark matter) is interesting and may provide other perspectives of DM phenomenology.

Chapter 5

Singlet scalar extension of inert doublet model (IDM) part-I

5.1 Introduction

Existence of a newly found Higgs-like scalar boson of mass about 125 GeV has been reported by recent LHC results. ATLAS [64] and CMS [63] independently confirmed the discovery of a new scalar and measured signal strengths of the Higgs-like scalar to various decay channels separately. ATLAS has reported a Higgs to di-photon signal strength ($R_{\gamma\gamma}$) of about $1.57^{+0.33}_{-0.29}$ at 95% C.L. [84]. On the other hand best fit value of Higgs to di-photon signal strength reported by CMS [85] experiment is $\sim 0.78^{+0.28}_{-0.26}$ for 125 GeV Higgs boson. Despite the success of Standard Model (SM) of particle physics, it fails to produce a plausible explanation of dark matter (DM) in modern cosmology. Existence of dark matter is now established by the observations such as rotation curves of spiral galaxies, gravitational lensing, analysis of cosmic microwave background (CMB) etc. Besides, particle constituent of dark

matter is still unknown and SM of particle physics appears inadequate to address the issues regarding dark matter. Among various extensions of SM, another simple model is to introduce an additional SU(2) scalar doublet which produces no VEV. The resulting model namely inert doublet model (IDM) provides a viable explanation for DM. Stability of this inert doublet is ensured by a discrete Z_2 symmetry and the lightest inert particle (can also be labeled as LIP, i.e., the lightest particle of the inert Higgs doublet) in this model can be assumed to be a plausible DM candidate. Phenomenology of IDM has been elaborately studied in literatures such as [86]-[96]. In this chapter, we propose an extension of inert doublet model (IDM) with an additional singlet scalar field S . We impose a discrete Z_2 symmetry, under which all SM particles and the singlet scalar S are even while the inert doublet is odd. This ensures the stability of the LIP (H_0) of the inert doublet to remain stable and serve as a viable dark matter candidate. Additional scalar singlet having a non zero VEV mixes with the SM Higgs, provides two CP even Higgs states. We consider one of the scalars, h_1 , to be the SM-like Higgs. Then h_1 should be compatible with SM Higgs and one can compare the relevant calculations for h_1 with that obtained in LHC experiment. The phenomenology of dark matter is explored in the context of this model. We also calculate the signal strength $R_{\gamma\gamma}$ for $h_1 \rightarrow \gamma\gamma$ channel in the present framework and compare them with the experimentally obtained limits for this quantity from CMS and ATLAS experiments which further constrain the model parameter space.

5.2 The Model

5.2.1 Scalar Sector

In our model we add an additional SU(2) scalar doublet and a real scalar singlet S to the SM of particle physics. Similar to the widely studied inert doublet model or IDM where the added SU(2) scalar doublet to the SM Lagrangian is made “inert” (by imposing a Z_2 symmetry that ensures no interaction with SM fermions and the inert doublet does not generate any VEV), here too the extra doublet is assumed to be odd under a discrete Z_2 symmetry. Under this Z_2 symmetry however, all SM particles as also the added singlet S remain unchanged. The potential is expressed as

$$\begin{aligned}
V = & m_{11}^2 \Phi_1^\dagger \Phi_1 + m_{22}^2 \Phi_2^\dagger \Phi_2 + \frac{1}{2} m_s^2 S^2 + \lambda_1 (\Phi_1^\dagger \Phi_1)^2 + \lambda_2 (\Phi_2^\dagger \Phi_2)^2 + \lambda_3 (\Phi_1^\dagger \Phi_1) (\Phi_2^\dagger \Phi_2) \\
& + \lambda_4 (\Phi_2^\dagger \Phi_1) (\Phi_1^\dagger \Phi_2) + \frac{1}{2} \lambda_5 [(\Phi_2^\dagger \Phi_1)^2 + (\Phi_1^\dagger \Phi_2)^2] + \rho_1 (\Phi_1^\dagger \Phi_1) S + \rho'_1 (\Phi_2^\dagger \Phi_2) S \\
& + \rho_2 S^2 (\Phi_1^\dagger \Phi_1) + \rho'_2 S^2 (\Phi_2^\dagger \Phi_2) + \frac{1}{3} \rho_3 S^3 + \frac{1}{4} \rho_4 S^4, \tag{5.1}
\end{aligned}$$

where $m_k (k = 11, 22, s)$ etc. and all the coupling parameters ($\lambda_i, \rho_i, \rho'_i, i = 1, 2, 3, \dots$ etc.) are assumed to be real. In Eq. 5.1, Φ_1 is the ordinary SM Higgs doublet and Φ_2 is the inert Higgs doublet. After spontaneous symmetry breaking Φ_1 and S acquires VEV and expressed as

$$\Phi_1 = \begin{pmatrix} 0 \\ \frac{1}{\sqrt{2}}(v+h) \end{pmatrix}, \quad \Phi_2 = \begin{pmatrix} H^+ \\ \frac{1}{\sqrt{2}}(H_0 + iA_0) \end{pmatrix}, \quad S = v_s + s. \tag{5.2}$$

In the above v_s denotes the VEV of the field S and s is the real singlet scalar. Relation among model parameters can be obtained from the extremum conditions of

the potential expressed in Eq. 5.1 and are given as

$$\begin{aligned} m_{11}^2 + \lambda_1 v^2 + \rho_1 v_s + \rho_2 v_s^2 &= 0, \\ m_s^2 + \rho_3 v_s + \rho_4 v_s^2 + \frac{\rho_1 v^2}{2v_s} + \rho_2 v^2 &= 0. \end{aligned}$$

Mass terms of various scalar particles as derived from the potential are

$$\begin{aligned} \mu_h^2 &= 2\lambda_1 v^2 \\ \mu_s^2 &= \rho_3 v_s + 2\rho_4 v_s^2 - \frac{\rho_1 v^2}{2v_s} \\ \mu_{hs}^2 &= (\rho_1 + 2\rho_2 v_s)v \\ m_{H^\pm}^2 &= m_{22}^2 + \lambda_3 \frac{v^2}{2} + \rho'_1 v_s + \rho'_2 v_s^2 \\ m_{H_0}^2 &= m_{22}^2 + (\lambda_3 + \lambda_4 + \lambda_5) \frac{v^2}{2} + \rho'_1 v_s + \rho'_2 v_s^2 \\ m_{A_0}^2 &= m_{22}^2 + (\lambda_3 + \lambda_4 - \lambda_5) \frac{v^2}{2} + \rho'_1 v_s + \rho'_2 v_s^2. \end{aligned} \quad (5.3)$$

The mass eigenstates h_1 and h_2 are linear combinations of h and s and can be written as

$$\begin{aligned} h_1 &= h \cos \alpha - s \sin \alpha, \\ h_2 &= h \sin \alpha + s \cos \alpha, \end{aligned} \quad (5.4)$$

α being the mixing angle between h_1 and h_2 , is given by

$$\tan \alpha \equiv \frac{x}{1 + \sqrt{1 + x^2}}, \quad (5.5)$$

where $x = \frac{2\mu_{hs}^2}{(\mu_h^2 - \mu_s^2)}$. Masses of the physical neutral scalars h_1 and h_2 are

$$m_{1,2}^2 = \frac{\mu_h^2 + \mu_s^2}{2} \pm \frac{\mu_h^2 - \mu_s^2}{2} \sqrt{1 + x^2}. \quad (5.6)$$

We consider h_1 with mass $m_1 = 125$ GeV as the SM-like Higgs boson and the mass of the other scalar h_2 in the model is denoted as m_2 with $m_2 > m_1$. Couplings of the physical scalars h_1 and h_2 with SM particles are modified by the factors $\cos\alpha$ and $\sin\alpha$ respectively. To ensure that h_1 is the SM-like Higgs, we constrain the mixing angle by imposing the condition $0 \leq \alpha \leq \pi/4$ [97]. The coupling λ_5 serves as a mass splitting factor between H_0 and A_0 . We consider H_0 to be the lightest inert particle (LIP) which is stable and is the DM candidate in this work. We take $\lambda_5 < 0$ in order to make H_0 to be the lightest stable inert particle. It is to be noted that for very small mixing, i.e., in the decoupling limit, the present model will be exactly identical to IDM providing a low mass DM ($m_{H_0} \leq 80$ GeV) and a high mass DM candidate ($m_{H_0} \geq 500$ GeV). In the present framework, both the scalars h_1 and h_2 couple with the lightest inert particle H_0 . Couplings of the scalar bosons (h_1 and h_2) with the inert dark matter H_0 are given by

$$\begin{aligned}\lambda_{h_1 H_0 H_0} v &= \left(\frac{\lambda_{345}}{2} c_\alpha - \frac{\lambda_s}{2} s_\alpha \right) v, \\ \lambda_{h_2 H_0 H_0} v &= \left(\frac{\lambda_{345}}{2} s_\alpha + \frac{\lambda_s}{2} c_\alpha \right) v\end{aligned}\tag{5.7}$$

where $\lambda_{345} = \lambda_3 + \lambda_4 + \lambda_5$, $\lambda_s = \frac{\rho'_1 + 2\rho'_2 v_s}{v}$ and $s_\alpha(c_\alpha)$ denotes $\sin\alpha(\cos\alpha)$. Couplings of scalar bosons with charged scalars H^\pm are

$$\begin{aligned}\lambda_{h_1 H^+ H^-} v &= (\lambda_3 c_\alpha - \lambda_s s_\alpha) v, \\ \lambda_{h_2 H^+ H^-} v &= (\lambda_3 s_\alpha + \lambda_s c_\alpha) v.\end{aligned}\tag{5.8}$$

5.2.2 Constraints

The model parameters are bounded by theoretical and experimental constraints.

- **Vacuum Stability** - Vacuum stability constraints requires the potential to remain bounded from below. Conditions for the stability of the vacuum are [98]

$$\begin{aligned}
 \lambda_1, \lambda_2, \rho_4 > 0, \quad \lambda_3 + 2\sqrt{\lambda_1\lambda_2} > 0, \quad \lambda_3 + \lambda_4 - |\lambda_5| + 2\sqrt{\lambda_1\lambda_2} > 0, \\
 \rho_2 + \sqrt{\lambda_1\rho_4} > 0, \quad \rho'_2 + \sqrt{\lambda_2\rho_4} > 0, \\
 \frac{2\rho_2\sqrt{\lambda_2} + 2\rho'_2\sqrt{\lambda_1} + \lambda_3\sqrt{\rho_4}}{+2\left(\sqrt{\lambda_1\lambda_2\rho_4} + \sqrt{\left(\lambda_3 + 2\sqrt{\lambda_1\lambda_2}\right)\left(\rho_2 + \sqrt{\lambda_1\rho_4}\right)\left(\rho'_2 + \sqrt{\lambda_2\rho_4}\right)}\right)} > 0, \\
 \frac{2\rho_2\sqrt{\lambda_2} + 2\rho'_2\sqrt{\lambda_1} + (\lambda_3 + \lambda_4 - \lambda_5)\sqrt{\rho_4}}{+2\left(\sqrt{\lambda_1\lambda_2\rho_4} + \sqrt{\left(\lambda_3 + \lambda_4 - \lambda_5 + 2\sqrt{\lambda_1\lambda_2}\right)\left(\rho_2 + \sqrt{\lambda_1\rho_4}\right)\left(\rho'_2 + \sqrt{\lambda_2\rho_4}\right)}\right)} > 0.
 \end{aligned} \tag{5.9}$$

- **Pertubativity** - For a theory to be acceptable in perturbative limits, we have to constrain high energy quartic interactions at tree level. The eigenvalues $|\Lambda_i|$ of quartic couplings (scattering) matrix must be smaller than 4π .

- **LEP** - LEP[99] results constrains the Z boson decay width and masses of scalar particles

$$\begin{aligned}
 m_{H_0} + m_{A_0} > m_Z, \\
 m_{H^\pm} > 79.3 \text{ GeV}.
 \end{aligned} \tag{5.10}$$

- **Relic Density** - Parameter space is also constrained by the experimental measurement of relic density (WMAP, PLANCK etc.)of dark matter candidate. Relic density of the lightest inert particle (LIP) serving as a viable candidate

for dark matter in the present model must satisfy PLANCK results [3],

$$\Omega_{\text{DM}}h^2 = 0.1199 \pm 0.0027 . \quad (5.11)$$

- **Higgs to Diphoton Rate $R_{\gamma\gamma}$** - Bound on Higgs to two photon channel has been obtained from experiments performed by LHC. The measured signal strength for the Higgs to diphoton channel obtained from ATLAS at 95% C.L. is

$$R_{\gamma\gamma}|_{\text{ATLAS}} = 1.57^{+0.33}_{-0.29} ,$$

whereas the best fit value of $R_{\gamma\gamma}$ for a 125 GeV Higgs with 3.2σ excess in local significance corresponding to an expected value of 4.2σ measured by CMS is

$$R_{\gamma\gamma}|_{\text{CMS}} = 0.78^{+0.28}_{-0.26} .$$

- **Direct Detection Experiments** - The bounds on dark matter from direct detection experiments are based on the elastic scattering of the dark matter particle off a scattering nucleus. Dark matter direct detection experiments set constraints on the dark matter - nucleus (nucleon) elastic scattering cross-section. Limits on scattering cross-sections for different dark matter mass cause further restrictions on the model parameters. Experiments like CDMS, DAMA, CoGeNT, CRESST etc. provide effective bounds on low mass dark matter. Stringent bounds on middle mass and high mass dark matter are obtained from XENON100 and LUX experiments.

5.3 Dark matter

5.3.1 Relic density

Relic density of dark matter is constrained by the results of PLANCK and WMAP. Dark matter relic abundance for the model is evaluated by solving the evolution of Boltzmann equation given as [26]

$$\frac{dn_{H_0}}{dt} + 3Hn_{H_0} = -\langle\sigma v\rangle(n_{H_0}^2 - n_{H_0\text{eq}}^2). \quad (5.12)$$

In Eq. 5.12, $n_{H_0}(n_{H_0\text{eq}})$ denotes the number density (equilibrium number density) of dark matter H_0 and H is the Hubble constant. In Eq. 5.12, $\langle\sigma v\rangle$ denotes the thermal averaged annihilation cross-section of dark matter particle to SM species. We solve for the dark matter relic density by using Eq. 4.17 given in Chapter 4. The freeze out temperature T_F for the dark matter candidate is obtained from the iterative solution to the Eq. 4.18.

5.3.2 Annihilation cross section

Annihilation of inert dark matter H_0 to SM particles is governed by processes involving scalar (h_1, h_2) mediated s($\simeq 4m_{H_0}^2$) channels. Thermal averaged annihilation cross-section $\langle\sigma v\rangle$ of dark matter H_0 to SM fermions are given as

$$\langle\sigma v_{H_0 H_0 \rightarrow f \bar{f}}\rangle = n_c \frac{m_f^2}{\pi} \beta_f^3 \left| \frac{\lambda_{h_1 H_0 H_0} \cos \alpha}{4m_{H_0}^2 - m_1^2 + i\Gamma_1 m_1} + \frac{\lambda_{h_2 H_0 H_0} \sin \alpha}{4m_{H_0}^2 - m_2^2 + i\Gamma_2 m_2} \right|^2. \quad (5.13)$$

In the above, m_x represents mass of the particle $x(\equiv f, H_0$ etc.), n_c is the colour quantum number (3 for quarks and 1 for leptons) with $\beta_a = \sqrt{1 - \frac{m_a^2}{m_{H_0}^2}}$ and $\Gamma_i (i = 1, 2)$ denotes the total decay width of each of the two scalars h_1 and h_2 . For DM mass

$m_{H_0} > (m_W, m_Z)$, annihilation of DM to gauge boson (W or Z) channels will yield high annihilation cross-section. Since $\Omega_{\text{DM}} \sim \langle \sigma v \rangle^{-1}$ (Eq. 4.17), the relic density for the dark matter with mass $m_{H_0} > m_W$ or m_Z in the present model in fact falls below the relic density given by WMAP or PLANCK as the four point interaction channel $H_0 H_0 \rightarrow W^+ W^-$ or ZZ will be accessible and as a result increase in total annihilation cross-section will be observed. Thus the possibility of a single component DM in the present framework is excluded for mass $m_{H_0} > m_W, m_Z$ ¹. Invisible decay of $h_i (i = 1, 2)$ depends on DM mass m_{H_0} and is kinematically forbidden for $m_{H_0} > m_i/2 (i = 1, 2)$. Contributions of invisible decay widths for h_1 and h_2 are taken into account when the condition $m_{H_0} < m_i/2 (i = 1, 2)$ is satisfied. Invisible decay width is represented by the relation

$$\Gamma_i^{\text{inv}}(h_i \rightarrow 2H_0) = \frac{\lambda_{h_i H_0 H_0}^2 v^2}{16\pi m_i} \sqrt{1 - \frac{4m_{H_0}^2}{m_i^2}}. \quad (5.14)$$

5.3.3 Modification of $R_{\gamma\gamma}$ and $R_{\gamma Z}$

Recent studies of IDM [101, 102, 103] and two Higgs doublet models [104, 105] have reported that a low mass charged scalar could possibly enhance the $h_1 \rightarrow \gamma\gamma$ signal strength $R_{\gamma\gamma}$. Correlation of $R_{\gamma\gamma}$ with $R_{\gamma Z}$ is also accounted for as well [102, 105]. The quantities $R_{\gamma\gamma}$ and $R_{\gamma Z}$ are expressed as

$$R_{\gamma\gamma} = \frac{\sigma(pp \rightarrow h_1)}{\sigma(pp \rightarrow h)^{\text{SM}}} \frac{Br(h_1 \rightarrow \gamma\gamma)}{Br(h \rightarrow \gamma\gamma)^{\text{SM}}} \quad (5.15)$$

$$R_{\gamma Z} = \frac{\sigma(pp \rightarrow h_1)}{\sigma(pp \rightarrow h)^{\text{SM}}} \frac{Br(h_1 \rightarrow \gamma Z)}{Br(h \rightarrow \gamma Z)^{\text{SM}}}, \quad (5.16)$$

¹Similar results for IDM are also obtained in previous work (Ref. [100]) where a two component dark matter was considered in order to circumvent this problem.

where σ is the Higgs production cross-section and Br represents the branching ratio of Higgs to final states. Branching ratio to any final state is given by the ratio of partial decay width for the particular channel to the total decay width of decaying particle. For IDM with additional singlet scalar, the ratio $\frac{\sigma(pp \rightarrow h_1)}{\sigma(pp \rightarrow h)^{\text{SM}}}$ in Eqs. 5.15-5.16 is represented by a factor $\cos^2 \alpha$. Standard Model branching ratios $Br(h \rightarrow \gamma\gamma)^{\text{SM}}$ and $Br(h \rightarrow \gamma Z)^{\text{SM}}$ for a 125 GeV Higgs boson is 2.28×10^{-3} and 1.54×10^{-3} respectively [82]. To evaluate the branching ratios $Br(h_1 \rightarrow \gamma\gamma)$ and $Br(h_1 \rightarrow \gamma Z)$, we compute the total decay width of h_1 . Invisible decay of h_1 to dark matter particle H_0 is also taken into account and evaluated using Eq. 5.14 when the condition $m_{H_0} < m_1/2$ is satisfied. Partial decay widths $\Gamma(h_1 \rightarrow \gamma\gamma)$ and $\Gamma(h_1 \rightarrow \gamma Z)$ according to the model are given as

$$\begin{aligned} \Gamma(h_1 \rightarrow \gamma\gamma) &= \frac{G_F \alpha_s^2 m_1^3}{128 \sqrt{2} \pi^3} \left| c_\alpha \left(\frac{4}{3} F_{1/2} \left(\frac{4m_t^2}{m_1^2} \right) + F_1 \left(\frac{4m_W^2}{m_1^2} \right) \right) + \frac{\lambda_{h_1 H^+ H^-} v^2}{2m_{H^\pm}^2} F_0 \left(\frac{4m_{H^\pm}^2}{m_1^2} \right) \right|^2, \\ \Gamma(h_1 \rightarrow \gamma Z) &= \frac{G_F^2 \alpha_s}{64 \pi^4} m_W^2 m_1^3 \left(1 - \frac{m_Z^2}{m_1^2} \right)^3 \left| -2c_\alpha \frac{1 - \frac{8}{3} s_W^2}{c_W} F'_{1/2} \left(\frac{4m_t^2}{m_1^2}, \frac{4m_t^2}{m_1^2} \right) \right. \\ &\quad \left. - c_\alpha F'_1 \left(\frac{4m_W^2}{m_1^2}, \frac{4m_W^2}{m_1^2} \right) + \frac{\lambda_{h_1 H^+ H^-} v^2 (1 - 2s_W^2)}{2m_{H^\pm}^2 c_W} I_1 \left(\frac{4m_{H^\pm}^2}{m_1^2}, \frac{4m_{H^\pm}^2}{m_1^2} \right) \right|^2, \end{aligned} \quad (5.17)$$

where G_F is the Fermi constant, m_x denotes the mass of particle x ($x \equiv 1, W, Z, t, H^\pm$) etc. and $s_W(c_W)$ represents $\sin \theta_W$ ($\cos \theta_W$), θ_W being the weak mixing angle. Expressions for various loop factors ($F_{1/2}$, F_1 , F_0 , $F'_{1/2}$, F'_1 and I_1) appeared in Eq. 5.17 are given in Appendix A. It is to be noted that a similar derivation of decay widths and signal strengths ($R'_{\gamma\gamma}$ or $R'_{\gamma Z}$) for the other scalar h_2 can be obtained by replacing m_1 , $\cos \alpha$, $\lambda_{h_1 H^+ H^-}$ with m_2 , $\sin \alpha$, $\lambda_{h_2 H^+ H^-}$ respectively and this is addressed in Sec. 5.5.

5.4 Analysis of $R_{\gamma\gamma}$ and $R_{\gamma Z}$

In this section we compute the quantities $R_{\gamma\gamma}$ and $R_{\gamma Z}$ in the framework of the present model. We restrict the allowed model parameter space for our analysis using the vacuum stability, perturbative unitarity, LEP bounds along with the relic density constraints described in Section 5.2.2. Dark matter relic density is evaluated by solving the Boltzmann equation presented in Section 5.3.1 with the expression for annihilation cross-section given in Eq. 5.13. Model parameters (λ_i, ρ_i) , should remain small in order to satisfy perturbative bounds and relic density constraints. Calculations are made for the model parameter limits given below,

$$\begin{aligned}
m_1 &= 125 \text{ GeV} , \\
80 \text{ GeV} &\leq m_{H^\pm} \leq 400 \text{ GeV} , \\
0 &< m_{H_0} < m_{H^\pm}, m_{A_0} , \\
0 &< \alpha < \pi/4 , \\
-1 &\leq \lambda_3 \leq 1 , \\
-1 &\leq \lambda_{345} \leq 1 , \\
-1 &\leq \lambda_s \leq 1 .
\end{aligned} \tag{5.18}$$

The enhancement of Higgs to di-photon signal depends on the contribution from the charged scalar loop (Eq. 5.17). Since for higher value of charged scalar mass (m_{H^\pm}), the contribution from charged scalar loop will reduce, we expect mass of the charged scalar to be small. Due to this reason, we kept charged scalar mass to be less than 400 GeV. As mentioned earlier, due to large DM annihilation cross-section to W or Z boson channel, high mass DM in the present scenario will fail to satisfy DM relic abundance unless we assume a TeV scale dark matter [106]. Hence, for the range considered for charged scalar mass, we explore the low mass region only where

enhancement is significant. The couplings $\lambda_{h_1 H_0 H_0}$ and $\lambda_{h_2 H_0 H_0}$ (Eq. 5.7) are required to calculate the scattering cross-section of the dark matter off a target nucleon. Dark matter direct detection experiments are based on these scattering processes whereby the recoil energy of the scattered nucleon is measured. Thus the couplings $\lambda_{h_1 H_0 H_0}$ and $\lambda_{h_2 H_0 H_0}$ can be constrained by comparing the computed values of the scattering cross-section for different dark matter masses with those given by different dark matter direct detection experiments. In the present work, $|\lambda_{h_1 H_0 H_0}, \lambda_{h_2 H_0 H_0}| \leq 1$ is adopted. The following bounds on parameters will also constrain the couplings $\lambda_{h_1 H^+ H^-}$ and $\lambda_{h_2 H^+ H^-}$ (Eq. 5.8). Using Eqs. 5.13-5.14 we solve for the Boltzmann equation for dark matter given in Section 5.3.1 scanning over the parameter space mentioned in Eq. 5.18 also imposing the conditions $|\lambda_{h_1 H^+ H^-}, \lambda_{h_2 H^+ H^-}| \leq 2$ to calculate $R_{\gamma\gamma}, R_{\gamma Z}$ in the present model. Comparing the experimentally observed dark matter relic density with the calculated value restricts the allowed model parameter space and gives the range of mass that satisfies observed DM relic density. We have made our calculations for two different values of singlet scalar (h_2) mass namely $m_2 = 150$ and 300 GeV. Scanning of the full parameter space yields that for all the cases considered, the limits $|\lambda_{h_1 H_0 H_0}, \lambda_{h_2 H_0 H_0}| \leq 0.7$ are required for satisfying observed DM relic abundance. Our calculation reveals that $|\lambda_{h_1 H^+ H^-}, \lambda_{h_2 H^+ H^-}| \leq 1.5$ are needed in order to satisfy observed relic density of dark matter. Using the allowed parameter space thus obtained, we calculate the signal strengths $R_{\gamma\gamma}$ and $R_{\gamma Z}$ (Eqs. 5.15-5.16) by evaluating the corresponding decay widths given in Eq. 5.17.

In Fig. 5.1(a-b), shown are the regions in the $R_{\gamma\gamma} - m_{H_0}$ plane for the parameter values that satisfy DM relic abundance. As mentioned earlier, results are presented for two values of h_2 mass namely 150 GeV and 300 GeV. Since for low mass DM region, invisible decay channel of h_1 to DM pair remains open, enhancement of $R_{\gamma\gamma}$ is not possible in this regime. $R_{\gamma\gamma}$ becomes greater than unity near the region of resonance where $m_{H_0} \approx m_2/2$ for $m_2 = 150$ GeV. Resonant enhancement is more pronounced for

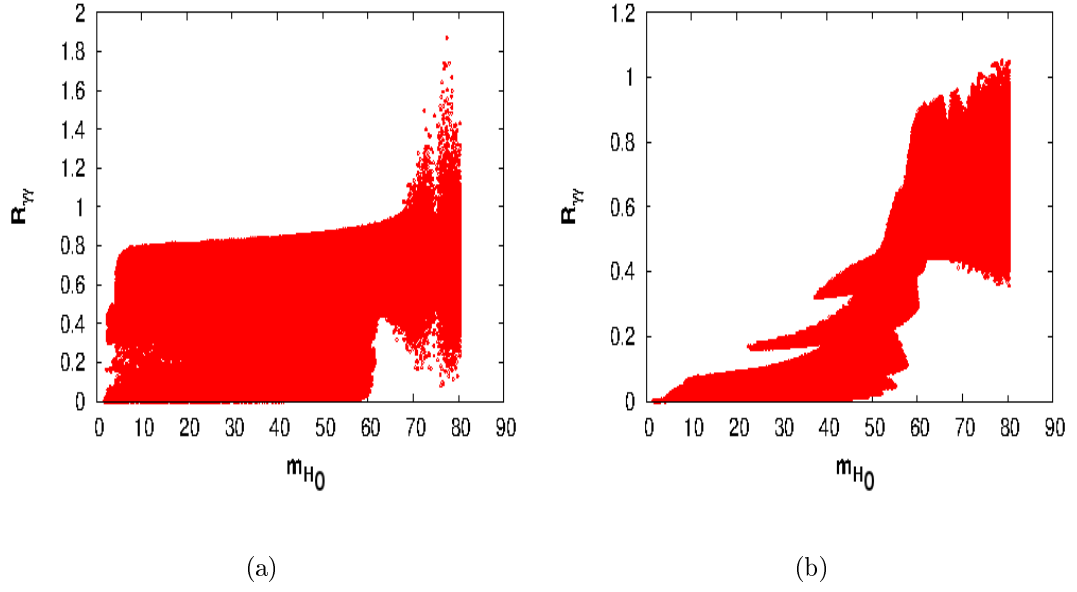


Figure 5.1: Variation of $R_{\gamma\gamma}$ with DM mass m_{H_0} satisfying DM relic density for $m_2 = 150$ and 300 GeV.

lighter values of m_{H^\pm} mass. However, no such resonant enhancement is obtained for $m_2 = 300$ GeV but a small enhancement occurs near $m_{H_0} \simeq 80$ GeV for light charged scalar ($m_{H^\pm} \leq 100$ GeV). The region that describes the $R_{\gamma\gamma}$ enhancement is reduced with increasing h_2 mass and thus enhancement is not favoured for higher values of h_2 mass. For the rest of the allowed DM mass parameter space, $R_{\gamma\gamma}$ remains less than 1 and decreases with higher values of h_2 mass. The results presented in Fig. 5.1 indicate that observed enhancement of the $h_1 \rightarrow \gamma\gamma$ signal could be a possible indication of the presence of h_2 since $R_{\gamma\gamma} \gtrsim 1$ occurs near the resonance of h_2 which contributes to the total annihilation cross section measured using Eq. 5.13. The $R_{\gamma\gamma}$ value depends on the coupling $\lambda_{h_1 H^+ H^-}$ and becomes greater than unity only for $\lambda_{h_1 H^+ H^-} < 0$ and interferes constructively with the other loop contributions. Technically, $R_{\gamma\gamma}$ depends on the values of h_2 mass, charged scalar mass m_{H^\pm} , coupling $\lambda_{h_1 H^+ H^-}$ and the decay width of invisible decay channel $\Gamma_{inv}(h_1 \rightarrow H_0 H_0)$. A similar variation for the $h_1 \rightarrow \gamma Z$ channel (computed using Eqs. 5.16-5.17 and Eq. 5.18) yields lesser

enhancement for $R_{\gamma Z}$ in comparison with $R_{\gamma\gamma}$. This phenomenon can also be verified from the correlation between $R_{\gamma\gamma}$ and $R_{\gamma Z}$. The correlation between the signals $R_{\gamma\gamma}$

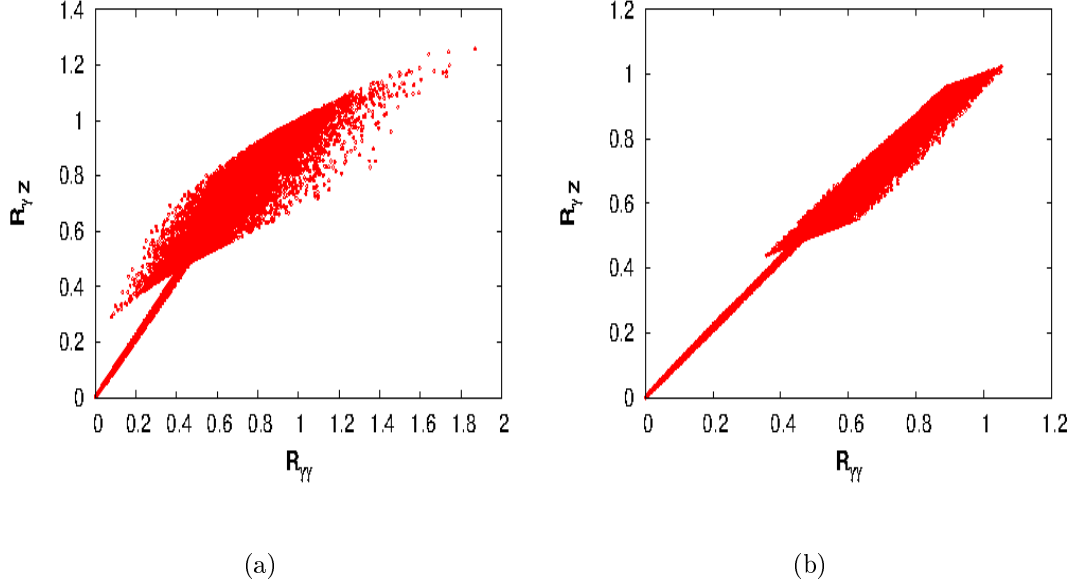


Figure 5.2: Correlation plots between $R_{\gamma\gamma}$ and $R_{\gamma Z}$ for two choices of h_2 mass (150 and 300 GeV).

and $R_{\gamma Z}$ is shown in Fig. 5.2a - Fig. 5.2b for $m_2 = 150, 300$ GeV respectively. Variations of $R_{\gamma\gamma}$ and $R_{\gamma Z}$ satisfy all necessary parameter constraints taken into account inclusive of the relic requirements for DM. Fig. 5.2 also indicates that, with increase in the mass (m_2) of h_2 , enhancement of $R_{\gamma\gamma}$ and $R_{\gamma Z}$ are likely to reduce. For $m_2 = 150$ GeV, $R_{\gamma\gamma}$ enhances up to two times whereas $R_{\gamma Z}$ increases nearly by a factor 1.2 with respect to corresponding values predicted by SM. On the other hand, for $m_2 = 300$ GeV, $R_{\gamma\gamma}$ varies linearly with $R_{\gamma Z}$ ($R_{\gamma\gamma} \simeq R_{\gamma Z}$) without any significant enhancement. For low mass dark matter ($m_{H_0} \lesssim m_1/2$), invisible decay channel of h_1 remains open and the processes $h_1 \rightarrow \gamma\gamma$ and $h_1 \rightarrow \gamma Z$ suffer considerable suppressions. These result in the correlation between the channels $h_1 \rightarrow \gamma\gamma$ and $h_1 \rightarrow \gamma Z$ appear to become stronger and $R_{\gamma\gamma}$ vs $R_{\gamma Z}$ plot shows more linearity with increase in h_2 mass. For larger h_2 masses, the corresponding charged scalar (H^\pm)

masses for which $R_{\gamma\gamma,\gamma Z} > 1$, tends to increase. Since any increase in H^\pm mass will affect the contribution from charged scalar loop, the decay widths $\Gamma(h_1 \rightarrow \gamma\gamma, \gamma Z)$ or signal strengths $R_{\gamma\gamma,\gamma Z}$ are likely to reduce. Our numerical results exhibit a positive correlation between the signal strengths $R_{\gamma\gamma}$ and $R_{\gamma Z}$. This is an important feature of the model. Since signal strengths tend to increase with relatively smaller values of m_2 , possibility of having a light singlet like scalar is not excluded. The coupling of h_2 with SM sector is suppressed by a factor $\sin \alpha$ which results in a decrease in the signal strengths from h_2 and makes their observations difficult.

5.5 Direct Detection

In this section we further investigate whether the allowed model parameter space (and enhancement of $R_{\gamma\gamma,\gamma Z}$) is consistent with dark matter direct search experiments. Within the framework of our model and allowed values of parameter region obtained in Sec. 5.4, we calculate spin independent (SI) elastic scattering cross-section for the dark matter candidate in our model off a nucleon in the detector material. We then compare our results with those given by various direct detection experiments and examine the plausibility of our model in explaining the direct detection experimental results. The DM candidate in the present model, interacts with SM via processes led by Higgs exchange. The spin-independent elastic scattering cross-section σ_{SI} is of the form

$$\sigma_{\text{SI}} \simeq \frac{m_r^2}{\pi} \left(\frac{m_N}{m_{H_0}} \right)^2 f^2 \left(\frac{\lambda_{h_1 H_0 H_0} \cos \alpha}{m_1^2} + \frac{\lambda_{h_2 H_0 H_0} \sin \alpha}{m_2^2} \right)^2, \quad (5.19)$$

where m_N and m_{H_0} are the masses of scattered nucleon and DM respectively, f represents the scattering factor that depends on pion-nucleon cross-section and quarks involved in the process and $m_r = \frac{m_N m_{H_0}}{m_N + m_{H_0}}$ is the reduced mass. In the present

framework $f = 0.3$ [14] is considered. The computations of σ_{SI} for the dark matter candidate in the present model are carried out with those values of the couplings restricted by the experimental value of relic density. In Fig. 5.3(a,b), we present the

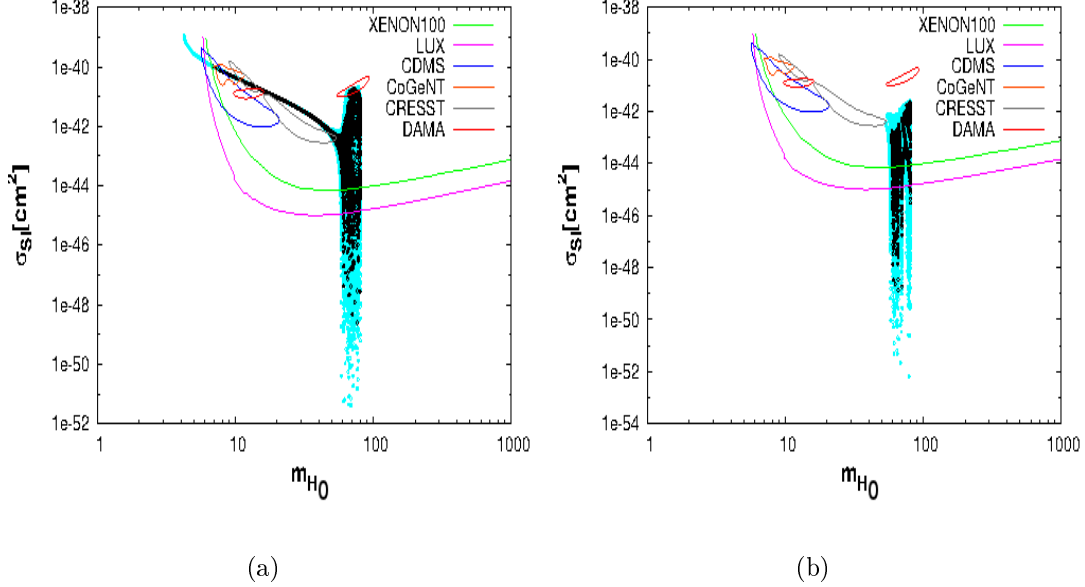


Figure 5.3: Allowed regions in $m_{H_0} - \sigma_{SI}$ plane for $m_2 = 150$ and 300 GeV.

variation of elastic scattering cross-section calculated using Eq. 5.19, with LIP dark matter mass (m_{H_0}) for two values of h_2 masses $m_2 = 150$ and 300 GeV satisfying the CMS limit of $R_{\gamma\gamma}$. We assume h_1 to be SM-like Higgs and restrict the mixing angle α such that the condition $\cos \alpha \gtrsim 1/\sqrt{2}$ is satisfied. In each of the $\sigma_{SI} - m_{H_0}$ plots of Fig. 5.3(a-b) the light blue region satisfies CMS limit of $R_{\gamma\gamma}$ for two chosen values of m_2 . Also marked in black are the specific zones that correspond to the central value of $R_{\gamma\gamma}|_{\text{CMS}} = 0.78$. The bounds on σ_{SI} – DM mass obtained from DM direct search experiments such as XENON100, LUX, CDMS, CoGeNT, CRESST are shown in Fig. 5.3(a-b), superimposed on the computed results for comparison. From Fig. 5.3(a-b) one notes that for the case of $m_2 = 150$ GeV, the DM candidate in our model partly satisfies bounds obtained from low mass dark matter direct detection experiments like CoGeNT, CDMS, CRESST, DAMA but are disfavoured for $m_2 = 300$ GeV. It is

therefore evident from Fig. 5.3(a-b) that imposition of signal strength ($R_{\gamma\gamma}$) results obtained from LHC, further constraints the allowed scattering cross-section limits obtained from direct detection experimental results for the DM candidate in our model. Investigating the region allowed by LUX and XENON100 experiments along with other direct dark matter experiments such as CDMS etc., it is evident from Fig. 5.3(a-b) that our model suggests a DM candidate within the range $m_{H_0} = 60 - 80$ GeV with scattering cross-section values $\sim 10^{-45} - 10^{-49}$ cm² with $m_1 = 125$ GeV, which is an SM-like scalar. There are however few negligibly small allowed parameter space with σ_{SI} below $\sim 10^{-49}$ cm². Hence, in the present model H_0 can serve as a potential dark matter candidate and future experiments with higher sensitivity like XENON1T [107], SuperCDMS [30] etc. are expected to constrain or rule out the viability of this model. Similar procedure has been adopted for restricting the $\sigma_{\text{SI}} - m_{H_0}$ space using $R_{\gamma\gamma}$ limits from ATLAS experiment. We found that the region of DM parameter space for the case of Higgs to di-photon signal strength predicted by ATLAS with 95% C.L. is completely ruled out as the allowed DM mass region in the model (for both $m_2 = 150$ and 300 GeV) cannot satisfy the latest direct detection bounds from XENON100 and LUX experiments. In the present model we so far adopt

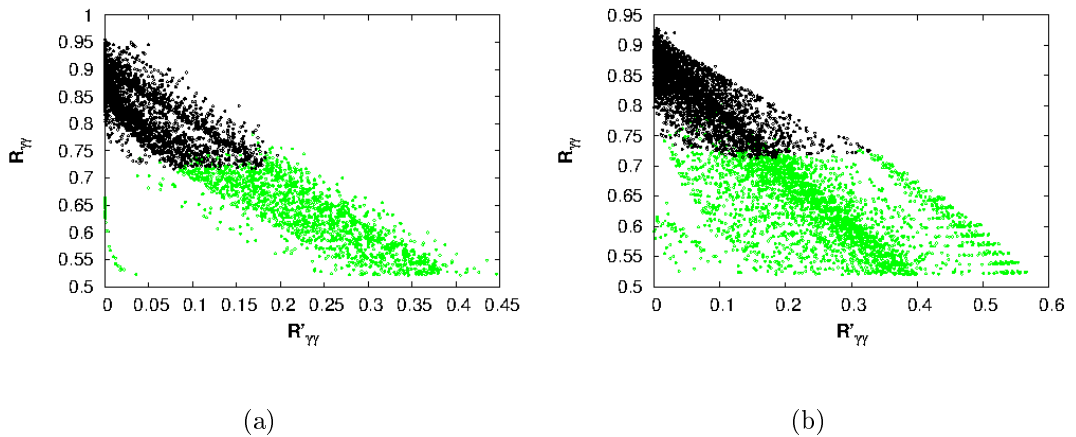


Figure 5.4: Allowed regions in $R_{\gamma\gamma} - R'_{\gamma\gamma}$ plane for $m_2 = 150$ and 300 GeV.

the consideration that h_1 plays the role of SM Higgs and hence in our discussion we consider $h_1 \rightarrow \gamma\gamma$ for constraining our parameter space. The model considered in this work also provides us with a second scalar namely h_2 . Since LHC has not yet observed a second scalar, it is likely that the other scalar h_2 is very weakly coupled to SM sector so that the corresponding branching ratios (signal strengths) are small. Also significant enhancement of the process $h_2 \rightarrow \gamma\gamma$ can occur due to the presence of charge scalar (H^\pm). Hence, in the present scenario we require $h_2 \rightarrow \gamma\gamma$ branching ratio or signal strength ($R'_{\gamma\gamma}$) to be very small compared to that for h_1 . Needless to mention that the couplings required to compute $R_{\gamma\gamma}$ and $R'_{\gamma\gamma}$ are restricted by dark matter constraints. We address these issues by computing $R'_{\gamma\gamma}$ values and comparing them with $R_{\gamma\gamma}$ ². The computations of $R_{\gamma\gamma}$ and $R'_{\gamma\gamma}$ initially involve the dark matter model parameter space that yields the dark matter relic density in agreement with PLANCK data [3] as also the stringent direct detection cross-section bound obtained from LUX [28]. $R_{\gamma\gamma}$ values thus obtained are not found to satisfy the experimental range given by ATLAS experiment. The resulting $R_{\gamma\gamma} - R'_{\gamma\gamma}$ is further restricted for those values of $R_{\gamma\gamma}$ which are within the limit of $R_{\gamma\gamma}|_{\text{CMS}}$ given by CMS experiment. The region with green scattered points in Fig. 5.4(a-b) corresponds to the $R_{\gamma\gamma} - R'_{\gamma\gamma}$ space consistent with the model parameters that are allowed by DM relic density obtained from PLANCK, direct detection experiment bound from LUX and $R_{\gamma\gamma}|_{\text{CMS}}$ for $m_2 = 150$ GeV and 300 GeV. It is to be noted that $R_{\gamma\gamma}$ is not the only constrain obtained from LHC experiments, we have to consider other decay channels of h_1 as well. In the present model, signal strengths (R_1) of h_1 to any particular decay channel (excluding $\gamma\gamma$ and γZ channel) can be expressed as

$$R_1 = c_\alpha^4 \frac{\Gamma_1^{\text{SM}}}{\Gamma_1} \quad (5.20)$$

²Since $R'_{\gamma\gamma}$ and $R'_{\gamma Z}$ are correlated, any suppression in $h_2 \rightarrow \gamma\gamma$ will be followed by similar effects in $h_2 \rightarrow \gamma Z$.

where Γ_1^{SM} represents the total SM decay width of h_1 , Γ_1 denotes the total decay width of h_1 in the present model. Since contribution of $h_1 \rightarrow \gamma\gamma$ and $h_1 \rightarrow \gamma Z$ channel to the total decay width is negligibly small, total decay width Γ_1 can be written as

$$\Gamma_1 = c_\alpha^2 \Gamma_1^{\text{SM}} + \Gamma_1^{\text{inv}} \quad (5.21)$$

where Γ_1^{inv} is the invisible decay width of h_1 as expressed in Eq. 5.14. Similarly signal strength of the singlet like scalar h_2 can be given as

$$R_2 = s_\alpha^4 \frac{\Gamma_2^{\text{SM}}}{\Gamma_2} \quad (5.22)$$

with $\Gamma_2 = s_\alpha^2 \Gamma_2^{\text{SM}} + \Gamma_2^{\text{inv}} + \Gamma_{211}$, where Γ_{211} is the decay width of singlet scalar h_2 to SM Higgs h_1 is given as

$$\Gamma_{211} = \frac{\lambda_{h_2 h_1 h_1}^2}{32\pi m_2} \sqrt{1 - \frac{4m_1^2}{m_2^2}}, \quad (5.23)$$

with

$$\begin{aligned} \lambda_{h_2 h_1 h_1} &= 3\lambda_1 v c_\alpha^2 s_\alpha + \frac{\rho_1}{2} (-2s_\alpha^2 c_\alpha + c_\alpha^3) + \rho_2 v (-2s_\alpha c_\alpha^2 + s_\alpha^3) + \rho_2 v_s (-2s_\alpha^2 c_\alpha + c_\alpha^3) \\ &+ \rho_3 s_\alpha^2 c_\alpha + 3\rho_4 v_s s_\alpha^2 c_\alpha. \end{aligned} \quad (5.24)$$

In the present work, we constraint the signal strength R_1 in order to invoke h_1 as the SM-like scalar and set $R_1 \geq 0.8$ [108]. In Fig.5.4(a,b) the region shown in black scattered points are in agreement with the condition $R_1 \geq 0.8$. We found that the signal strength R_2 for the other scalar involved remains small ($R_2 \leq 0.2$) and may also suffer appreciable reduction due to $h_2 \rightarrow H_0 H_0$ channel for $m_{H_0} < m_2/2$.

Constraints from the signal strength R_1 along with direct detection bound

m_2 (GeV)	m_{H_0} (GeV)	m_{H^\pm} (GeV)	α (deg)	$\lambda_{h_1 H_0 H_0}$	$\lambda_{h_2 H_0 H_0}$	$R_{\gamma\gamma}$	$R'_{\gamma\gamma}$	$Br(h_2 \rightarrow \gamma\gamma)$	σ_{SI} in cm^2	Br_{inv}
150.00	61.06	125.00	06	-5.5e-03	8.5e-02	0.875	3.59e-05	4.627e-06	5.890e-47	1.51e-02
	67.05	132.00	09	9.0e-03	-8.0e-02	0.874	4.62e-04	2.659e-05	3.745e-48	-
	73.07	171.00	07	-2.0e-03	5.8e-02	0.883	4.79e-04	4.541e-05	7.001e-46	-
300.0	61.72	97.00	01	-2.5e-03	-8.3e-04	0.906	2.93e-04	1.238e-05	7.245e-46	2.31e-02
	64.78	144.50	08	7.0e-03	-0.30	0.876	2.88e-02	1.917e-05	2.290e-47	-
	70.12	117.00	15	-2.0e-02	0.48	0.857	3.35e-03	6.461e-07	4.659e-46	-

Table 5.1: Benchmark points satisfying observed DM relic density obtained from PLANCK data and direct detection cross-section reported by LUX results for two different choices of h_2 mass.

predicted by LUX restricts the allowed model parameter space with $|\lambda_{h_1 H_0 H_0}| \leq 0.04$ and $|\lambda_{h_2 H_0 H_0}| \leq 0.5$ for $m_2 = 300$ GeV and couplings are even smaller for the other scenario $m_2 = 150$ GeV. Further reduction to the allowed limit of $\lambda_{h_1 H_0 H_0}$ occurs for DM mass $m_{H_0} \leq m_1/2$ satisfying the range $|\lambda_{h_1 H_0 H_0}| \leq 0.01$ which indicates that invisible decay branching ratio is small. Hence, according to the model, even if we restrict the results with the conditions $R'_{\gamma\gamma} \leq 0.1$ and $R_1 \geq 0.8$ [108] along with the DM relic density obtained from PLANCK and direct detection bounds obtained from LUX ($\sigma_{SI} \leq 10^{-45} \text{cm}^2$), the model still provides a feasible DM candidate with an appreciable range of allowed parameter space. In Table 5.1 we further demonstrate that within the framework of our proposed model for LIP dark matter, $R'_{\gamma\gamma}$ is indeed small compared to $R_{\gamma\gamma}$. We tabulate the values of both $R_{\gamma\gamma}$ and $R'_{\gamma\gamma}$ for some chosen values of LIP dark matter mass m_{H_0} fulfilling the bound obtained from signal strength $R_1 \geq 0.8$ [108]. These numerical values are obtained from the computational results consistent with LUX direct DM search bound. Also given in Table 5.1 the corresponding mixing angles α between h_1 and h_2 , couplings $\lambda_{h_i H_0 H_0}$ ($i = 1, 2$), the scalar masses m_{H^\pm} , h_2 to di-photon branching ratio, the scattering cross-section σ_{SI} and invisible branching ratio Br_{inv} of h_1 for two different values of m_2 considered in the work. It is also evident from Table 5.1 that $R_{\gamma\gamma} \gg R'_{\gamma\gamma}$ and mixing angles corresponding to respective values are small. In fact for some cases such as for

$m_{H_0} = 61.06$ GeV ($m_2 = 150$ GeV) $R_{\gamma\gamma} = 0.875$ whereas $R'_{\gamma\gamma} \sim 10^{-5}$ and α is as small as 6. Coupling $\lambda_{h_1 H_0 H_0}$ remains small and is responsible for small invisible decay branching ratio (denoted by BR_{inv} in Table 5.1) of SM-like scalar h_1 . This demonstrates that the scalar h_1 in Eq. 5.4 is mostly dominated by SM-like Higgs component and the major component in the other scalar is the real scalar singlet s of the proposed model.

5.6 Summary and Outlook

We have investigated a dark matter model with an extended two Higgs doublet model with an additional singlet scalar. The DM candidate follows by considering one of the Higgs doublet to be an inert Higgs doublet. A Z_2 symmetry imposed on the potential ensures the lightest inert particle or LIP dark matter from the added inert doublet is stable. The inert doublet does not generate any VEV and hence cannot couple to Standard Model fermions directly. The scalar singlet, having no such discrete symmetry acquires a non zero VEV and mixes up with SM Higgs. The unknown couplings of the model, which are basically the model parameters, are restricted with theoretical and experimental bounds. The mixing of the SM Higgs and the singlet scalar gives rise to two scalar states namely h_1 and h_2 . For small mixing, h_1 behaves as the SM Higgs and h_2 as the added scalar. We extensively explored the scalar sector of the model and studied the signal strengths $R_{\gamma\gamma}$ and $R_{\gamma Z}$ for the SM-like Higgs (h_1) in the model. The range and the region of enhancement of $R_{\gamma\gamma}$ depend on the mass of the singlet like scalar h_2 . Appreciable enhancements of both $h_1 \rightarrow \gamma\gamma$ and $h_1 \rightarrow \gamma Z$ signals depend on h_2 mass and occurs near the resonance of h_2 . Increase in signal strengths is not allowed for heavier values of h_2 mass. Enhancement of signals is forbidden when the invisible decay channel remains open. The extent of

enhancement depends on the charged scalar mass and occurs only when the Higgs-charged scalar coupling $\lambda_{h_1 H^+ H^-} < 0$. We first restrict our parameter space by calculating the relic density of LIP dark matter in the framework of our model. Using the resultant parameter space obtained from observed relic density bounds we evaluate the signal strengths $R_{\gamma\gamma}$ and $R_{\gamma Z}$ for different dark matter masses. We then restrict the parameter space by calculating the spin independent scattering cross-section and comparing it with the existing limits from ongoing direct detection experiments like CDMS, CoGeNT, DAMA, XENON100, LUX etc. Employing additional constraints by requiring that $R_{\gamma\gamma}$ and $R_{\gamma Z}$ will satisfy the CMS bounds and ATLAS bounds, we see that the present model provides a good and viable DM candidate in mass region 60-80 GeV consistent with LUX and XENON100 bounds. We obtain that $R_{\gamma\gamma}(> 1.0)$ in the present framework does not seem to be favoured by LUX and XENON100 data. Therefore, we conclude that under the present framework, the inert doublet model with additional scalar singlet provide a viable DM candidate with mass range 60 – 80 GeV which not only is consistent with the direct detection experimental bounds and PLANCK results for relic density but also in agreement with the Higgs search results of LHC. A singlet like scalar that couples weakly with SM Higgs may also exist that could enrich the Higgs sector and may be probed in future collider experiments.

Chapter 6

Singlet scalar extension of inert doublet model (IDM) part-II

6.1 Introduction

Recent results from Fermi-Lat data [48, 49] have confirmed the existence of GeV scale γ -ray excess which appear to be emerging from the region of galactic centre (GC) [50]-[59]. This excess in γ -ray can be treated as a result of dark matter (DM) annihilation in proximity of galactic centre. There are also studies which claim that the observed gamma ray excess can be explained by millisecond pulsar [57] or unresolved point sources near GC [58]. In this thesis, we consider the excess gamma ray observed purely originates from annihilation of dark matter at galactic centre. The γ -ray excess in the energy range 1-3 GeV observed by Fermi-LAT from the direction of galactic centre is addressed in a recent work by Dan Hooper et al [59]. In that work they show that a dark matter candidate within the mass range of 31-40 GeV primarily annihilating into $b\bar{b}$ or a 7-10 GeV dark matter primarily

annihilating into $\tau\bar{\tau}$ [59],[109]-[112] can well explain this observed phenomenon of excess gamma in 1-3 GeV energy range. Some works [55],[113] even suggest a DM candidate with mass $61.8_{-4.9}^{+6.9}$ GeV can also explain this observed excess when their annihilation cross-section $\langle\sigma v\rangle_{b\bar{b}}$ to $b\bar{b}$ is $\sim 3.30_{-0.49}^{+0.69} \times 10^{-26} \text{cm}^3/\text{s}$. Different particle physics models are studied and proposed in the literature in order to explain the anomalous excess of gamma ray in the energy range $\sim 1-3$ GeV [114]-[126]. In this work we attempt to explore whether a dark matter candidate within the framework of the inert doublet model can explain this reported gamma ray excess of 1-3 GeV. Study of inert doublet model (IDM) have been pursued vigorously in literatures [86]-[96]. In the inert doublet model, an additional scalar SU(2) doublet is added to the Standard Model (SM) which is assumed to develop no vacuum expectation value (VEV). An unbroken Z_2 symmetry ensures that the added scalar is stable and does not interact with the SM fermions (inert). The lightest stable inert particle (LIP) in this model can be a viable DM candidate. Inert doublet model provides a plausible DM candidate in low mass region that could address the observed GC γ -rays excess. We show in this work that although LIP dark matter in IDM model may indeed provide a 31-40 GeV dark matter which satisfies observed DM relic density, but this candidate (of mass $\sim 31 - 40$ GeV) does not withstand the latest bounds from dark matter direct detection experiments as well as the LHC bound on $R_{\gamma\gamma}$. We also found that the inert doublet model can account for a DM of mass around 60-63 GeV (i.e., near the SM Higgs resonance) that can satisfy the allowed relic density limits from PLANCK experiment and direct detection limits but fails to explain the observed GC γ -ray excess. In this work we have revisited the extension of this IDM model proposed in Chapter 5 where an additional singlet scalar is added to the IDM model mentioned above. This newly added scalar singlet acquires a non zero VEV and mixes up with the SM Higgs, thus provides an extra scalar boson and scalar resonance. The LIP dark matter candidate in this resulting extended IDM can obtain an LIP dark

matter candidate in the mass range of 31-40 GeV which simultaneously satisfy the relic density bound from PLANCK experiment, direct detection experimental results and the bound on signal strength of SM Higgs from LHC experiment. We show that the calculation of gamma ray flux obtained from the annihilation of such a dark matter from the extended IDM model proposed in this work can explain the 1-3 GeV γ -ray excess observed by Fermi-LAT from GC region.

6.2 Dark matter in inert doublet model and Fermi-LAT observed gamma ray excess

IDM is a simple extension of SM of particle physics which includes an additional Higgs doublet that acquires no VEV. The added doublet do not interact with the SM sector due to imposition of a discrete Z_2 symmetry under which all the SM particles are even but the doublet is odd. The most general CP conserving potential for IDM is given as,

$$\begin{aligned}
 V = & m_{11}^2 \Phi_H^\dagger \Phi_H + m_{22}^2 \Phi_I^\dagger \Phi_I + \lambda_1 (\Phi_H^\dagger \Phi_I)^2 + \lambda_2 (\Phi_I^\dagger \Phi_I)^2 + \lambda_3 (\Phi_H^\dagger \Phi_H) (\Phi_I^\dagger \Phi_I) \\
 & + \lambda_4 (\Phi_I^\dagger \Phi_H) (\Phi_H^\dagger \Phi_I) + \frac{1}{2} \lambda_5 [(\Phi_I^\dagger \Phi_H)^2 + (\Phi_H^\dagger \Phi_I)^2],
 \end{aligned} \tag{6.1}$$

where Φ_H is the SM Higgs doublet and Φ_I is the inert doublet assuming all the couplings (λ_i , $i = 1, 5$) in Eq. 6.1 are real. After spontaneous symmetry breaking (SSB), Φ_H generates a VEV $v = 246$ GeV whereas the inert doublet does not produce any VEV and the Z_2 symmetry remains unbroken. The doublets are given as

$$\Phi_H = \begin{pmatrix} \chi^+ \\ \frac{1}{\sqrt{2}}(v + h + i\chi^0) \end{pmatrix}, \quad \Phi_I = \begin{pmatrix} H^+ \\ \frac{1}{\sqrt{2}}(H_0 + iA_0) \end{pmatrix}, \tag{6.2}$$

where χ^+ and χ^0 are absorbed in W^\pm , Z after spontaneous symmetry breaking. After SSB, the masses of various scalar particles obtained are given as,

$$\begin{aligned}
 m_h^2 &= 2\lambda_1 v^2 \\
 m_{H^\pm}^2 &= m_{22}^2 + \lambda_3 \frac{v^2}{2} \\
 m_{H_0}^2 &= m_{22}^2 + (\lambda_3 + \lambda_4 + \lambda_5) \frac{v^2}{2} \\
 m_{A_0}^2 &= m_{22}^2 + (\lambda_3 + \lambda_4 - \lambda_5) \frac{v^2}{2} .
 \end{aligned} \tag{6.3}$$

where $m_h = 125$ GeV, is the mass of newly found SM Higgs boson h , as observed by LHC experiments CMS [63] and ATLAS [64]. With $\lambda_5 < 0$, the lightest inert particle (LIP) H_0 is the stable DM candidate in the model. The potential described in Eq. 6.1 must be bounded from below and the corresponding vacuum stability conditions are given as,

$$\lambda_1, \lambda_2 > 0, \quad \lambda_3 + 2\sqrt{\lambda_1\lambda_2} > 0, \quad \lambda_3 + \lambda_4 - |\lambda_5| + 2\sqrt{\lambda_1\lambda_2} > 0. \tag{6.4}$$

Apart from the bounds obtained from vacuum stability, there are several other constraints on the model such as perturbative bounds requiring all the couplings Λ_i to be less than 4π . From LEP [99] experiment constraints of the Z boson decay width and charged scalar mass m_{H^\pm} , we have

$$\begin{aligned}
 m_{H_0} + m_{A_0} &> m_Z , \\
 m_{H^\pm} &> 79.3 \text{ GeV}.
 \end{aligned} \tag{6.5}$$

Apart from the constraints presented in Eqs. 6.3-6.4, the present DM candidate H_0 must also satisfy the correct relic abundance of DM obtained from PLANCK [3]

$$\Omega_{\text{DM}} h^2 = 0.1199 \pm 0.0027 , \tag{6.6}$$

where h is the Hubble parameter in the unit of $100 \text{ km s}^{-1} \text{ Mpc}^{-1}$. Dark matter relic density is obtained by solving the Boltzmann equation for the DM species and is given as

$$\frac{dn_{H_0}}{dt} + 3Hn_{H_0} = -\langle\sigma v\rangle(n_{H_0}^2 - n_{H_0\text{eq}}^2). \quad (6.7)$$

In Eq. 6.7 $\langle\sigma v\rangle$ is the total annihilation cross-section of the DM summing over all possible annihilation channels, n_{H_0} is the number density of dark matter particle H_0 and $n_{H_0\text{eq}}$ is the equilibrium number density of the same. The Hubble parameter is denoted as H in Eq. 6.7. For the case of low mass dark matter scenario ($m_{H_0} \leq m_W$, m_W is the mass of W boson), total annihilation cross-section of DM candidate H_0 to SM particles expressed as

$$\langle\sigma v_{H_0H_0 \rightarrow f\bar{f}}\rangle = n_c \sum_f \frac{m_f^2}{\pi} \beta_f^3 \frac{(\lambda_L/2)^2}{(4m_{H_0}^2 - m_h^2)^2 + \Gamma_h^2 m_h^2}. \quad (6.8)$$

In Eq. 6.8 above, Γ_h is the total decay width of SM Higgs boson (including the contribution from invisible decay channel), m_f is the mass of the fermion species involved with $\beta_f = \sqrt{1 - \frac{m_f^2}{m_{H_0}^2}}$. The Higgs-DM coupling denoted as λ_L in Eq. 6.8 is of the form $\lambda_L = (\lambda_3 + \lambda_4 + \lambda_5)$ and n_c is the colour quantum number with $n_c = 3$ for quarks and $n_c = 1$ for leptons respectively. Invisible decay width of Higgs boson to DM particle as also the branching fraction Br_{inv} for such invisible decay is written as

$$\begin{aligned} \Gamma^{\text{inv}}(h \rightarrow H_0H_0) &= \frac{\lambda_L^2 v^2}{64\pi m_h} \sqrt{1 - \frac{4m_{H_0}^2}{m_h^2}}, \\ \text{Br}_{\text{inv}} &= \frac{\Gamma^{\text{inv}}(h \rightarrow H_0H_0)}{\Gamma_h}. \end{aligned} \quad (6.9)$$

DM relic density is then calculated by solving the Boltzmann equation expressed in Eq. 6.7, is given as

$$\Omega_{\text{DM}} h^2 = \frac{1.07 \times 10^9 x_F}{\sqrt{g_*} M_{\text{Pl}} \langle \sigma v \rangle}, \quad (6.10)$$

where $x_F = m_H/T_F$ is the freeze out or decoupling temperature of the DM species H_0 , M_{Pl} is the Planck mass ($M_{\text{Pl}} = 1.22 \times 10^{19}$ GeV) and g^* is the number of effective degrees of freedom. The quantity x_F (and subsequently the freeze out temperature T_f) can be obtained from the iterative solution to the equation

$$x_F = \ln \left(\frac{m_{H_0}}{2\pi^3} \sqrt{\frac{45 M_{\text{Pl}}^2}{2g_* x_F} \langle \sigma v \rangle} \right). \quad (6.11)$$

The relic density of the dark matter can be obtained using Eqs. 6.7-6.11 with the constraints given in Eqs. 6.4-6.6. It is to be noted that in addition to the constraints mentioned above, the present DM candidate must also satisfy the DM direct detection experimental limits provided by the experiments like XENON [27], LUX [28]. These experiments provide the upper bound of dark matter scattering cross-sections for different dark matter masses. The spin independent direct dark matter-nucleon scattering cross-section for the LIP dark matter H_0 of mass m_{H_0} is expressed as

$$\sigma_{\text{SI}} = \frac{\lambda_L^2}{4\pi} \frac{1}{m_h^4} f^2 \frac{m_N^4}{(m_{H_0} + m_N)^2}, \quad (6.12)$$

where m_N is the mass of scattering nucleon and f is related to the matrix element of Higgs-nucleon coupling is taken to be $\simeq 0.3$ [14]. We further restrict the allowed model parameter space by assuming the invisible decay branching ratio of SM Higgs $\text{Br}_{\text{inv}} < 20\%$ [127]. The branching ratio Br_{inv} is the ratio of the Higgs invisible decay width to the total Higgs decay width as discussed below. We compute, using Eq. 6.12 and with the constraints given in Eqs. 6.4-6.6, the LIP dark matter scattering cross-

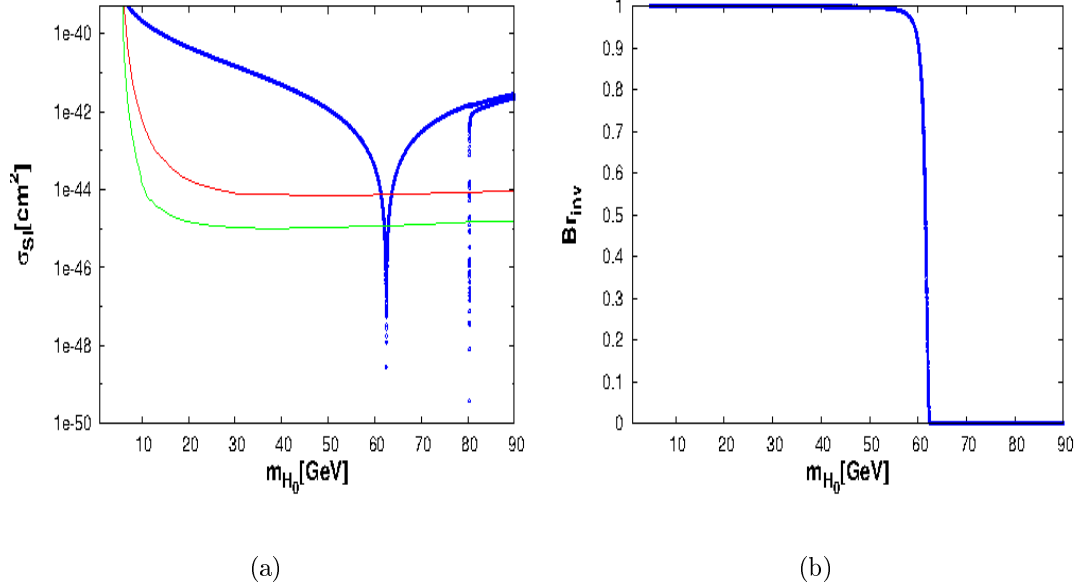


Figure 6.1: The left panel shows the $m_{H_0} - \sigma_{\text{SI}}$ space allowed by DM relic density obtained from PLANCK. The right panel presents the variation of invisible decay branching ratio Br_{inv} with DM mass m_{H_0} for the same.

section, σ_{SI} for different values of LIP dark matter mass, m_{H_0} . It is therefore ensured that these calculations are performed for those LIP dark matter masses for which the relic density criterion (Eq. 6.6) is satisfied. The results are plotted in Fig. 6.1a (in $\sigma_{\text{SI}} - m_{H_0}$ plane). Superimposed on this plot in Fig. 6.1a are the the bounds obtained from XENON100 (red line) and LUX (green line) experimental results for comparison. It is clear from Fig. 6.1a that an LIP dark matter within the framework of IDM does not have a mass region in the range 31-40 GeV that satisfies the allowed bounds given by both the XENON100 and LUX experiments in $\sigma_{\text{SI}} - m_{H_0}$ plane. One may recall that the previous analysis to explain the Fermi-LAT γ -ray excess in the gamma ray energy range of 1 – 3 GeV [59] from the annihilation of dark matter at the galactic centre requires a dark matter candidate having mass in the range 31 – 40 GeV. We also compute the Higgs invisible decay branching ratio Br_{inv} for the allowed range of DM mass obtained in Fig. 6.1a and the results are plotted in Fig. 6.1b. It is also evident from Fig. 6.1b that the LIP mass (m_{H_0}) in the range 31-40 GeV does

not satisfy the Br_{inv} limit of $\text{Br}_{\text{inv}} < 20\%$ [127]. Thus from both Fig 1a and Fig 1b, it can be concluded that an LIP dark matter in the inert doublet model cannot account for a viable dark matter candidate in the mass range of 31-40 GeV.

However, from Fig 1a and 1b, it is clear we have a viable dark matter candidate in the IDM framework in the region of Higgs resonance with mass ($m_{H_0} \simeq m_h/2$) that not only satisfies the relic density bound for dark matter but also is consistent with DM direct detection results and the bounds for Higgs invisible decay as well. Earlier model independent analysis [55],[113] have reported that a dark matter with mass near Higgs resonance can produce the observed excess of γ -ray in the gamma energy range 1 – 3 GeV if the secondary γ -ray is produced out of the primary annihilation process $\text{DM DM} \rightarrow b\bar{b}$ with the annihilation cross-section $\langle\sigma v\rangle_{b\bar{b}} \sim 3.30_{-0.49}^{+0.69} \times 10^{-26} \text{ cm}^3/\text{s}$. However for IDM with mass $m_{H_0} \sim m_h/2$, the respective annihilation cross-section of LIP dark matter H_0 into $b\bar{b}$ ($\langle\sigma v\rangle_{b\bar{b}}$) channel is found to be $\sim 1.7 \times 10^{-26}$ which is almost half the required annihilation cross-section. Hence the gamma ray flux computed for this LIP dark matter (with $b\bar{b}$ to be the primary annihilation channel) does not comply with the observed excess in γ -ray.

Thus it is apparent that a viable dark matter candidate (mass $\sim m_h/2$) in the IDM model discussed so far where only an inert SU(2) doublet is added to SM, fails to explain the excess gamma ray in the energy range 1-3 GeV as observed by Fermi-LAT in the direction of galactic centre. Apart from the SM Higgs resonance, there also exists another allowed region appearing in IDM (in the vicinity of W^+W^- threshold shown in Fig. 6.1a¹) which satisfies the PLANCK DM relic density and direct detection limits provided by XENON100 and LUX experiments. However, LIP dark matter of mass ~ 80 GeV in this narrow allowed region cannot explain the observed GC gamma ray excess. In fact the gamma flux obtained for this latter case

¹This feature have also been reported in Ref. [95] by T. A. Chowdhury *et al.*

is even smaller when compared to that obtained from the IDM dark matter with mass $m_{H_0} \sim m_h/2$. Hence we consider a feasible extension of the inert doublet model.

6.3 Inert doublet model with additional singlet scalar

We modify the IDM formalism given in Sect. 6.2 by adding another singlet scalar with the model as discussed earlier in Chapter 5. The resulting theory now includes an inert SU(2) doublet as before and an additional scalar singlet added to the Standard Model. The newly added scalar singlet generates a VEV and is even under the discrete Z_2 symmetry. The LIP of the inert doublet is the dark matter candidate in this formalism too. We demonstrate that our proposed extended IDM provides a viable LIP dark matter candidate in the mass range of 31 – 40 GeV and the annihilation cross-section to $b\bar{b}$ channel for such a candidate can be calculated to be in the right ballpark required to explain the excess γ peak from GC seen by Fermi-LAT in 1-3 GeV energy range and is also consistent with the LHC constraint. We restrict the model parameter space using the conditions from vacuum stability, unitarity, LEP, DM relic density from PLANCK, direct detection constraints on DM-nucleon scattering cross-section from LUX etc. as mentioned previously in Chapter 5. The phenomenology of the singlet extension of IDM is already explored in Chapter 5. We use the formalism of the model developed in Chapter 5 and explore the dark matter phenomenology of this model. We have used Eqs. 5.1-5.8 to build the singlet extended inert doublet model as given in Chapter 5. The model parameter space is then restricted by vacuum stability, LEP etc. using Eqs. 5.9-5.10. However, instead of taking m_1 as Higgs like scalar and m_2 to be the non-SM scalar (in Chapter 5), here we consider h_2 with mass m_2 to be the SM-like Higgs boson having mass 125 GeV

assuming $m_2 > m_1$ where m_1 is the mass of the singlet scalar. The relic density for the LIP is then calculated by solving Eqs. 4.17-4.18,5.12. In order to solve for the Boltzmann equation for dark matter we have used the expression of annihilation cross-section given by Eq. 5.13. We obtain the valid model parameter space in the present model satisfying PLANCK dark matter relic density and direct detection cross-section for the dark matter is then calculated using Eq. 5.19. The invisible decay widths for the scalar h_1 and h_2 are also obtained from Eq. 5.14. Since in the present model h_2 is SM-like scalar, we constrain the model parameter space further by the condition $Br_{\text{inv}} < 0.2$ [127] ($Br_{\text{inv}} = \frac{\Gamma_2^{\text{inv}}(h_2 \rightarrow 2H_0)}{\Gamma_2}$, where Γ_2 is the total decay width of Higgs like scalar with mass $m_2 = 125$ GeV). The modification of signal strength of SM Higgs (h_2) to any particular channel that may occur due to the mixing with other scalar (h_1) is also taken into account. The signal strength to any specific channel is given as,

$$R = \frac{\sigma}{\sigma^{\text{SM}}} \frac{\text{Br}}{\text{Br}^{\text{SM}}} \quad (6.13)$$

where σ and σ^{SM} are the Higgs production cross-section in the present model and in SM respectively whereas Br and Br^{SM} are the respective branching ratios to any channel for the present model and SM. As the present model (extended IDM) involves two scalars h_1 and h_2 , signal strengths R_1 and R_2 for both the scalars are given as

$$R_1 = \frac{\sigma^1(pp \rightarrow h_1)}{\sigma^{\text{SM}}(pp \rightarrow h_1)} \frac{\text{Br}(h_1 \rightarrow xx)}{\text{Br}^{\text{SM}}(h_1 \rightarrow xx)}, \quad R_2 = \frac{\sigma^2(pp \rightarrow h_2)}{\sigma^{\text{SM}}(pp \rightarrow h_2)} \frac{\text{Br}(h_2 \rightarrow xx)}{\text{Br}^{\text{SM}}(h_2 \rightarrow xx)} \quad (6.14)$$

where xx is any SM final state with $\frac{\sigma^i}{\sigma^{\text{SM}}} = \cos^2 \alpha$ or $\sin^2 \alpha$ for $i = 1, 2$ respectively. Since h_2 is the SM-like scalar with mass $m_2 = 125$ GeV, we take $R_2 \geq 0.8$ [108] for SM-like scalar to satisfy LHC results. It is to be noted that some of the channels (γZ , $\gamma\gamma$) will suffer considerable changes due to the presence of inert charged scalars (H^\pm) addressed in [101]-[103]. Effect of the charged scalars on those channels are

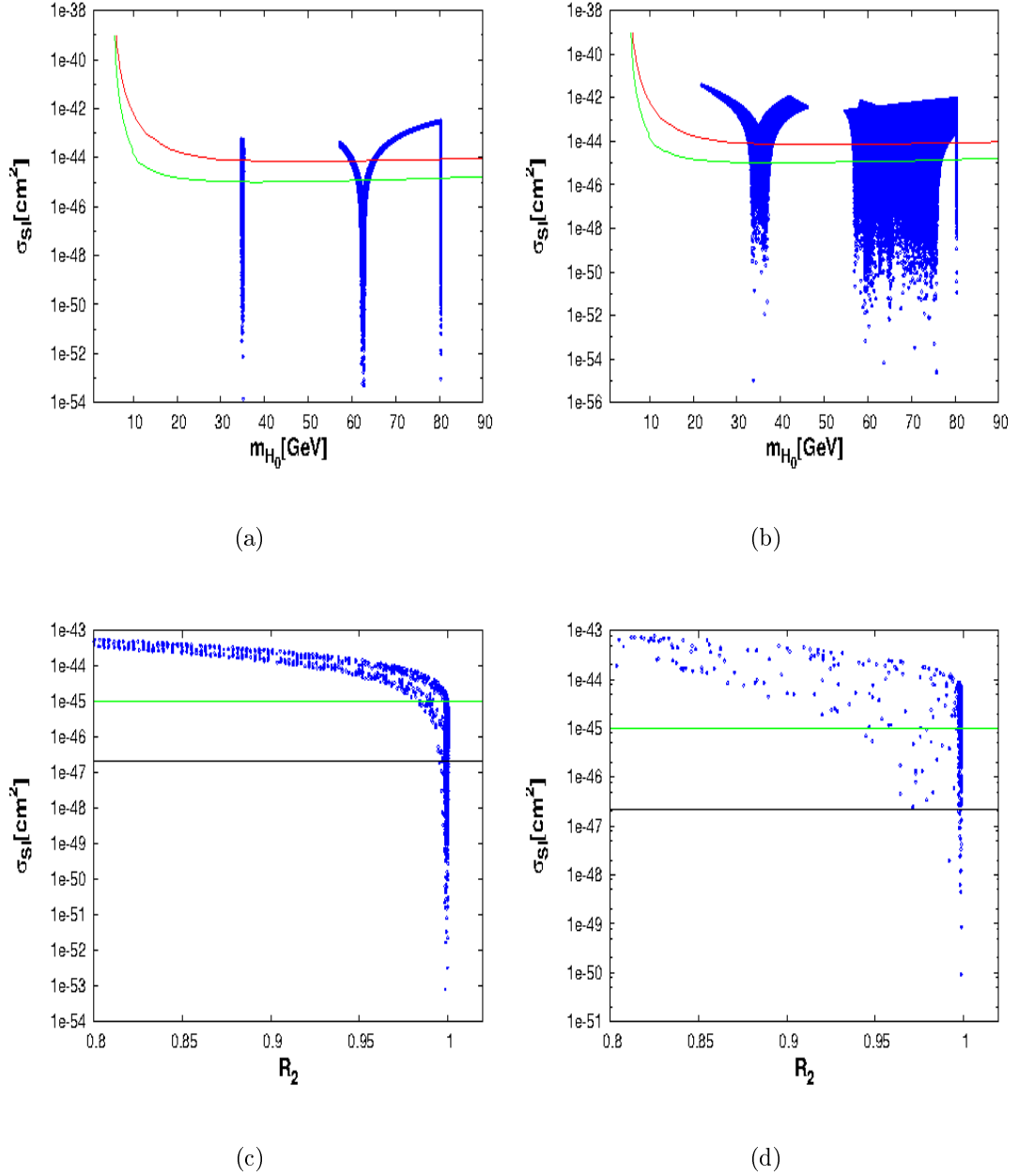


Figure 6.2: The upper panel shows the valid $m_{H_0} - \sigma_{SI}$ plane obtained for $m_1 = 70$ GeV with $\cos \alpha = 0.9 \times 10^{-3}$ and 3.5×10^{-2} . The lower panel shows the variation of signal strength R_2 with σ_{SI} for $m_{H_0} = 35$ GeV for the same.

also taken into account (for details see Appendix A). We put further bound on model parameter space from the experimental limits for Higgs to diphoton signal strength $R_{\gamma\gamma}$ given by ATLAS [84] with 95% C. L. along with the best fit value of $R_{\gamma\gamma}$ from

CMS [85] for 125 GeV Higgs. Our calculation yields that for the allowed parameter space obtained from vacuum stability, relic density, LEP constraints as also with the condition $R_2 \geq 0.8$, $\text{Br}_{\text{inv}} \leq 0.2$, the Higgs to diphoton signal strength predicted by ATLAS is not favoured by the present model and hence we constrain the model with the experimental value of $R_{\gamma\gamma}$ only from CMS experiment. Taking all these constraints into account, we now compute the LIP dark matter (in extended IDM) scattering cross-sections σ_{SI} (Eq. 5.19) for the LIP masses (m_{H_0}) for two different mixing angles α given by $\cos \alpha = 9.0 \times 10^{-3}$ and 3.5×10^{-2} . The results for two chosen mixing angles are plotted in Fig. 6.2a and Fig. 6.2b respectively in $m_{H_0} - \sigma_{\text{SI}}$ parameter space. The calculations are performed with a chosen value $m_1 = 70$ GeV for the mass of the scalar singlet h_1 . Direct detection bounds from XENON100 and LUX are shown in Fig. 6.2a-b with the same color definitions used in Fig. 6.1a. It is

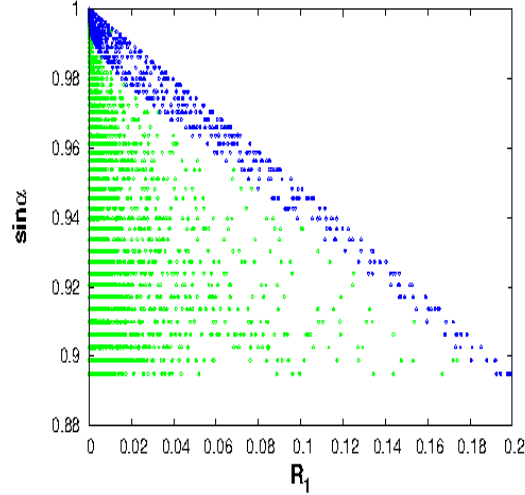


Figure 6.3: Allowed parameter space in $R_1 - \sin \alpha$ plane for $m_1 = 70$ GeV. Also shown in blue corresponds to the parameter space for $m_{H_0} = 35$ GeV.

clear from Fig. 6.2a-b that apart from obtaining a LIP dark matter of mass $\sim m_2/2$ (Higgs resonance) allowed by both XENON100 and LUX, we also obtain another allowed LIP mass of 35 GeV (due to the resonance of the added scalar involved in the model). Thus, the present modified inert doublet model produces a viable

DM candidate with a mass of 35 GeV. Fig. 6.2a-b also indicate that the resonant behaviour is prominent for smaller values of mixing angle α . Increase in the mixing angle broadens the allowed $m_{H_0} - \sigma_{\text{SI}}$ parameter space resulting appreciable increase in DM-nucleon cross-section. Study of Fig. 6.2a-b reveals that, similar to the case of IDM discussed earlier in Section 6.2, a resonance like narrow allowed region appears just near W^+W^- threshold in our scalar singlet extended IDM model too. However, this allowed region near the W^+W^- threshold also cannot explain the GC gamma ray excess problem unless a different case ($m_1 < m_{H_0}$ discussed in Section 6.4) is taken into account. In Fig. 6.2c-d we show the variation of R_2 with σ_{SI} where LIP dark matter mass $m_{H_0} = 35$ GeV is considered for the two mixing angles as chosen for Fig. 6.2a-b. Horizontal lines in green and black are the values of σ_{SI} as obtained from the allowed regions from LUX [28] and XENON1T [107] respectively for the dark matter mass of 35 GeV. Fig. 6.2c shows that as R_2 approaches to unity there is a sharp decrease in σ_{SI} . A similar conclusion also follows from the nature of Fig. 6.2d. Observation of Fig. 6.2c-d reveals that a 35 GeV DM satisfying relic density obtained from PLANCK and direct detection bounds from LUX and XENON1T does not affect the signal strength ($R_2 \sim 1$) of the SM Higgs observed in LHC. Fig. 6.2c-d clearly demonstrate that the presence of a low mass scalar is necessary in order to achieve a DM of mass ~ 35 GeV that (a) satisfy PLANCK relic density result, (b) agree with the latest dark matter direct detection experimental bounds and also (c) yields the experimental bound for Higgs invisible decay.

Since the model involves an additional scalar of low mass, yet undetected by LHC, the corresponding signal strength for that singlet like scalar must remain small compared to that of h_2 . In order to demonstrate this, we compute the signal strength R_1 (Eq. 6.14) for different values of the mixing angle α . In Fig. 6.3 we plot the results in $R_1 - \sin \alpha$ plane for low mass DM ($\leq m_W$). These results satisfy the conditions $R_2 \geq 0.8$ [108] and $\text{Br}_{\text{inv}} \leq 0.2$ [127] with $m_1 = 70$ GeV and also consistent with relic

density reported by PLANCK. Scattered blue region in Fig. 6.3 corresponds to 35 GeV DM mass ($m_{H_0} = 35$ GeV) with $\langle\sigma v\rangle_{b\bar{b}} \sim (1.62 - 1.68) \times 10^{-26} \text{cm}^3/\text{s}$. We show latter in Sec. 6.4 that such a value for $\langle\sigma v\rangle_{b\bar{b}}$ in case of a dark matter mass of 35 GeV can indeed explain the Fermi-LAT observed excess of γ -ray in the energy range of 1-3 GeV. Variation of $\sin\alpha$ with R_1 in Fig. 6.3 depicts that for the parameter space constrained by different experimental and theoretical bounds, the value of the signal strength R_1 remains small (≤ 0.2). Therefore, non-observance of such a scalar by LHC is justified and can possibly be probed in future experiment.

6.4 Calculation of gamma ray flux

In this section we calculate the gamma ray flux from the galactic centre due to the annihilation of 35 GeV dark matter in the extended IDM discussed in Sect.6.3. The gamma ray flux produced from DM annihilation in galactic centre is given by

$$\Phi = \frac{\langle\sigma v\rangle}{8\pi m_{DM}^2} \frac{dN}{dE_\gamma} J(\psi) . \quad (6.15)$$

In Eq. 6.15, $\langle\sigma v\rangle$ is the annihilation cross-section, m_{DM} is the mass of the dark matter (m_{H_0} in the present scenario), $\frac{dN}{dE_\gamma}$ is the spectrum of photon produced due to DM annihilation. The factor $J(\psi)$ in Eq. 6.15 is the line of sight integral given as

$$J(\psi) = \int_{\text{los}} \rho^2(l, \psi) dl , \quad (6.16)$$

where ψ is angle between the direction of line of sight and the direction from GC to Earth, l is the distance from line of sight. We use the generalised NFW [5] halo

m_1 in GeV	m_{H_0} in GeV	m_H^\pm in GeV	$\cos \alpha$	λ_L	λ_s	$\langle \sigma v \rangle_{b\bar{b}}$ in cm^3/s	σ_{SI} in cm^2
70.0	35.0	174.0	0.9×10^{-3}	-7.89e-05	-7.91e-02	1.66×10^{-26}	4.58×10^{-49}
		110.0	3.5×10^{-2}	7.87e-04	1.26e-02	1.65×10^{-26}	2.52×10^{-48}

 Table 6.1: Benchmark points of singlet extended IDM with DM mass $m_{H_0} = 35$ GeV.

profile for the DM distribution $\rho(r)$ given by

$$\rho(r) = \rho_0 \frac{(r/r_s)^{-\gamma}}{(1 + r/r_s)^{3-\gamma}}. \quad (6.17)$$

In Eq. 6.17, $\rho_0 = 0.3 \text{ GeV cm}^{-3}$ is the local DM density at a distance 8.5 kpc from GC. For the present work we consider $r_s = 20$ kpc and $\gamma = 1.26$ [59]. Using Eqs. 6.15 - 6.17, we calculate the gamma ray flux for the present 35 GeV DM candidate in our model with two values of mixing angles given by $\cos \alpha = 0.9 \times 10^{-3}$ and 3.5×10^{-2} . A chosen set of values for other parameters and the corresponding values of $\langle \sigma v \rangle_{b\bar{b}}$ and σ_{SI} for each of these two mixing angles are tabulated in Table 1. The gamma ray spectrum for these two set of parameter values given in Table 6.1 are plotted in Fig. 6.4. The plots in Fig. 6.4 are produced using NFW profile with inner profile slope $\gamma = 1.26$ at 5° from the galactic centre assuming local DM density $\rho_0 = 0.3 \text{ GeV cm}^{-3}$ at a distance 8.5 kpc from GC. Green and blue lines shown in Fig. 6.4 correspond to the benchmark points given in Table 6.1 for two sets of mixing angles (α) with values given by $\cos \alpha = 0.9 \times 10^{-3}$ and 3.5×10^{-2} respectively. Also shown in Fig. 6.4, the data points for the observed γ -ray by Fermi-LAT for comparison obtained from Ref. [59]. Fig. 6.4 clearly demonstrates that the viable LIP DM candidate in our model can very well explain the observed γ -ray flux and its excess in the 1-3 GeV energy range while remains consistent with the bounds from LHC and DM direct search experiments.

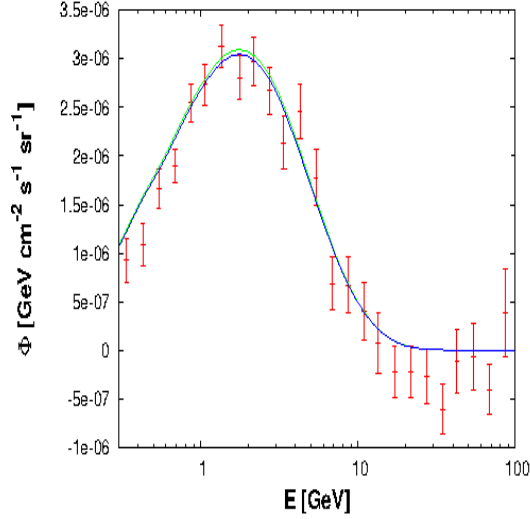


Figure 6.4: γ -ray flux obtained from the benchmark points in Table 6.1 and compared with the results from [59] for two different mixing angles.

A discussion is in order. Throughout the work, we have considered the case $m_1 > m_{H_0}$, i.e., the additional singlet scalar h_1 is heavier than the lightest inert particle H_0 in order to provide a DM of mass 31-40 GeV and produce the required DM annihilation cross-section (into $b\bar{b}$) to explain the observed GC γ -ray excess. We found that in our model, DM mass in the range of 31-40 GeV can be achieved by adding a singlet scalar of mass $m_1 \sim 2m_{H_0}$ to IDM. However, it is also possible in our model to provide an alternative explanation to GC γ -ray considering the singlet mass to be less than the LIP dark matter ($m_1 < m_{H_0}$). In this case, the lightest inert particle H_0 can annihilate into two singlet scalar particles (h_1) which then decay into two $b\bar{b}$ pairs. As shown in Fig. 6.3a-b, apart from the resonances near the masses of h_1 and h_2 , there is also a resonance like appearance near W^+W^- threshold when $H_0H_0 \rightarrow W^+W^-$ channel opens. Hence, dark matter particle H_0 having mass ~ 80 GeV annihilating into the scalar singlet h_1 with mass $m_1 < m_{H_0}$, can also explain the observed γ -ray excess in GC. Such possibilities have been explored in Ref. [119, 120].

6.5 Summary

We have revisited the inert doublet model (IDM) of dark matter and test the viability of the model to provide a suitable explanation for the observed excess in low energy (1-3 GeV) γ -ray emission from GC assumed to have originated out of the annihilation of dark matter in the mass range 31-40 GeV DM into $b\bar{b}$. We show that a dark matter candidate within mass range 31-40 GeV in IDM cannot satisfy the latest direct detection bounds on DM-nucleon cross-section predicted by experiments like LUX or XENON100 and also is inconsistent with the limits on Higgs invisible decay. Our calculations also yield that although IDM can provide a DM of mass $\sim m_h/2$ (m_h is the mass of SM Higgs) that is consistent with direct detection and invisible decay bounds but eventually fails to produce the value of $\langle\sigma v\rangle_{b\bar{b}}$ required to explain the excess emission of γ -ray. In order to comply with the observed γ emission results as obtained from Fermi-LAT in 1-3 GeV energy range, we extend the IDM with an additional singlet scalar and explore the viability of the model. The extension of IDM provides an additional scalar singlet that mixes with the SM-Higgs. We found that presence of a low mass singlet like scalar in the model can yield a 31-40 GeV DM that satisfies relic density bounds from PLANCK and direct detection cross-section constraints from LUX or XENON100 experiments and also yields the right DM annihilation cross-section $\langle\sigma v\rangle_{b\bar{b}}$, that would explain the observed excess in γ -ray. The singlet like scalar having a small mixing with the SM Higgs couples weakly to the SM sector and acquires a very small signal strength but this signal is beyond the present LHC detection limit and may be probed in future collider experiments.

Chapter 7

Hidden sector Fermionic dark matter Model

7.1 Introduction

So far, in this thesis, we have explored dark matter models with discrete symmetries. This discrete symmetry assures the stability of dark matter to provide a viable candidate for dark matter. However, in SM, there is no such discrete symmetry to ensure stability of particles. In this work, we consider a “hidden sector” framework of dark matter without pretending any such discrete symmetry associated with it. We propose the existence of a hidden sector which has $SU(2)_H$ gauge structure. Dark fermions in this hidden sector are charged under this $SU(2)_H$ gauge group while all the SM particles behave like a singlet. Hence, the SM sector is decoupled from the dark sector and could interact only through the exchange of scalar bosons that exist in both the sector. Gauge bosons charged under $SU(2)_H$ are heavy and decay into dark fermions. Thus, the lightest one among dark fermions is stable and can

be treated as a viable DM candidate. We check for the viability of the model by constraining the model parameter space by vacuum stability, LHC phenomenology, DM relic density, direct detection cross-section and also probe whether DM in present model can account for the indirect search results from GC and dwarf galaxy γ -ray signals.

7.2 The Model

We consider the existence of a “dark sector” that governs the particle candidate of dark matter. Just as the “visible sector” related to the known fundamental particles successfully explained by the Standard Model, we propose the existence of a hidden “dark sector” that relates the dark matter particles. We also presume that the Lagrangian of this hidden sector remains invariant under the transformations of a local $SU(2)_H$ as well as a global $U(1)_H$ gauge symmetries. Therefore we consider two fermion generations χ_i ($i = 1, 2$) where each generation consists of two fermions. Consequently, in the dark sector we have altogether four fermions namely f_i ($i = 1, 4$). The left handed component of each fermion (f_{iL}) transforms like a part of a doublet under $SU(2)_H$ while its right handed part f_{iR} behaves like a singlet under the same gauge group. Thus, the left handed components of f_1, f_2 and f_3, f_4 form two separate $SU(2)_H$ doublets¹. However, both the left handed as well as the right handed fermionic components are charged under the postulated global $U(1)_H$ symmetry. The interactions between the dark sector fermions and the SM particles are possible by the presence of an $SU(2)_H$ scalar doublet Φ through the gauge invariant interaction term $\lambda_3 H^\dagger H \Phi^\dagger \Phi$ which introduces a finite mixing between the SM Higgs boson and the neutral component of the hidden sector scalar doublet Φ . This scalar doublet does

¹In order to cancel the Witten anomaly [128] we need at least two (even numbers) of left handed fermionic $SU(2)_H$ doublets in our model.

not have any global $U(1)_H$ charge. As a result, the global $U(1)_H$ symmetry does not break spontaneously. However, being an $SU(2)_H$ doublet Φ breaks the local $SU(2)_H$ symmetry spontaneously when its neutral component acquires vacuum expectation value (VEV) v_s . Besides the local $SU(2)_H$ gauge symmetry, the scalar doublet Φ , which is in the fundamental representation of $SU(2)_H$ gauge group, also possesses a custodial $SO(3)$ symmetry. As a result of this residual $SO(3)$ symmetry, three dark gauge bosons $A'_{i\mu}$ ($i = 1$ to 3) which get mass due to the spontaneous breaking of the local $SU(2)_H$ symmetry, become degenerate in mass. Non abelian nature of the $SU(2)_H$ forbids the mixing between SM gauge bosons with dark gauge bosons $A'_{i\mu}$ ($i = 1$ to 3) [16], [129]. The scalar doublets H , Φ and the fermionic doublets can be written as²

$$H = \begin{pmatrix} G_1^+ \\ \frac{h^0 + iG_1^0}{\sqrt{2}} \end{pmatrix}, \quad \Phi = \begin{pmatrix} G_2^+ \\ \frac{\phi^0 + iG_2^0}{\sqrt{2}} \end{pmatrix}, \quad \chi_{1L} = \begin{pmatrix} f_1 \\ f_2 \end{pmatrix}_L, \quad \chi_{2L} = \begin{pmatrix} f_3 \\ f_4 \end{pmatrix}_L. \quad (7.1)$$

Therefore, the most general Lagrangian of the present proposed model contains the following gauge invariant terms

$$\begin{aligned} \mathcal{L} \supset & -\frac{1}{4}F'_{\mu\nu}F'^{\mu\nu} + (D_\mu H)^\dagger(D^\mu H) + (D'_\mu \Phi)^\dagger(D'^\mu \Phi) - \mu_1^2 H^\dagger H - \mu_2^2 \Phi^\dagger \Phi \\ & -\lambda_1(H^\dagger H)^2 - \lambda_2(\Phi^\dagger \Phi)^2 - \lambda_3 H^\dagger H \Phi^\dagger \Phi + \sum_{i=1,2} \bar{\chi}_{iL}(i\not{D}'\chi_{iL}) + \sum_{i=1,4} \bar{f}_{iR}(i\not{D}f_{iR}) \\ & -y'_1 \bar{\chi}_{1L} \Phi f_{1R} - y'_2 \bar{\chi}_{1L} \tilde{\Phi} f_{2R}, -y'_3 \bar{\chi}_{2L} \Phi f_{3R} - y'_4 \bar{\chi}_{2L} \tilde{\Phi} f_{4R} + hc, \end{aligned} \quad (7.2)$$

²Although, in order to keep similarity with the expression of the Standard Model Higgs doublet H , we have introduced the notation of three scalar fields, in the expression of Φ , as G_2^+ , ϕ^0 and G_2^0 , however the symbols $+$ and 0 appearing in the superscript of dark sector scalar fields do not represent the electric charge of the corresponding scalar field as electric charge itself is not defined in the dark sector which is invariant only under $SU(2)_H$.

with

$$\begin{aligned}
 D_\mu &= \left(\partial_\mu + i\frac{g}{2} \sum_{a=1,3} \sigma_a W^a{}_\mu + i\frac{g'}{2} B_\mu \right), \\
 D'_\mu &= \left(\partial_\mu + i\frac{g_H}{2} \sum_{a=1,3} \sigma^a A'_{a\mu} \right),
 \end{aligned} \tag{7.3}$$

are the covariant derivatives of the $SU(2)_L \times U(1)_Y$ doublet H and the $SU(2)_H$ doublets Φ, χ_{iL} respectively while $\tilde{\Phi} = i\sigma_2 \Phi^*$ with σ_2 is the Pauli spin matrix. Moreover, g, g' and g_H are the respective gauge couplings corresponding to the gauge groups $SU(2)_L, U(1)_Y$ and $SU(2)_H$. In the above equation (Eq. 7.2) $F'_{\mu\nu}$ is the field strength tensor for the gauge fields $A'_{i\mu}$ ($i = 1$ to 3) of the $SU(2)_H$ gauge group while H is the usual SM Higgs doublet. The global $U(1)_H$ invariance of the dark sector Lagrangian forbids the presence of any Majorana type mass terms of the fermionic fields ($f_i, i = 1, 4$) in Eq. 7.2. We have assumed at the beginning that the dark sector fermions are charged under a global $U(1)_H$ symmetry. Therefore invariance of the dark sector Lagrangian (Eq. 7.2) under this $U(1)_H$ symmetry requires an equal and opposite $U(1)_H$ charges between each fermion and its antiparticle. Thus we can say that there is some conserved quantum number in the theory which can differentiate between a fermion and its antiparticle. In other words this can be stated the dark sector fermions in the present theory are Dirac type fermions. We have also assumed that the dark sector fermions ($f_i, i = 1, 4$) are in “mass basis” or “physical basis” so that the Lagrangian (Eq. 7.2) does not contain any mixing term between these fermionic states³. The dark sector fermions can interact among themselves by exchanging dark gauge bosons $A'_{i\mu}$ and due to the presence of these interaction modes all the heavier fermions such as f_i ($i = 2$ to 4) decay into the lightest one (f_1). Consequently, the

³ Alternatively, one may think that the fermions in dark sector may have mixing between themselves similar to the case of SM fermions in quark and lepton sectors. Following the CKM mechanism in the quark sector of SM we can assume that the mass matrix of up-type fermion generations i.e. f_1 and f_3 is diagonal while the mixing takes place between down-type fermionic states (f_2, f_4). Now, since we have considered the up-type fermion f_1 to be the lightest of all fermions in dark sector, thus in the present framework, the study of fermion mixing is redundant.

lightest fermion f_1 is stable and can be a viable dark matter candidate. Like the hidden sector gauge fields $A'_{i\mu}$, the dark matter candidate f_1 also gets mass when the postulated $SU(2)_H$ symmetry of the hidden sector breaks spontaneously by the VEV of Φ . Thus, the expression of mass of the fermionic dark matter candidate can easily be obtained using Eq. 7.2 which is

$$m_{f_1} = \frac{y'_1 v_s}{\sqrt{2}}. \quad (7.4)$$

We have already mentioned before, that due to the presence of the gauge invariant term $\lambda_3 H^\dagger H \Phi^\dagger \Phi$, the neutral components of both the scalar doublets, namely h^0 and ϕ^0 , possess mass mixing between themselves. The mass squared mixing matrix between these two real scalar fields are given by,

$$\mathcal{M}_{\text{scalar}}^2 = \begin{pmatrix} 2\lambda_1 v^2 & \lambda_3 v v_s \\ \lambda_3 v v_s & 2\lambda_2 v_s^2 \end{pmatrix}. \quad (7.5)$$

After diagonalising the mass squared matrix $\mathcal{M}_{\text{scalar}}^2$, we obtain two physical eigenstates h_1 and h_2 which are related to the old basis states h^0 and ϕ^0 by an orthogonal transformation matrix $O(\alpha)$ where α is the mixing angle between the resulting physical scalars. The relation between physical scalars h_1 and h_2 with the scalar fields h^0 and ϕ^0 are given as

$$h_1 = \cos \alpha h^0 - \sin \alpha \phi^0, \quad h_2 = \sin \alpha h^0 + \cos \alpha \phi^0.$$

The expressions of the mixing angle α and the masses of the physical real scalars h_1

and h_2 are given by

$$\alpha = \frac{1}{2} \tan^{-1} \left(\frac{\frac{\lambda_3 v}{\lambda_2 v_s}}{1 - \frac{\lambda_1 v^2}{\lambda_2 v_s^2}} \right), \quad (7.6)$$

$$\begin{aligned} m_1 &= \sqrt{\lambda_1 v^2 + \lambda_2 v_s^2 + \sqrt{(\lambda_1 v^2 - \lambda_2 v_s^2)^2 + (\lambda_3 v v_s)^2}}, \\ m_2 &= \sqrt{\lambda_1 v^2 + \lambda_2 v_s^2 - \sqrt{(\lambda_1 v^2 - \lambda_2 v_s^2)^2 + (\lambda_3 v v_s)^2}}. \end{aligned} \quad (7.7)$$

We assume the physical scalar h_1 is the SM-like Higgs boson which has been observed by the ATLAS and the CMS detector [63, 64]. Therefore we have adopted the mass (m_1) of h_1 and VEV v of h^0 to be ~ 125.5 GeV and 246 GeV respectively. Thus, we have three unknown model parameters which control the interactions of the dark matter candidate f_1 in the early Universe, namely the mixing angle α , the mass (m_2) of the extra physical scalar boson h_2 and more importantly, the mass m_{f_1} of the dark matter particle f_1 . In the rest of our work we have computed the allowed ranges of these model parameters using various theoretical, experimental as well as observational results. Throughout the work, for simplicity we take mass of fermionic DM candidate (f_1) to be m .

7.3 Constraints

In this section we will discuss various constraints and bounds on model parameters that arise from both theoretical aspects and experimental observations.

- **Vacuum Stability** - To ensure the stability of the vacuum, the scalar potential for the model must remain bounded from below. The quartic terms of the scalar potential is given as

$$V_4 = \lambda_1 (H^\dagger H)^2 + \lambda_2 (\Phi^\dagger \Phi)^2 + \lambda_3 H^\dagger H \Phi^\dagger \Phi, \quad (7.8)$$

where H is the SM Higgs doublet and Φ is the hidden sector Higgs doublet. Conditions for the vacuum stability in this framework is given as

$$\lambda_1 > 0, \quad \lambda_2 > 0, \quad \lambda_3 + 2\sqrt{\lambda_1\lambda_2} > 0. \quad (7.9)$$

- LHC Phenomenology** - In the present model of hidden sector ($SU(2)_H$) fermionic dark matter discussed earlier in Sect. 7.2, an extra Higgs doublet is added to the SM. This dark $SU(2)_H$ Higgs doublet provides an additional Higgs like scalar that mixes up with the SM Higgs. Large Hadron Collider (LHC) performing the search of Higgs particle (ATLAS and CMS Collaboration) have already discovered a Higgs like particle having mass about 125 GeV. The excess in $\gamma\gamma$ channel reported independently by ATLAS [64] and CMS [63] confirmed the existence of Higgs like bosons. In the case of Hidden sector $SU(2)_H$ model, the mixing between SM Higgs with Dark Higgs results in two Higgs like scalars. In the the present scenario we take one of the scalar (h_1) as the SM Higgs with mass $m_1 = 125$ GeV. We further assume that the signal strength of scalar h_1 also satisfies the limits on the same obtained for the newly discovered boson. Thus, h_1 in the present framework is identical with the SM-like Higgs as reported by LHC Higgs search experiments (ATLAS and CMS). The signal strength of Higgs boson (h), decaying into a particular final state (xx , x is any SM particle), is defined as

$$R = \frac{\sigma(pp \rightarrow h)}{\sigma^{\text{SM}}(pp \rightarrow h)} \frac{\text{Br}(h \rightarrow xx)}{\text{Br}^{\text{SM}}(h \rightarrow xx)}, \quad (7.10)$$

where $\sigma(pp \rightarrow h)$ and $\text{Br}(h \rightarrow xx)$ are the Higgs production cross-section and its branching ratio of any particular decay mode ($x = \text{quark, lepton or gauge boson}$), obtained from LHC experiments. The corresponding quantities computed using Standard Model of electroweak interaction are denoted by $\sigma^{\text{SM}}(pp \rightarrow h)$ and

$\text{Br}^{\text{SM}}(h \rightarrow xx)$ respectively. For the present model, the signal strength of the SM-like scalar h_1 is then defined as,

$$R_1 = \frac{\sigma(pp \rightarrow h_1)}{\sigma^{\text{SM}}(pp \rightarrow h)} \frac{\text{Br}(h_1 \rightarrow xx)}{\text{Br}^{\text{SM}}(h \rightarrow xx)}, \quad (7.11)$$

where the quantities in the numerator of Eq. 7.11 are the production cross-section and branching ratio of SM-like Higgs boson h_1 which are computed using the present formalism. Now due to the mixing of scalar bosons, the coupling of SM-like Higgs boson to the SM fermions and gauge bosons are modified with respect to SM Higgs boson (h) by the cosine of mixing angle α whereas, the couplings of non-SM scalar boson h_2 to SM particles are multiplied by a factor $\sin \alpha$. Hence the ratio $\frac{\sigma(pp \rightarrow h_1)}{\sigma^{\text{SM}}(pp \rightarrow h)} = \cos^2 \alpha$ and from the similar argument one can yield $\frac{\sigma(pp \rightarrow h_2)}{\sigma^{\text{SM}}(pp \rightarrow h)} = \sin^2 \alpha$. The SM branching ratio can be expressed as $\text{Br}^{\text{SM}}(h \rightarrow xx) = \frac{\Gamma^{\text{SM}}(h \rightarrow xx)}{\Gamma^{\text{SM}}}$ where $\Gamma^{\text{SM}}(h \rightarrow xx)$ is the decay width of SM Higgs boson h into any final state particles and Γ^{SM} is the total SM Higgs decay width having mass $m_1 = 125$ GeV. Similarly one can derive the expression for branching ratio of h_1 into any specific decay channel in the present model $\text{Br}(h_1 \rightarrow xx) = \frac{\Gamma_1(h_1 \rightarrow xx)}{\Gamma_1}$ where $\Gamma_1(h_1 \rightarrow xx) = \cos^2 \alpha \Gamma^{\text{SM}}(h \rightarrow xx)$ is the decay width of h_1 decaying into xx final state while Γ_1 is the total decay width of h_1 in the present model. Hence, the signal strength of h_1 in Eq. 7.11 can be written in the form

$$R_1 = c_\alpha^4 \frac{\Gamma^{\text{SM}}}{\Gamma_1}, \quad (7.12)$$

where we have denoted $\cos \alpha$ as c_α . It is to be noted that apart from the decay into SM particles the SM-like scalar h_1 can also have invisible decay mode into dark matter particles. Therefore the total decay width of h_1 , in the present

model, can be written as

$$\Gamma_1 = c_\alpha^2 \Gamma^{\text{SM}} + \Gamma_1^{\text{inv}} . \quad (7.13)$$

In Eq. 7.13, Γ_1^{inv} is the invisible decay width h_1 for the channel $h_1 \rightarrow f_1 \bar{f}_1$. For $m_1 > 2m$ the expression of invisible decay width of h_1 is given by

$$\Gamma_1^{\text{inv}} = \frac{m_1 m^2}{8\pi v_s^2} s_\alpha^2 \left(1 - \frac{4m^2}{m_1^2} \right)^{3/2} , \quad (7.14)$$

since coupling between h_1 and dark matter candidate is proportional to $\frac{m}{v_s} s_\alpha$. In the above, v_s is the VEV of $\text{SU}(2)_H$ Higgs doublet Φ and $s_\alpha = \sin \alpha$. Similarly for the other scalar involved in our model, the signal strength R_2 is expressed as

$$R_2 = \frac{\sigma(pp \rightarrow h_2) \text{Br}(h_2 \rightarrow xx)}{\sigma^{\text{SM}}(pp \rightarrow h) \text{Br}^{\text{SM}}(h \rightarrow xx)} \quad (7.15)$$

with $\sigma(pp \rightarrow h_2)$ being the production cross-section of h_2 and $\text{Br}(h_2 \rightarrow xx)$ is decay branching ratio of h_2 to any final state. However in this case, the Standard Model predictions $\sigma^{\text{SM}}(pp \rightarrow h)$ and $\text{Br}^{\text{SM}}(h \rightarrow xx)$ are computed for the mass of SM Higgs boson $m_h = m_2$. Using the similar approach we used to calculate R_1 and replacing $h_1, \cos \alpha$ etc. by $h_2, \sin \alpha$ the signal strength R_2 of h_2 can be expressed as

$$R_2 = s_\alpha^4 \frac{\Gamma^{\text{SM}}(m_h = m_2)}{\Gamma_2} , \quad (7.16)$$

where $\Gamma^{\text{SM}}(m_h = m_2)$ is the total decay width of SM Higgs boson if it has mass $m_h = m_2$ while Γ_2 is the total decay width for the non-SM scalar boson h_2

$$\Gamma_2 = s_\alpha^2 \Gamma^{\text{SM}}(m_h = m_2) + \Gamma_2^{\text{inv}} . \quad (7.17)$$

The coupling between dark matter and h_2 depends on the factor $\frac{m}{v_s} \cos \alpha$. Hence, invisible decay width of h_2 (Γ_2^{inv}) for $m_2 > 2m$ is given as

$$\Gamma_2^{\text{inv}} = \frac{m_2 m^2}{8\pi v_s^2} c_\alpha^2 \left(1 - \frac{4m^2}{m_2^2}\right)^{3/2}. \quad (7.18)$$

As stated earlier, we consider h_1 with mass $m_1 = 125$ GeV to be the Higgs like scalar and infer $R_1 > 0.8$ [108] and invisible decay branching ratio $\text{Br}_{\text{inv}}^1 \leq 0.2$ [127] where $\text{Br}_{\text{inv}}^1 = \Gamma_{\text{inv}}^1/\Gamma^1$ is defined as the ratio of invisible decay width to the total decay width.

- **Dark matter relic density** - The DM relic density as measured by PLANCK

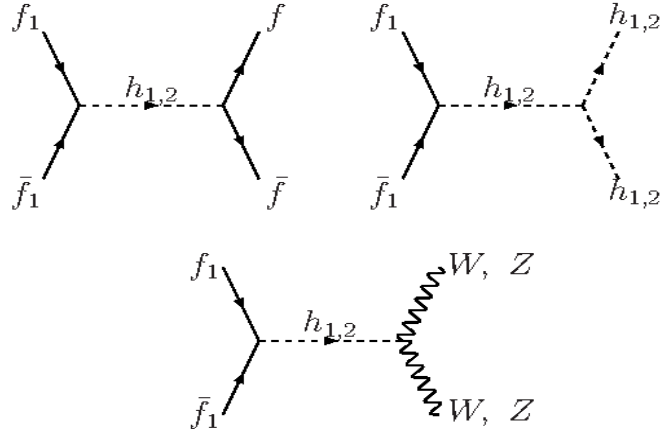


Figure 7.1: Feynman diagrams for dark matter annihilation into fermions (quarks and leptons), gauge bosons and scalars contributing to DM annihilation cross-section.

satellite experiment is given as [3]

$$\Omega_{\text{DM}} h^2 = 0.1199 \pm 0.0027. \quad (7.19)$$

In Eq. 7.19, h is the Hubble parameter measured in the unit of $100 \text{ km s}^{-1} \text{ Mpc}^{-1}$. Using Eqs. 4.16-4.18 described earlier in Chapter 4 (see Sect. 4.4), we calculate the relic density for the fermionic ($\text{SU}(2)_{\text{H}}$) dark matter

candidate in dark sector in our model by solving the Boltzmann equation. In order to obtain the freeze out temperature of DM and hence its relic density using Eqs. 4.17-4.18 we need to calculate the thermal average of the product between total DM annihilation cross-section (σ) and the relative velocity (v) of two annihilating DM particles. The expression for the thermally averaged DM annihilation cross-section into all possible final states is given as

$$\langle\sigma v\rangle = \frac{1}{8m^4 T_F K_2^2(m/T_F)} \int_{4m^2}^{\infty} ds \sigma(s) (s - 4m^2) \sqrt{s} K_1(\sqrt{s}/T_F), \quad (7.20)$$

where the factors K_i , ($i = 1, 2$) are the modified Bessel functions and \sqrt{s} being the centre of mass energy. In the present formalism dark matter candidate f_1 can annihilate into the SM particles through s -channel processes mediated by the scalar bosons h_1 and h_2 . In the above Eq. 7.20, $\sigma(s)$ denotes the total annihilation cross-section of dark matter into all possible final states which are allowed by the Lagrangian given in Eq. 7.2. Feynman diagrams for different annihilation channels of f_1 are shown in Fig. 7.1. The expressions of σv for different final state annihilation of dark matter into SM particles are derived from the Feynman diagrams shown in Fig. 7.1. The value of σv obtained for DM annihilation into SM fermion and antifermion pairs ($f\bar{f}$) at the final state is of the form

$$\sigma_{v f\bar{f}} = N_c \frac{m^2}{v_s^2} \frac{s_\alpha^2 c_\alpha^2}{8\pi} \frac{m_f^2}{v^2} \left(1 - \frac{4m_f^2}{s}\right)^{3/2} F(s, m_1, m_2) \quad (7.21)$$

where

$$F(s, m_1, m_2) = (s - 4m^2) \left[\frac{1}{(s - m_1^2)^2 + m_1^2 \Gamma_1^2} + \frac{1}{(s - m_2^2)^2 + m_2^2 \Gamma_2^2} - \frac{2(s - m_1^2)(s - m_2^2) + 2m_1 m_2 \Gamma_1 \Gamma_2}{[(s - m_1^2)^2 + m_1^2 \Gamma_1^2][(s - m_2^2)^2 + m_2^2 \Gamma_2^2]} \right].$$

In Eq. 7.21, m is the DM mass and m_f is the mass of specific fermion ($f =$ quark or lepton). The terms v and v_s in Eq. 7.21 are the vacuum expectation values of SM Higgs doublet and dark Higgs doublet, N_c is the colour quantum number (3 for quarks and 1 for leptons). Γ_1, Γ_2 in the expression of $F(s, m_1, m_2)$ are the total decay widths of the scalar bosons h_1, h_2 and the expressions of Γ_1 and Γ_2 are given in Eqs. 7.13, 7.17. We also calculate σv for W^+W^- and ZZ channels which proceed through the s -channel exchange of scalar bosons h_1, h_2 (see Fig. 7.1). The expressions of $\sigma v_{W^+W^-}$ and σv_{ZZ} are furnished below

$$\sigma v_{W^+W^-} = \frac{m^2}{v_s^2} \frac{s_\alpha^2 c_\alpha^2}{8\pi s} \left(1 - \frac{4m_W^2}{s}\right)^{1/2} \left(\frac{2m_W^2}{v}\right)^2 \left(1 + \frac{(s/2 - m_W^2)^2}{2m_W^4}\right) F(s, m_1, m_2), \quad (7.22)$$

and

$$\sigma v_{ZZ} = \frac{m^2}{v_s^2} \frac{s_\alpha^2 c_\alpha^2}{16\pi s} \left(1 - \frac{4m_Z^2}{s}\right)^{1/2} \left(\frac{2m_Z^2}{v}\right)^2 \left(1 + \frac{(s/2 - m_Z^2)^2}{2m_Z^4}\right) F(s, m_1, m_2). \quad (7.23)$$

In the above, m_W and m_Z denotes the respective masses of W and Z bosons. Annihilations of DM particles into scalar bosons h_1 and h_2 are also taken into account. The process of DM annihilation into scalars h_1 or h_2 is also scalar mediated, depends on scalar couplings between h_1 and h_2 . The s -channel annihilation cross-section of f_1 annihilating into the pairs of h_1 and h_2 , calculated using $f_1 \bar{f}_1 \rightarrow h_i h_i$, $i = 1, 2$ annihilation diagram, takes the following form

$$\begin{aligned} \sigma v_{h_1 h_1} = & \frac{1}{16\pi s} \frac{m^2}{v_s^2} \left(1 - \frac{4m_1^2}{s} + \frac{4m_1^2(m_1^2 - 1)}{s^2}\right)^{1/2} (s - 4m^2) \left[\frac{s_\alpha^2 \lambda_{111}^2}{(s - m_1^2)^2 + m_1^2 \Gamma_1^2} \right. \\ & \left. + \frac{c_\alpha^2 \lambda_{211}^2}{(s - m_2^2)^2 + m_2^2 \Gamma_2^2} - \frac{2s_\alpha c_\alpha \lambda_{111} \lambda_{211} ((s - m_1^2)(s - m_2^2) + 2m_1 m_2 \Gamma_1 \Gamma_2)}{[(s - m_1^2)^2 + m_1^2 \Gamma_1^2][(s - m_2^2)^2 + m_2^2 \Gamma_2^2]} \right], \end{aligned} \quad (7.24)$$

and

$$\begin{aligned} \sigma_{\nu h_2 h_2} = & \frac{1}{16\pi s} \frac{m^2}{v_s^2} \left(1 - \frac{4m_2^2}{s} + \frac{4m_2^2(m_2^2 - 1)}{s^2} \right)^{1/2} (s - 4m^2) \left[\frac{s_\alpha^2 \lambda_{122}^2}{(s - m_1^2)^2 + m_1^2 \Gamma_1^2} \right. \\ & \left. + \frac{c_\alpha^2 \lambda_{222}^2}{(s - m_2^2)^2 + m_2^2 \Gamma_2^2} - \frac{2s_\alpha c_\alpha \lambda_{122} \lambda_{222} ((s - m_1^2)(s - m_2^2) + 2m_1 m_2 \Gamma_1 \Gamma_2)}{[(s - m_1^2)^2 + m_1^2 \Gamma_1^2][(s - m_2^2)^2 + m_2^2 \Gamma_2^2]} \right], \end{aligned} \quad (7.25)$$

where, λ_{ijk} is the coupling for the vertex involving three scalar fields $h_i h_j h_k$. The expressions for the scalar couplings λ_{111} , λ_{211} , λ_{122} and λ_{222} are given as follows

$$\begin{aligned} \lambda_{111} &= \lambda_1 v c_\alpha^3 - \lambda_2 v_s s_\alpha^3 + \frac{1}{2} \lambda_3 (v c_\alpha s_\alpha^2 - v_s s_\alpha c_\alpha^2), \\ \lambda_{222} &= \lambda_1 v s_\alpha^3 + \lambda_2 v_s c_\alpha^3 + \frac{1}{2} \lambda_3 (v s_\alpha c_\alpha^2 + v_s c_\alpha s_\alpha^2), \\ \lambda_{211} &= 3(\lambda_1 v c_\alpha^2 s_\alpha - \lambda_2 v_s s_\alpha^2 c_\alpha) + \frac{1}{2} \lambda_3 (v_s (c_\alpha^3 - 2s_\alpha^2 c_\alpha) + v (s_\alpha^3 - 2c_\alpha^2 s_\alpha)), \\ \lambda_{122} &= 3(\lambda_1 v s_\alpha^2 c_\alpha - \lambda_2 v_s c_\alpha^2 s_\alpha) + \frac{1}{2} \lambda_3 (v_s (-s_\alpha^3 + 2c_\alpha^2 s_\alpha) + v (c_\alpha^3 - 2s_\alpha^2 c_\alpha)). \end{aligned}$$

We calculate the thermally averaged annihilation cross-section of the present DM candidate using Eqs. 7.20-7.25 We then compute the freeze out temperature T_F by solving Eq. 4.18 and finally obtain the relic density of f_1 at the present epoch from Eq. 4.17.

- **DM Direct Detection** - Direct detection of DM particle is based on the scattering of the DM particle with the target nucleus of the detector material. Fermionic dark matter in the present model can undergo elastic scattering with the detector nucleus. This elastic scattering of the DM and the nucleus will transfer a recoil energy to the target nucleus which is then calibrated. From the non-observance of such elastic scattering events the direct detection experiments give the upper bound of elastic scattering cross-sections for different possible masses of dark matter. The scattering cross-section is expressed as cross-

section per nucleon for enabling direct comparison of the results from different experiments. In the present model DM fermion of mass m can interact with the target nucleus through t-channel Higgs mediated processes through both h_1 and h_2 . The spin-independent (SI) elastic scattering cross-section off the detector material normalised to per nucleon can be written as [130]

$$\sigma_{\text{SI}} = \frac{\sin^2 2\alpha m^2}{4\pi v_s^2} m_r^2 \left(\frac{1}{m_1^2} - \frac{1}{m_2^2} \right)^2 \lambda_p^2 \quad (7.26)$$

where $m_r = \frac{mm_p}{m+m_p}$ is the reduced mass for the DM-nucleon system and λ_p [130] is given in terms of the form factors f_q , proton mass m_p as

$$\lambda_p = \frac{m_p}{v} \left[\sum_q f_q + \frac{2}{9} \left(1 - \sum_q f_q \right) \right] \simeq 1.3 \times 10^{-3}. \quad (7.27)$$

Using Eqs. 7.26-7.27, we calculate the spin independent elastic scattering cross-section of the DM fermion off the nucleon and compare it with the experimental bounds from LUX [28].

Note that both DM annihilation cross-section and DM-nucleon scattering cross-section depend on an effective coupling $g_{eff} = \left| \frac{m}{v_s} s_\alpha c_\alpha \right|$ (Eqs. 7.21-7.26). This effective coupling is a useful parameters to explain the dark matter phenomenology in the present framework. Further discussions on the effective coupling are given later in Sec. 7.4.

- **DM Indirect Detection** The existence of DM has now been well established from gravitational evidences in astrophysical scale. Indirect search of DM focuses on the non-gravitational search of DM candidate and explores the particle physics nature of DM. The astrophysical sites such as galactic centre (GC), dwarf galaxies etc. are of great interest since dark matter can be trapped and accumulate at GC due to the enormous gravity in the region of GC and

the mass to luminosity ratio of dwarf galaxies indicate the presence of dark matter in large magnitude. These sites are suitable for indirect search of DM as DM particles trapped in these regions can undergo annihilation into various SM particles which can further produce gamma rays, neutrinos etc. Thus any observed excess in the fluxes of γ -ray, positron, anti-proton from such sites can indicate DM annihilation processes in those sites if other astrophysical phenomena cannot explain the observed excess. Fermi-LAT [131] searches for the excess emission of γ -rays originating from GC and dwarf galaxies. Observation of the excess in e^+/e^- and p/\bar{p} flux is performed by AMS [45] experiment. In this Section we will study Fermi-LAT observed gamma ray flux results from the centre of Milky Way and surrounding dwarf spheroidal galaxies (dSphs).

The expression for the differential γ -ray flux obtained from a region of interest (ROI) subtends a solid angle $d\Omega$ centered at GC is given as

$$\frac{d\Phi}{dE d\Omega} = \frac{1}{8\pi m_{DM}^2} J \sum_f \langle \sigma v \rangle_f \frac{dN_f}{dE_\gamma}, \quad (7.28)$$

where $\langle \sigma v \rangle_f$ is the average thermal annihilation cross-section of DM particles annihilating into final state particle f and $\frac{dN_f}{dE_\gamma}$ is the photon energy spectrum of DM annihilation into the same. The factor J appearing in Eq. 7.28 is related to the quantity of dark matter present at the astrophysical site considered and is expressed in terms of dark matter density as

$$J = \int_{\text{los}} \rho^2(r(s, \theta)) ds. \quad (7.29)$$

In Eq. 7.29 the line of sight (los) integral is performed over an angle θ , is the angular aperture between the line connecting GC to the Earth and the direction of line of sight. In the above Eq. 7.29, $r = \sqrt{r_\odot^2 + s^2 - 2r_\odot s \cos \theta}$

where $r_\odot = 8.5$ kpc, is the distance to the Sun from GC. It is clear from the expression of Eq. 7.29 that value of J factor is dependent on the nature of the chosen $\rho(r)$ factor i.e, DM halo density profile $\rho(r)$. In the present work, we consider Navarro-Frenk-White (NFW) [5] halo profile. DM density distribution for the NFW halo profile is given as

$$\rho(r) = \rho_0 \frac{(r/r_s)^{-\gamma}}{(1 + r/r_s)^{3-\gamma}}. \quad (7.30)$$

where $r_s = 20$ kpc is the characteristic distance and ρ_0 is normalised to local DM density i.e., $\rho_\odot = 0.4 \text{ GeV cm}^{-3}$ at a distance r_\odot from GC.

The analysis by Daylan et. al. [59] of Fermi-LAT data suggests an excess in γ -ray in the γ energy range of 2-3 GeV at GC. The same analysis demonstrates that this excess can be explained by the annihilation of 31-40 GeV DM into $b\bar{b}$ with $\langle\sigma v\rangle_{b\bar{b}} = 1.4 - 2.0 \times 10^{-26} \text{ cm}^3\text{s}^{-1}$. In this work [59], inner galaxy gamma ray flux (5° from GC) is calibrated using NFW halo profile with $\gamma = 1.26$ and local DM density $\rho_\odot = 0.3 \text{ GeV cm}^{-3}$. In a recent work by Calore, Cholis and Weniger (CCW) [60] detailed analysis is performed for the GC γ -rays along with the systematic uncertainties using 60 galactic diffusion excess (GDE) models. Results from CCW analysis provides a best fit for DM annihilation into $b\bar{b}$ having mass $49_{-5.4}^{+6.4} \text{ GeV}$ with $\langle\sigma v\rangle_{b\bar{b}} = 1.76_{-0.27}^{+0.28} \times 10^{-26} \text{ cm}^3\text{s}^{-1}$. However, CCW analysis of galactic centre excess (GCE) for gamma ray have also considered generalised NFW profile ($\gamma=1.2$, $\rho_\odot = 0.4 \text{ GeV cm}^{-3}$) for a different region of interest (ROI) with galactic latitude $|l| \leq 20^\circ$ and longitude $|b| \leq 20^\circ$ masking out inner $|b| \leq 2^\circ$. In another work P. Agrawal et. al. [132] reported that annihilation of heavier dark matter (upto 165 GeV for $b\bar{b}$ channel) can also explain the observed GCE in γ -ray when uncertainties in DM halo profile (NFW) and the J -factor are taken into account. However in the present work,

we do not consider any such uncertainties in halo profiles or J values and use the canonical NFW halo profile used in CCW analysis. Using Eqs. 7.28-7.30, we calculate the γ -ray flux (in $\text{GeV cm}^{-2} \text{s sr}^{-1}$) for the ROI described in CCW analysis for Fermi-LAT data. As mentioned earlier we consider for our calculations the NFW profile with $\gamma = 1.2$ and $\rho_{\odot} = 0.4 \text{ GeV cm}^{-3}$.

Apart from the GC region, dwarf galaxies of the Milky-Way galaxy are also of great significance for indirect search of DM as these galaxies are supposed to be rich in dark matter. Recent analyses of γ -ray fluxes from 15 Milky-Way dSphs reported by Fermi-LAT [61] provide a limit on DM mass and corresponding thermally averaged annihilation cross-section $\langle\sigma v\rangle_f$ into different channels f (τ and b). Fermi-LAT have used their 6 year data collected by Fermi Large area Telescope and performed an analysis for 15 dSphs using “pass-8 event level analysis” (see [61] and references therein). In another work [62] Fermi-LAT in collaboration along with Dark Energy Survey (DES) collaboration also provide similar bound on $\langle\sigma v\rangle_f$ where they include data for 8 new dSphs. For both the analysis presented in [61, 62] a canonical NFW halo profile ($\gamma = 1$) is considered, and the astrophysical J factors are measured over a solid angle $\Delta\Omega = 2.4 \times 10^{-3} \text{ sr}$ with angular radius 0.5° . Independent searches carried out by Fermi-LAT [61] and DES-Fermi-LAT collaboration on 15 previously discovered and 8 recently discovered different dSphs reported no significant excess in observed γ -ray. Results from the DES dSphs [62] also predicts an upper bound to the observed γ -ray energy flux with 95% confidence limit (C.L.) for 8 newly found dSphs. Gamma ray flux for dwarf galaxies when integrated for an energy range extending over a region of solid angle $\Delta\Omega$ is expressed as

$$\Phi = \frac{\langle\sigma v\rangle}{8\pi m_{DM}^2} J \int_{E_{\min}}^{E_{\max}} \frac{dN}{dE_{\gamma}} dE_{\gamma} , \quad (7.31)$$

where $\frac{dN}{dE_\gamma}$ is the γ -ray. The expression of flux presented in Eq. 7.31 is calculated for a single final state annihilation of DM. Hence, summation over different final channels is not needed. Form of J factor appearing in Eq. 7.31 is different from Eq. 7.29 and written as

$$J = \int_{\Delta\Omega} \int_{\text{los}} \rho^2(r(s, \theta)) ds, \quad (7.32)$$

calculated over a solid angle $\Delta\Omega = 2.4 \times 10^{-3}$ sr subtended by the ROI (0.5 $^\circ$ angular radius) for NFW halo profile ($\gamma = 1$). The density distribution function for NFW profile with $\gamma = 1$ is then

$$\rho(r) = \rho_0 \frac{r_s^3}{r(r_s + r)^2}, \quad (7.33)$$

where r_s is the NFW scale radius and ρ_0 represents the characteristic density for the dSphs. In the case of Fermi-LAT analysis, J factors for different dSphs are adopted from Ref. [61]. We use values of J factor from [62] for computing gamma ray flux for 8 DES dSphs for the dark matter candidates in our model. However, it is to be noted that J factors for DES dSphs candidates are obtained assuming the point like dSphs instead of having spatial extension (as in the case of [61]) to avoid the uncertainties in halo profile arising from spatial extension. Calculation of gamma ray flux is also based on the assumption that the spectrum $\frac{dN}{dE_\gamma}$ follows the conventional power law $\frac{dN}{dE_\gamma} \sim \frac{1}{E^2}$. As mentioned earlier, study of 15 dSphs by Fermi-LAT and 8 other dSphs by DES-Fermi-LAT collaboration found no significant excess in γ -ray from these dwarf galaxies. However, a recent search on a newly discovered dwarf galaxy Reticulum 2 (Ret2) in a work by Geringer-Sameth et. al [133] has reported an excess in observed γ -ray signal. In the present work, we calculate the γ -ray flux for annihilation of hidden $SU(2)_H$ fermionic dark matter into γ -ray through different SM final states and explore

whether the model can account for GCE in γ -ray and also satisfies the bounds on gamma ray flux from dwarf satellite galaxies.

As mentioned earlier, in the present model dark matter candidate (f_1) is fermionic in nature and it interacts with the visible world (SM particles) through the exchange of two real scalar bosons h_1 and h_2 . As a result the annihilation cross-sections of the DM dark candidate f_1 into the final states that composed of SM particles (mainly light quarks and leptons) are proportional to the square of relative velocity (v^2) between the annihilating dark matter particles (p wave process). Now the averaged DM relative velocity is proportional to $\sim \sqrt{3/x}$ [134]-[135] with $x = \frac{m}{T}$ is a dimensionless quantity and T being the temperature of the Universe. Hence, in our model, the thermally averaged annihilation cross-section used for computing DM relic density, at $x \sim 20 - 30$, is different from the annihilation cross-section (for $x \sim 3 \times 10^6$ [134]-[135]) needed to calculate γ -ray flux at the galactic centre and dwarf galaxies. The latter quantity is velocity suppressed as the average DM relative velocity is $\sim 10^{-3}$ when the annihilation of DM occurs at the GC. Among all the annihilation channels of f_1 , the annihilation mode $f_1 \bar{f}_1 \rightarrow b \bar{b}$ plays a significant role for the γ -ray excess observed from GC and dwarfs satellite galaxies as it is the most dominant annihilation channel for the considered mass range of DM. In order to explain the GC gamma-excess by DM annihilation to $b \bar{b}$, the annihilation cross-section should be $\sim 1.76_{-0.27}^{+0.28} \times 10^{-26} \text{ cm}^3/\text{s}$ [60]. Although in the present case, the thermally averaged annihilation cross-section for the $b \bar{b}$ annihilation is quite small, however the quantity $\langle \sigma v \rangle_{b \bar{b}}$ can be significantly enhanced using Breit-Wigner resonant enhancement mechanism [134]-[135]. Breit-Wigner enhancement occurs only when the mass of the dark matter (m) is nearly equal to half of the mediator mass (in our case it is the mass of h_2). Therefore, we have defined the mass of the hidden sector scalar boson (h_2) and the centre of mass energy \sqrt{s} in the

following way

$$m_2^2 = 4m^2(1 - \delta) \text{ and } s = 4m^2(1 + z) , \quad (7.34)$$

where $\delta < 0$ represents the physical pole and z is the measure of excess centre of momentum energy scaled by $4m^2$. In terms of z , Eq. 7.20 for the $b\bar{b}$ annihilation channel, can now be written as

$$\langle \sigma v \rangle_{b\bar{b}} = \frac{4x}{K_2^2(x)} \int_0^{z_{eff}} dz \sigma(z)_{b\bar{b}} z \sqrt{1+z} K_1(2x \sqrt{1+z}) \quad (7.35)$$

with the expression of $\sigma(z)_{b\bar{b}}$ is given by ⁴

$$\sigma(z)_{b\bar{b}} = \frac{g_c}{4m^2} \frac{\sqrt{z}}{1+z} \frac{\left(1 + z - \frac{m_b^2}{m^2}\right)^{3/2}}{[(z + \delta)^2 + \gamma_2^2(1 - \delta)^2]} , \quad (7.36)$$

and

$$g_c = \frac{N_c}{16\pi} \left(\frac{m \cos \alpha}{v_s} \frac{m_b \sin \alpha}{v} \right)^2 \quad (7.37)$$

where $\gamma_2 = \frac{\Gamma_2}{m_2}$, Γ_2 being the total decay width of h_2 of mass m_2 . It is to be noted that the upper limit of the above integration should be ∞ (see Eq. 7.20), however the integrand becomes negligibly small when z approaches to $z_{eff} \sim \max[4/x, 2|\delta|]$ for $\delta < 0$ [124],[135]. Using the above prescription, we calculate the thermally averaged annihilation cross-section $\langle \sigma v \rangle_{b\bar{b}}$ of the dark matter candidate f_1 for GC and dwarf spheroidal galaxies. The actual values of $\langle \sigma v \rangle_{b\bar{b}}$, γ_2 and δ for the two chosen bench mark points (BP1, BP2) are given in Table 7.1 of Sec. 7.4. We have found that for $|\delta| \sim 10^{-3}$ the annihilation

⁴Since the Breit-Wigner enhancement occurs when $m \sim m_2/2$, as a result only the term proportional to $\frac{1}{(s-m_2^2)^2 + m_2^2 \Gamma_2^2}$ will dominantly contribute to the annihilation cross-section appearing in Eq. 7.21.

cross-section $\langle\sigma v\rangle_{b\bar{b}} \sim 1.9 \times 10^{-26} \text{ cm}^3/\text{s}$ which can explain the excess of gamma ray flux in GC⁵.

7.4 Calculational procedures and Results

In this section we present the computation of dark matter annihilation cross-sections as also the DM-nucleon elastic scattering cross-sections. They are required for the calculation of relic densities and the comparison of the latest DM scattering cross-section bound given by the LUX direct detection experiment. The invisible decay widths and signal strengths for the SM-like scalar is also calculated in order to constrain the model parameter space. The gamma ray flux are then computed within the framework of $SU(2)_H$ fermionic dark matter for galactic centre as also for dwarf galaxies and the results are compared with the experimental analysis.

7.4.1 Constraining the model parameter space

The fermionic dark matter in the present model can annihilate through scalar mediated (h_1 and h_2) s -channel processes. As mentioned in Sec. 7.3, the model parameter space is first constrained by the vacuum stability conditions given in Eq. 7.9. The signal strengths R_1 and R_2 for the Higgs doublets h_1 (SM) and h_2 (dark sector) are then computed using Eq. 7.12 and Eq. 7.16. With the chosen constraints on R_1 ($R_1 \geq 0.8$, Ref. [108]) the invisible decay branching ratio of SM-like Higgs Br_{inv}^1 is calculated and the parameter space is further constrained by LHC experiment limit of Br_{inv}^1 ($\text{Br}_{\text{inv}}^1 \leq 0.2$ [127]). The parameter space thus constrained is then used to compute the thermal averaged annihilation cross-section $\langle\sigma v\rangle$ of the

⁵Similar results for Breit-Wigner enhancement of dark matter annihilation cross-section have been reported in [124].

present fermionic dark matter candidate and the relic density is obtained by solving the Boltzmann equation (using Eqs. 4.16-4.18 and Eq. 7.20). The annihilation cross-sections are computed with the calculated analytical formulae given in Eqs. 7.21-7.25 with two choices of VEV for Φ (dark Higgs doublet) namely $v_s = 246$ GeV and 500 GeV. In our calculation we consider the mass m_1 of the SM-like Higgs boson h_1 to be 125 GeV. The calculation is performed for two values of the dark sector scalar h_2 masses and they are $m_2 = 100$ GeV and 110 GeV. These relic densities are compared with the dark matter relic density given by PLANCK [3]. Thus PLANCK result further constrains the parameter space of our model. With this available parameter space we evaluate the dark matter-nucleon spin independent scattering cross-section (σ_{SI}) for the purpose of comparing our results with those given by the dark matter direct detection experiments such as LUX, XENON100 etc. In this way we restrict our model parameter space by different experimental results.

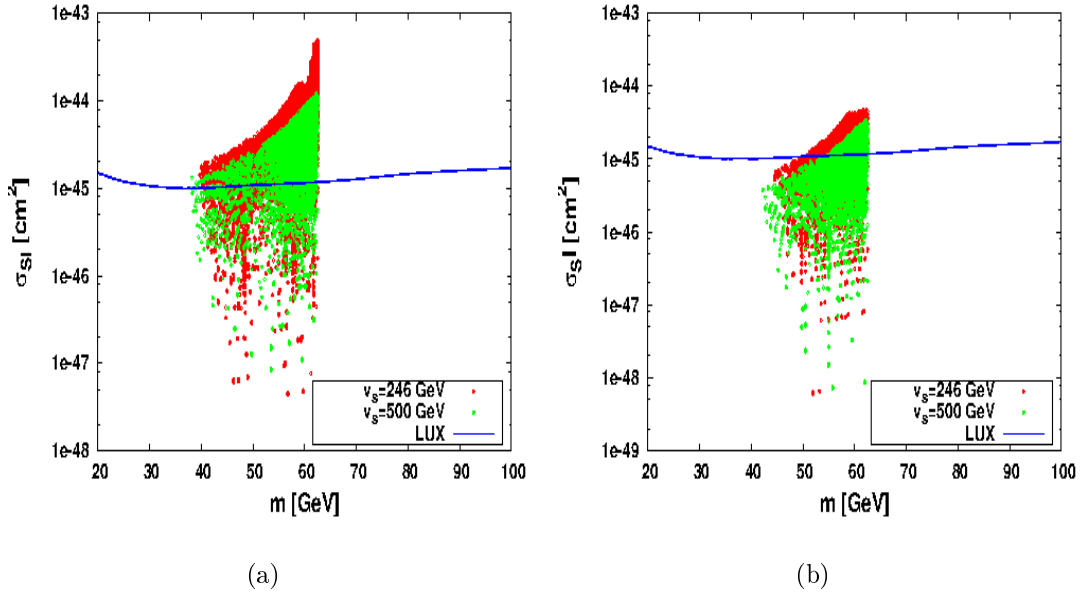


Figure 7.2: The allowed range of $m - \sigma_{\text{SI}}$ parameter space obtained for $m_2 = 100$ GeV (left panel) and $m_2 = 110$ GeV (right panel) plotted using the bounds from vacuum stability, LHC constraints on SM Higgs and relic abundance of DM obtained from PLANCK [3]. Limits on DM-nucleon cross-section from LUX [28] is also plotted (blue line) for comparison.

In Fig. 7.2a and Fig. 7.2b we show the calculated values of σ_{SI} with different DM mass in the present model where the conditions from vacuum stability, bound on SM Higgs signal strength and DM relic density results from PLANCK have been imposed. We first choose certain values of m_1 and m_2 and vary the couplings λ_i , $i = 1$ to 3 (satisfying vacuum stability conditions given in Eq. 7.9) for two different values of v_s which also constrain the mixing angle α through the Eq. 7.7. Here we want to mention that we have varied λ_1 and λ_2 in the range 0 to 0.2 with the values of both λ 's are evenly spread within the considered range. Consequently the value of the parameter λ_3 becomes fixed by the vacuum stability criteria given in Eq. 7.9 which is also varied with equal interval in the range $|\lambda_3| < 2\sqrt{\lambda_1\lambda_2}$. The model parameter space thus obtained is then further constrained by imposing the conditions $R_1 > 0.8$ and $Br_{\text{inv}}^1 < 0.2$ from LHC results. Using this restricted model parameter space satisfying both vacuum stability and LHC bounds, we therefore calculate the relic density of the dark matter candidate f_1 by solving the Boltzmann equation (Eq. 4.16) for different values of DM mass. Finally, we consider specific range of model parameter space which is in agreement with DM relic density reported by PLANCK experiment and for these parameter space we compute the spin-independent direct detection cross-section using Eqs. 7.26-7.27. In this way the viable model parameter space for the dark matter candidate f_1 is obtained. Fig. 7.2a is for the case $m_2 = 100$ GeV while Fig. 7.2b is for the case $m_2 = 110$ GeV. The upper limit on σ_{SI} for different values of DM mass, obtained from LUX DM direct search experiment, are also shown in Fig. 7.2a-b by the blue line for comparison. The red and green scattered regions as shown in Fig. 7.2a-b correspond to two choices of $v_s=246$ GeV and 500 GeV respectively. From Fig. 7.2a it can be observed that only the region near the resonances of scalar bosons h_1 and h_2 is in agreement with the upper limit on σ_{SI} predicted by LUX. It is also seen from Fig. 7.2a that the choice of v_s do not alter the allowed range of parameter space. Observation of Fig. 7.2b yields that, apart from

SM Higgs resonance region ($m \sim m_1/2$) there exists another allowed range of $m - \sigma_{\text{SI}}$ parameter space in the vicinity of non-SM scalar resonance ($m \sim m_2/2$). Note that variation of m with σ_{SI} depicted in Fig. 7.2b depends only on the masses of scalar bosons and does not suffer any significant change due to change in v_s . The non-SM Higgs signal strength R_2 (calculated using Eq. 7.16) for the valid $m - \sigma_{\text{SI}}$ parameter space shown in Figs. 7.2a-b is very small and $R_2 < 0.2$.

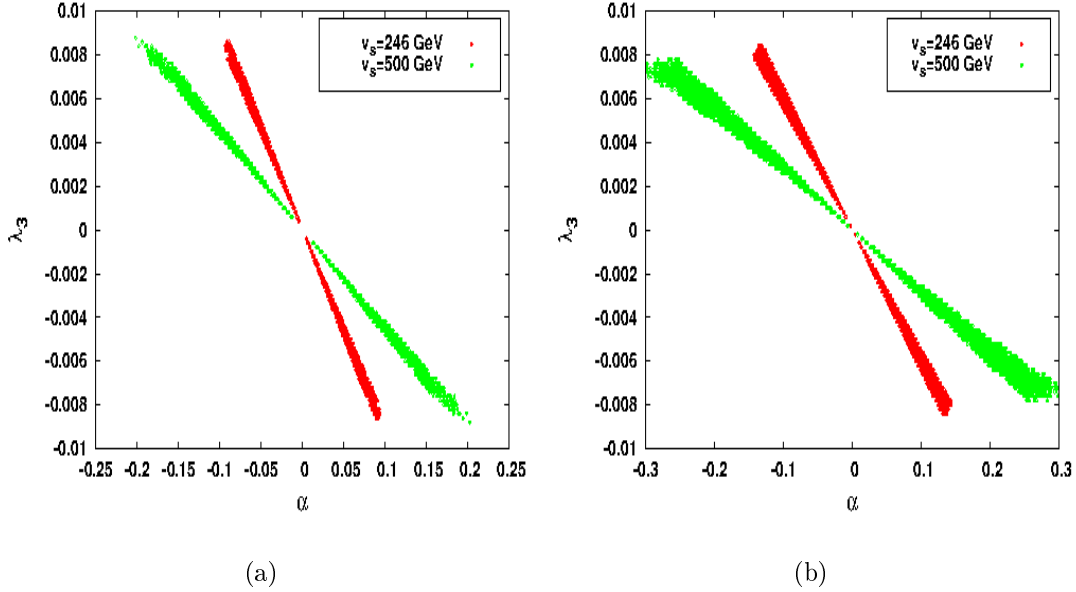


Figure 7.3: The valid model parameter space in $\lambda_3 - \alpha$ (in deg) plane obtained for the case of $m_2 = 100$ GeV (lef panel) and $m_2 = 110$ GeV (right panel) satisfying the limits from vacuum stability, LHC findings, PLANCK DM relic abundance and direct detection limits on σ_{SI} from LUX experiment.

In this work, we assumed two values for VEV v_s (246 GeV and 500 GeV) for the hidden sector Higgs doublet Φ_{HS} . From Eq. 7.6, we observe that the mixing between the scalars h_1 and h_2 depends on the VEV of Φ_{HS} and H . Hence, the choice of v_s may change the range of available model parameter space. In Figs. 7.3a-b, we plot the variation of Higgs mixing angle α between h_1 and h_2 with λ_3 for $m_2=100$ GeV and 110 GeV with $m_1=125$ GeV (mass of SM-like Higgs). Needless to mention the region of $\alpha - \lambda_3$ space shown in Figs. 7.3a-b are consistent with the bounds form

vacuum stability, SM Higgs signal strength from LHC, relic abundance of DM from PLANCK and limits on DM-nucleon scattering cross-section from LUX direct DM search experiment. Plots in Fig. 7.3 are produced using similar method we have applied previously to obtain viable model parameter space for Fig. 7.2. However $\alpha - \lambda_3$ plane in Fig. 7.3 is further constrained by imposing LUX DM direct detection bound. The plots in Fig. 7.3a are for the case when $m_1 = 125$ GeV and $m_2 = 100$ GeV while plots in Fig. 7.3b represent the allowed $\alpha - \lambda_3$ parameter space when $m_2 = 110$ GeV for the fixed value of $m_1 = 125$ GeV. The green and blue regions in Fig. 7.3a and Fig. 7.3b correspond to two different values for VEV of dark Higgs doublet, $v_s = 246$ GeV and $v_s = 500$ GeV respectively. From Fig. 7.3a ($m_2 = 100$ GeV case) one observes that for both the considered values of VEV v_s , the mixing parameter λ_3 remains small and is confined within the region $|\lambda_3| < 0.01$. For the case when $v_s = 246$ GeV (the red region of Fig. 7.3a), the limit of mixing angle α ranges between -0.1 to 0.1 . However these range (of mixing angle) varies within the limit $|\alpha| \leq 0.2$ when $v_s = 500$ GeV is chosen (green region shown in Fig. 7.3a). Study of the $\lambda_3 - \alpha$ plots in Fig. 7.3b (plotted for $m_2 = 110$ GeV) reveals that for both the values of v_s considered in Fig. 7.3, the mixing parameter is small ($|\lambda_3| < 0.01$). The mixing angle α is bounded in the range $|\alpha| < 0.15$ and $|\alpha| \leq 0.30$ for $v_s = 246$ GeV and 500 GeV respectively.

7.4.2 Calculation of gamma ray signals from galactic centre and dwarf galaxies

In this Section, we calculate the γ -ray flux from the galactic centre and dwarf galaxies for the fermionic dark matter in framework of the present model and compare our results with the experimental observations. For these calculations we consider two benchmark points (BPs) from the restricted parameter space that satisfy both

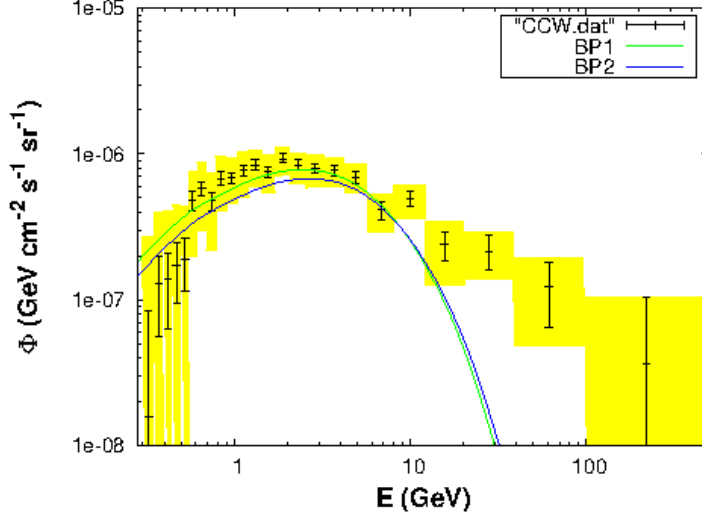


Figure 7.4: Comparison of the GC γ -ray flux data from [60] with those calculated for benchmark points in Table 7.1.

BP	v_s in GeV	m_2 in GeV	m in GeV	δ	γ_2	σ_{SI} in cm^2	$\langle\sigma v\rangle_{b\bar{b}}$ cm^3/s
BP1	246.0	100.242	50.0	-4.86e-03	0.60e-06	2.89e-46	1.98e-26
BP2	500.0	110.321	55.0	-5.85e-03	0.43e-06	1.13e-46	1.90e-26

Table 7.1: Benchmark points obtained from the constrained model parameter space in agreement with the bounds from vacuum stability, SM Higgs signal strength from LHC, DM relic density from PLANCK and LUX DM search bounds on DM-nucleon scattering cross-section.

theoretical and experimental bounds (mainly vacuum stability, LHC constraints on SM Higgs signal, PLANCK results for relic abundance and direct detection limit on $m - \sigma_{SI}$ from LUX) for two choices of h_2 mass, mainly, $m_2 = 100$ GeV and 200 GeV. In Table 7.1 we tabulate the chosen BPs along with model parameters. There are two chosen sets of benchmark points in Table 7.1 and we denote them as BP1 and BP2. The GC gamma ray flux is calculated using Eqs. 7.28-7.30 for the BPs tabulated in Table 7.1. The annihilation cross-section $\langle\sigma v\rangle_{b\bar{b}}$ for the dark matter particle is calculated using Breit-Wigner enhancement technique using Eqs. 7.34-7.37 discussed in Sec. 7.3. The gamma ray spectrum $\frac{dN}{dE}$ in Eq. 7.28 is obtained from

Cirelli [136] for annihilation of DM into any specific channel. The gamma ray spectra for BP1 and BP2 are then calculated for the specified region of interest adopted from Ref. [60] ($|l| \leq 20^{\circ}$, $2^{\circ} \leq |b| \leq 20^{\circ}$) using NFW halo profile (with $\gamma = 1.2$, $\rho_{\odot} = 0.4 \text{ GeV cm}^{-3}$). In Fig. 7.4, we show the calculated GC gamma ray flux (in $\text{GeV cm}^{-2} \text{ sr}^{-1}$) for our proposed DM candidate with BP1 and BP2. We also show in Fig. 7.4 the CCW data for comparison. Green and blue lines in Fig. 7.4 represent the calculated γ -ray spectra for BP1 and BP2 respectively. Both the benchmarks points are in agreement with the findings from GC gamma ray study presented in CCW [60]. From Fig. 7.4 it can be observed that flux calculated using the set BP1 ($m=50 \text{ GeV}$) is in better agreement with the findings from CCW analysis.

We now further investigate how well the DM candidate in our model can explain the observed extragalactic γ -ray signatures from various dwarf galaxies. From their six years observations on 15 dwarf galaxies, the Fermi-LAT experiment did not obtain any significant excess of γ -rays. Fermi-LAT collaboration [61] however in a recent work provides combined bound on DM mass and thermally averaged DM annihilation cross-section into SM particles for these 15 dSphs. A similar bound in $m - \langle\sigma v\rangle_f$ plane is also presented recently in an another work [62] for eight new dSphs jointly by Fermi-LAT and DES collaboration. In this work we calculate thermally averaged annihilation cross-section of DM annihilating into SM sector in our model and compare them with experimental results given by [61, 62]. In Fig. 7.5, we plot the bounds on DM annihilation cross-section $\langle\sigma v\rangle_{b\bar{b}}$ (for the annihilation channel $DMDM \rightarrow b\bar{b}$) with dark matter mass m obtained from galactic [60] and extragalactic [61, 62] γ -ray search experiments. We calculate the variations of the same plotted in Fig. 7.5 for the benchmark points BP1 (for $m_2 = 100 \text{ GeV}$) and BP2 (for $m_2 = 110 \text{ GeV}$) considered in our model.

Black contours shown in Fig. 7.5 are the 1σ , 2σ and 3σ contours given by the

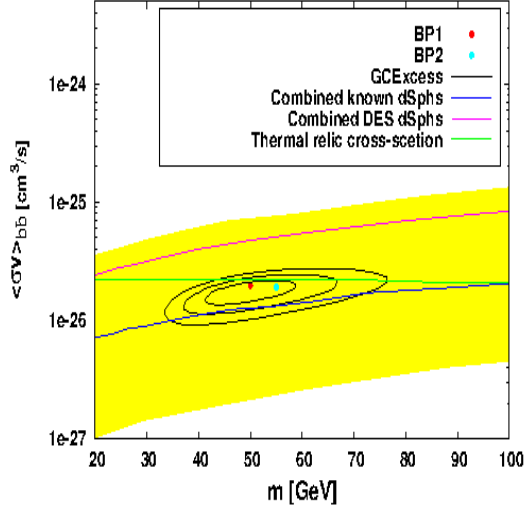


Figure 7.5: The allowed range of $m - \langle\sigma v\rangle$ space (for annihilation into $b\bar{b}$) along with the bounds on $\langle\sigma v\rangle$ (into $b\bar{b}$ channel only) obtained from GC γ ray search results CCW [60] and dwarf galaxies [61, 62] compared with the same obtained from benchmark points in Table 7.1.

CCW [60] analysis of GC gamma ray excess observations. The blue line in Fig. 7.5 describes the bounds in $m - \langle\sigma v\rangle_{b\bar{b}}$ plane given by the analysis of gamma rays from previously discovered 15 dSphs and they are adopted from [61]. Also shown in Fig. 7.5, the yellow band which is the 95% confidence limit (C.L.) region adopted from the analysis in Ref. [61] for DM annihilation into $b\bar{b}$. The combined bounds on $\langle\sigma v\rangle_{b\bar{b}}$ for different DM mass m from a recent study of the newly discovered 8 DES dwarf galaxies [62] are given by the pink coloured line in Fig. 7.5. The green horizontal line in Fig. 7.5 shows the annihilation cross-section for thermal dark matter that may yield the right DM relic abundance obtained from the PLANCK experiment.

From Fig. 7.5 one readily observes that the calculated values of $\langle\sigma v\rangle_{b\bar{b}}$ for the benchmark points BP1 and BP2 in our model broadly agrees with the 1σ , 2σ and 3σ allowed regions in $m - \langle\sigma v\rangle_{b\bar{b}}$ plane obtained from the experimental results. This can also be noted from Fig. 7.5 that these benchmark points are consistent the combined limit from DES dwarf satellite data and falls within the 95% C.L. limit predicted by Fermi-LAT for 15 dSphs. Also the calculated values of $\langle\sigma v\rangle_{b\bar{b}}$ for the benchmark

points considered in our work lie below the upper bound on thermal DM annihilation cross-section. Hence, DM fermion in the present model can account for the galactic centre excess in γ -ray and is also consistent with the bounds on gamma ray flux from Milky-Way dwarf satellite galaxies.

We now calculate the gamma ray flux for 8 new dwarf satellite galaxies discovered by the DES experiment for the hidden sector fermionic dark matter candidate proposed in this work. These calculations are performed with each of the benchmark parameter sets BP1 and BP2 given in Table 7.1. The gamma ray flux for each of these 8 dSphs in the work [62] is computed using Eq. 7.31 and the values of the J factors (Eq. 7.32) for each of the eight dSphs adopted from Ref. [62]. In Ref. [62] these J factors are estimated by integrating the dark matter density (adopting NFW halo profile for DM density distribution) along the line of sight over a solid angle $\Delta\Omega = 2.4 \times 10^{-4} \text{ sr}^{-1}$. As previously mentioned the gamma ray spectrum $\frac{dN}{dE}$ is also obtained from Ref. [136] for this calculation. The calculated flux for each of the eight dSphs are shown in eight plots (a-h) of Fig. 7.6. Also shown in each of the eight plots of Fig. 7.6, the respective upper bounds of the flux given by the experimental observations of gamma rays from each of the eight dSphs. These are shown as red coloured points while the computed flux in this work for the respective dSphs are given by continuous lines in Fig. 7.6. The green and blue continuous lines in each of the plots (a-h) of Fig. 7.6 correspond to the calculated flux using the benchmark points BP1 and BP2 respectively. It is clear from Fig. 7.6 that the fluxes calculated, assuming the annihilation of the DM candidate in our proposed model, for all the eight dSphs do not exceed the upper limit of γ flux set by the experimental observations of DES collaboration.

Besides the 15 dwarf galaxies investigated earlier and the eight other recently explored dwarf galaxies, one more dwarf galaxy namely Reticulum 2 (Ret2) has been

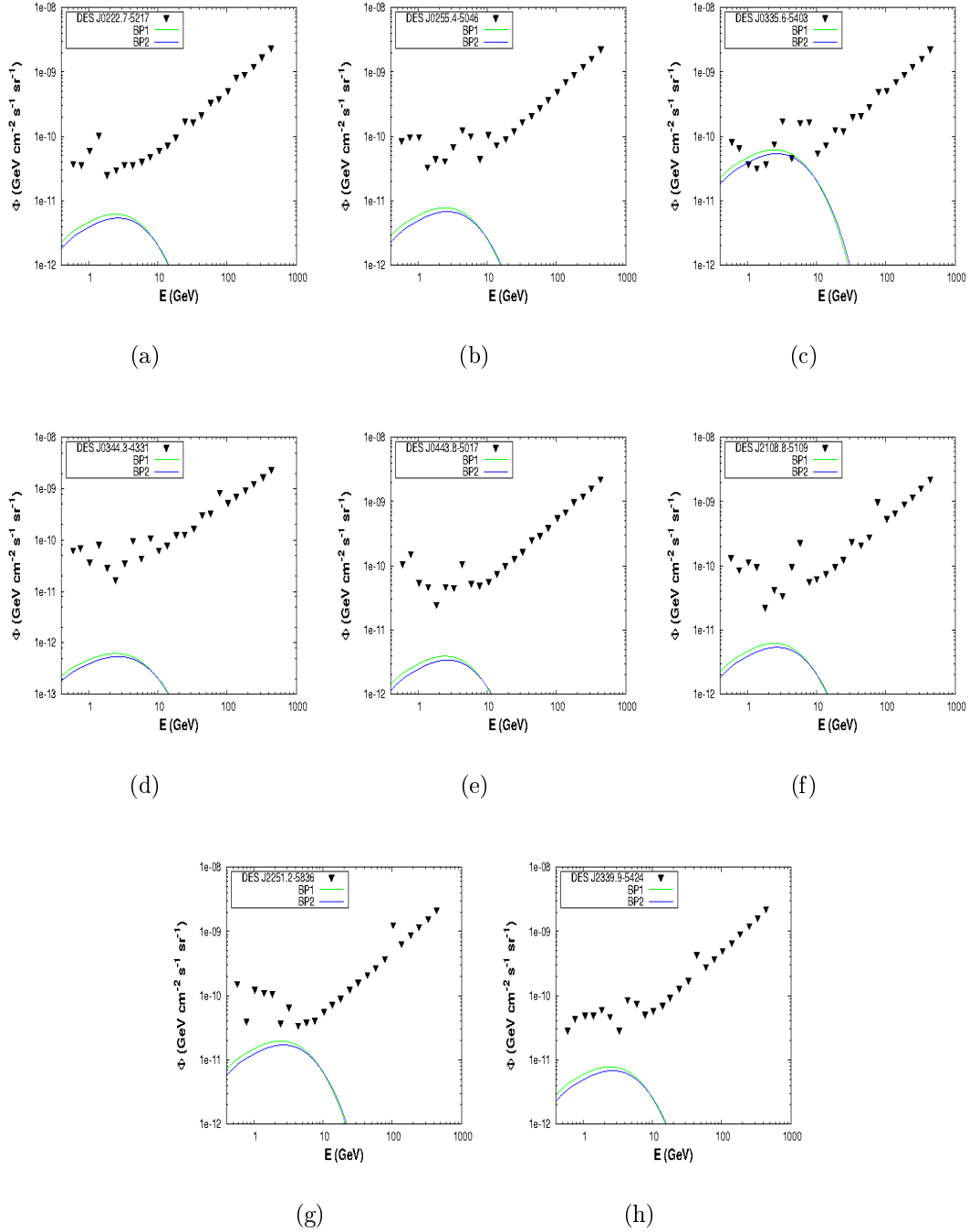


Figure 7.6: Comparison of the observed upper bound on γ -ray flux for 8 DES dSphs with the calculated γ -ray flux from BP1 and BP2 tabulated in Table 7.1.

probed very recently. Geringer-Sameth et. al. [133], after an analysis of observed gamma rays from Ret2 dwarf galaxy reported an excess of gamma ray emission from Ret2. From their analysis of Ret2 data Geringer-Sameth et. al. provide different C.L.

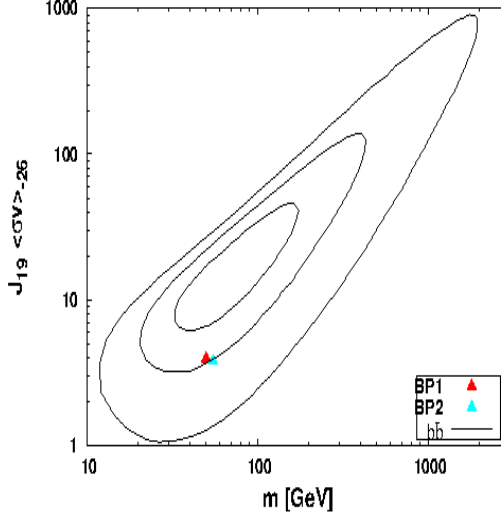


Figure 7.7: Benchmark points BP1 and BP2 compared with the allowed region of model parameter space shown in $m - J_{19}\langle\sigma v\rangle_{-26}$ plane obtained from [133]

allowed contours in $m - J_{19}\langle\sigma v\rangle_{-26}$ plane where m is the mass of the dark matter and $J_{19}\langle\sigma v\rangle_{-26}$ is the product of the J factor in the units of $10^{19} \text{ GeV}^2 \text{ cm}^{-5}$ and thermal averaged product $\langle\sigma v\rangle$ of annihilation cross-section and relative velocity in the units of $10^{-26} \text{ cm}^3 \text{ s}^{-1}$ for various final state SM channels. As mentioned earlier in this work DM candidate primarily annihilates into $b\bar{b}$, only the contours for the DM pair annihilation into $b\bar{b}$ channel are adopted. For the present dark matter model with the constrained parameter space discussed earlier we compute the quantity $J_{19}\langle\sigma v\rangle_{-26}$ for different dark matter mass m annihilating into $b\bar{b}$ channel. However the value of the J factor for Ret2 has been adopted from [133]. In their work Geringer-Sameth et. al. [133] estimated the J values by performing line of sight integral over a circular region with angular radius 0.5° surrounding the dwarf and over a solid angle $\Delta\Omega = 2.4 \times 10^{-4} \text{ sr}^{-1}$. All these calculations are performed for two values of non-SM scalar mass accounted in the present model namely $m_2 = 100 \text{ GeV}$ and $m_2 = 110 \text{ GeV}$. The results are presented for the two benchmark points BP1 and BP2 corresponding to the calculations with $m_2 = 100 \text{ GeV}$ and $m_2 = 110 \text{ GeV}$ are shown in red and skyblue points in Fig. 7.7. In Fig. 7.7, the contours from the experimental data analysis by

Geringer-Sameth et. al. are given for comparison. In Fig. 7.7 the contours for 68%, 95% and 99.7% C.L. are shown in black coloured lines in increasing order of area enclosed by each contour. The valid regions of $m - J_{19}\langle\sigma v\rangle_{-26}$ plane in our model (calculated for DM annihilating into $b\bar{b}$ pair) are presented by green coloured patches in both the plots of Fig. 7.7. From Fig. 7.7, it can be easily observed that $J_{19}\langle\sigma v\rangle_{-26}$ in the present model calculated for DM annihilating into $b\bar{b}$ channel (for benchmark points with $m_2=100$ GeV and 110 GeV) is within the 3σ C.L. limit. Hence fermionic DM candidate in the present framework can also explain the observed excess in γ -ray from Ret2.

7.5 Discussions and Conclusions

We have proposed the existence of a hidden sector which obeys a local $SU(2)_H$ and a global $U(1)_H$ gauge symmetries. In order to introduce fermions which are charged under this $SU(2)_H$ gauge group one should have at least two fermion doublets in order to avoid “Witten anomaly”. The particle and the antiparticle of these dark fermions are different as they possess equal and opposite $U(1)_H$ charges. However, similar to the usual Higgs doublet in the visible sector, this hidden sector also has an $SU(2)_H$ scalar doublet which does not have any $U(1)_H$ charge. The $SU(2)_H$ gauge symmetry breaks spontaneously when the neutral component of the scalar doublet Φ gets VEV and thereby generates masses to the dark gauge bosons (A'_μ) and dark fermions (f_i). In this work this lightest fermion is the candidate for particle dark matter. The dark sector scalar can interact with the SM Higgs like scalar in the visible sector and only through this interaction two sectors are mutually connected. However the dark fermions and dark gauge bosons remain unaffected by the visible sector due to the non abelian $SU(2)_H$ structure of the dark sector.

We constrain the model parameters from theoretical and experimental bounds such as vacuum stability, relic abundance of DM from PLANCK, direct detection experimental limits on DM-nucleon scattering cross-section from LUX etc. and test the viability of the model. Bounds from LHC on SM Higgs signal strength and invisible decay are also used to constrain the parameter space. Implementing these theoretical and experimental limits on the model suggests that only a small region of the available parameter space (region near the scalar resonances) is consistent with these bounds taken into account. Study of the model parameters thus constrained show that the mixing between the two scalars of the model is very small and depends on the VEV of the scalar doublets. With the allowed region of the parameter space for the present DM candidate (dark fermion) we compute the gamma ray flux from the GC region by explicitly calculating the annihilation cross-section for the DM candidate f_1 in the $b\bar{b}$ channel ($f_1\bar{f}_1 \rightarrow b\bar{b}$). These computational results are then compared with the experimental analysis of the Fermi-LAT observed GC gamma ray flux data considering the dark matter at the GC primarily pair annihilates into $b\bar{b}$. Our proposed DM candidate can indeed explain the results from these experimental analyses.

In search of indirect evidence of dark matter from astrophysical sources, the gamma rays from various dwarf satellite galaxies are also explored for possible signature of excess gamma rays from these sites. To this end 15 such dwarf galaxies have earlier been investigated and more recently the gamma ray observation is also reported from eight more newly discovered dSphs. From the analyses of these observational results different C.L. bounds have been given in the parameter space of $\langle\sigma v\rangle_{b\bar{b}} - m$ plane. We compare our computational results with these experimental bounds and found that the γ -rays that the DM candidate in our model produce on pair annihilation can simultaneously satisfy the observational results from GC and dwarf galaxies. We also demonstrate that the calculated fluxes in our model for

each of the recently discovered eight dwarf galaxies lie below the corresponding upper limits of the fluxes obtained from the observational results of these dwarf galaxies. We further demonstrate that our calculations are also in good agreement with the analysis of Ret2 dwarf galaxy observations.

Our work clearly demonstrate that the dark matter candidate proposed in this work is a viable one to explain the γ -rays from both the GC region and dwarf galaxies simultaneously. However the dark matter can also pair annihilate into fermion-antifermion pairs and there are experiments such as AMS-02 that look for the excess of e^+/e^- or p/\bar{p} in cosmos. In a recent work, AMS-02 collaboration have reported their first measurement of p/\bar{p} flux [47]. A model independent analysis of this AMS-02 p/\bar{p} data is performed by Jin et.al. [137]. In this work [137], the upper limits in $\langle\sigma v\rangle$ value for DM annihilation into SM particles (quarks and gauge bosons) for different considered DM halo profiles (NFW, Isothermal, Moore) are obtained. The analysis presented in the work [137] also considered four different propagation models namely conventional, MED, MIN and MAX⁶. We have also checked that the DM in our model satisfies upper bound on $\langle\sigma v\rangle_{b\bar{b}}$ given in Ref. [137] when NFW profile is considered. This is found to be true for both the cases of dark sector scalar mass $m_2 = 100$ GeV and $m_2 = 110$ GeV. Hence, fermionic dark matter explored in the present model can serve as a potential candidate for dark matter. Upcoming results from LHC as also DM direct and indirect search experiments may provide stringent limits on the available model parameter space.

⁶For further studies see [137] and references therein.

Chapter 8

Summary

In this thesis, different particle physics models for viable particle dark matter candidate have been proposed by simple extension of Standard Model of particle physics. Viability of these dark matter models are then investigated keeping in consideration, the observational results from LHC experiment, direct detection and indirect dark matter search experiments and more importantly verifying that for each of the models, the relic density results given by PLANCK CMBR anisotropy probe. Dark matter phenomenology in the models proposed here in this thesis includes the study of extended Higgs sector with extra Higgs doublets and singlets. Also the thesis contains a brief overview of dark matter in the Universe, its properties and relic densities.

In Chapter 1, preliminary ideas of dark matter such as evidences of dark matter, distribution of dark matter halo in the Universe, possible dark matter candidates etc. are discussed which have been used later for phenomenological studies of dark matter. In the next Chapter (Chapter 2), Standard Model (SM) of particle physics is revisited and limitations of SM are addressed which provides a strong motivation for beyond

Standard Model (BSM) studies. Thermal evolution of dark matter particle (cold) and solution to its Boltzmann equation in order to calculate the relic abundance is described in Chapter 3. In addition, direct and indirect detection methodology of dark matter due to interactions of dark matter with SM particles (scattering and annihilation) is also addressed in this Chapter.

In Chapter 4 we have proposed and explored a model of fermionic dark matter with a possible extension of Standard Model (SM) of particle physics into two Higgs doublet model. Higgs doublets couple to the singlet fermionic dark matter (FDM) through a non-renormalisable coupling providing a new physics scale. We explore the viability of such dark matter candidate and constrain the model parameter space by collider search, relic density of DM, direct detection measurements of DM-nucleon scattering cross-section. Limitations of this non-renormalisable model is also discussed in this chapter.

In the next Chapter (Chapter 5) we have considered a model for particle dark matter where an extra inert Higgs doublet and an additional scalar singlet is added to the Standard Model (SM) Lagrangian. The dark matter candidate is obtained from only the inert doublet. The stability of this one component dark matter is ensured by imposing a Z_2 symmetry on this additional inert doublet. The additional singlet scalar has a non zero vacuum expectation value (VEV) and mixes with the Standard Model Higgs doublet resulting in two CP even scalars h_1 and h_2 . We treat one of these scalars, h_1 , to be consistent with the SM Higgs like boson of mass around 125 GeV reported by the LHC experiment. These two CP even scalars contribute to the annihilation cross-section of this inert doublet dark matter resulting an allowed region of dark matter mass that satisfies the observed relic density given by PLANCK satellite borne experiment. Detailed analysis of the processes $h_1 \rightarrow \gamma\gamma$, $h_1 \rightarrow \gamma Z$ are presented and compared with LHC results to constrain the dark matter parameter

space in the present model. We have found that the dark matter candidate in the mass region 60-80 GeV is in agreement with the recent bound from LUX direct detection experiment.

Recent studies of gamma rays originating from the region of galactic centre have confirmed anomalous γ -ray excess within the energy range 1-3 GeV. This can be explained as the consequence of pair annihilation of a 31-40 GeV dark matter into $b\bar{b}$ with thermal annihilation cross-section $\sigma v \sim 1.4 - 2.0 \times 10^{-26} \text{ cm}^3/\text{s}$. In Chapter 6 we revisited the inert doublet model (IDM) in order to explain this gamma ray excess. Assuming the lightest inert particle (LIP) as a stable DM candidate we show that a 31-40 GeV dark matter derived from IDM will fail to satisfy experimental limits on dark matter direct detection cross-section obtained from ongoing direct detection experiments and is also inconsistent with LHC findings. We show that a singlet extended inert doublet model can easily explain the reported γ -ray excess which is as well in agreement with Higgs search results at LHC and other observed results like DM relic density and direct detection constraints.

In Chapter 7, a hidden sector dark matter model is explored assuming new particles in the dark sector (both fermionic and bosonic) invariant under a local $SU(2)_H$ gauge symmetry while behaving like a singlet under the SM gauge group. However, the fermionic fields of the dark sector also possess another global $U(1)_H$ symmetry which remains unbroken. The local $SU(2)_H$ invariance of the dark sector is broken spontaneously when a scalar field in this sector acquires a vacuum expectation value (VEV) and thereby generating masses to the dark gauge bosons and dark fermions charged under the $SU(2)_H$. The lightest fermion in this dark $SU(2)_H$ sector can be a potential dark matter candidate. We first examine the viability of the model and constrain the model parameter space by theoretical constraints such as vacuum stability and by the experimental constraints such as PLANCK limit on

relic density, LHC data, limits on spin independent scattering cross-section from dark matter direct search experiments etc. We then investigate the gamma rays from the pair annihilation of the proposed dark matter candidate at the galactic centre region. We also extend our calculations of gamma rays flux for the case of dwarf galaxies and compare the signatures of gamma rays obtained from these astrophysical sites.

Throughout the work, we have explored phenomenological models for cold dark matter and tested the viability of these models from direct dark matter search experiments, collider search results, vacuum stability of the model, dark matter relic abundance etc. We further investigated whether these models can explain observed astrophysical results obtained from indirect detection searches of dark matter (such as excess of γ -rays from galactic centre, dwarf galaxies etc.). Apart from cold dark matter, there are also other types of dark matter namely hot dark matter, warm dark matter which are of great interest in order to explain the structure formation, nature of Universe at early epoch etc. Asymmetric dark matter models are also encouraged to explain the dark matter problem along with leptogenesis, neutrino mass etc. Study of these dark matter models will be interesting which may enrich the physics of dark matter and provide a better understanding of the evolution of our Universe. In this thesis, we have considered only models with single dark matter component. However, there is possibility that dark matter may be multicomponent in nature. Relic abundance of dark matter in multicomponent dark matter models is calculated by solving coupled Boltzmann equations for dark matter candidates appearing in the model. Non thermal dark matter models are pursued in literatures to explain self interaction of dark matter. Elaborative study of these different dark matter models can be explored to solve the dark matter puzzle in the Universe which may also provide feasible explanation to other unsolved problems in the Universe. In future, I wish to study these above mentioned dark matter models in detail. Besides, collider searches of dark matter can also provide valuable information about the property of

dark matter. I am willing to study the collider aspects of the dark matter in light of present results of LHC and future results from both LHC and ILC.

Appendix A

Diphoton and γZ decay width of scalar bosons

Earlier in Chapter 5 and Chapter 6, we have discussed Inert Doublet Model with additional singlet scalar. The inert charged scalar appearing in the model will contribute to Higgs decay channels like $\gamma\gamma$ and γZ through the charged scalar loop involved in the process. Decay widths of $h_i \rightarrow \gamma\gamma, \gamma Z$ ($i = 1, 2$) are given as

$$\begin{aligned}\Gamma(h_i \rightarrow \gamma\gamma) &= \frac{G_F \alpha_s^2 m_i^3}{128\sqrt{2}\pi^3} \left| c_i \left(\frac{4}{3} F_{1/2} \left(\frac{4m_t^2}{m_i^2} \right) + F_1 \left(\frac{4m_W^2}{m_i^2} \right) \right) + \frac{\lambda_{h_i H^+ H^-} v^2}{2m_{H^\pm}^2} F_0 \left(\frac{4m_{H^\pm}^2}{m_i^2} \right) \right|^2, \\ \Gamma(h_i \rightarrow \gamma Z) &= \frac{G_F^2 \alpha_s}{64\pi^4} m_W^2 m_i^3 \left(1 - \frac{m_Z^2}{m_i^2} \right)^3 \left| -2c_i \frac{1 - \frac{8}{3}s_W^2}{c_W} F'_{1/2} \left(\frac{4m_t^2}{m_i^2}, \frac{4m_t^2}{m_Z^2} \right) \right. \\ &\quad \left. - c_i F'_1 \left(\frac{4m_W^2}{m_i^2}, \frac{4m_W^2}{m_Z^2} \right) + \frac{\lambda_{h_i H^+ H^-} v^2 (1 - 2s_W^2)}{2m_{H^\pm}^2 c_W} I_1 \left(\frac{4m_{H^\pm}^2}{m_i^2}, \frac{4m_{H^\pm}^2}{m_Z^2} \right) \right|^2,\end{aligned}$$

where G_F is the Fermi constant and s_W (c_W) is $\sin \theta_W$ ($\cos \theta_W$) with θ_W representing the weak mixing angle. Factor c_i in the above is given as $\cos \alpha$ or $\sin \alpha$ for $i = 1, 2$.

Couplings $\lambda_{h_1 H^+ H^-}$ and $\lambda_{h_2 H^+ H^-}$ in the expressions of decay widths are of the form

$$\begin{aligned}\lambda_{h_1 H^+ H^-} v &= (\lambda_3 c_\alpha - \lambda_s s_\alpha) v, \\ \lambda_{h_2 H^+ H^-} v &= (\lambda_3 s_\alpha + \lambda_s c_\alpha) v.\end{aligned}$$

In Chapter 5,6 we have calculated the decay widths $h_i \rightarrow \gamma\gamma, \gamma Z$ ($i = 1, 2$) in terms of the loop factors $F_{1/2}, F_1, F_0, F'_{1/2}, F'_1$ and I_1 . Expressions of the factors $F_{1/2}, F_1, F_0$ (for the measurement of $h_1 \rightarrow \gamma\gamma$ decay width) are given as [66]

$$\begin{aligned}F_{1/2}(\tau) &= 2\tau[1 + (1 - \tau)f(\tau)], \\ F_1(\tau) &= -[2 + 3\tau + 3\tau(2 - \tau)f(\tau)], \\ F_0(\tau) &= -\tau[1 - \tau f(\tau)],\end{aligned}$$

where the function $f(x)$ is given as

$$f(x) = \begin{cases} \arcsin^2\left(\frac{1}{\sqrt{x}}\right) & \text{for } x \geq 1, \\ -\frac{1}{4} \left[\log\left(\frac{1+\sqrt{1-x}}{1-\sqrt{1-x}}\right) - i\pi \right]^2 & \text{for } x < 1. \end{cases}$$

Similarly the loop factor for $h_i \rightarrow \gamma Z$ channel are [66]

$$\begin{aligned}F'_{1/2}(\tau, \lambda) &= I_1(\tau, \lambda) - I_2(\tau, \lambda), \\ F'_1(\tau, \lambda) &= c_W \left(4 \left(3 - \frac{s_W^2}{c_W^2} \right) I_2(\tau, \lambda) + \left[\left(1 + \frac{2}{\tau} \right) \frac{s_W^2}{c_W^2} - \left(5 + \frac{2}{\tau} \right) \right] I_1(\tau, \lambda) \right).\end{aligned}$$

Expressions of the factors I_1 and I_2 are of the form

$$\begin{aligned}I_1(a, b) &= \frac{ab}{2(a-b)} + \frac{a^2 b^2}{2(a-b)^2} [f(a) - f(b)] + \frac{a^2 b}{(a-b)^2} [g(a) - g(b)], \\ I_2(a, b) &= -\frac{ab}{2(a-b)} [f(a) - f(b)].\end{aligned}$$

where $f(x)$ is same as used in $h_i \rightarrow \gamma\gamma$ channel and $g(x)$ is given as

$$g(x) = \begin{cases} \sqrt{x-1} \arcsin \sqrt{\frac{1}{x}} & \text{for } x \geq 1, \\ \frac{\sqrt{1-x}}{2} \left(\log \frac{1+\sqrt{1-x}}{1-\sqrt{1-x}} - i\pi \right) & \text{for } x < 1. \end{cases}$$

Bibliography

- [1] G. Jungman, M. Kamionkowski and K. Griest, Phys. Rept. **267** 195 (1996).
- [2] D. Clowe, M. Bradac, A. H. Gonzalez, M. Markevitch, S. W. Randall, C. Jones and D. Zaritsky, Astrophys. J. **648**, L109 (2006).
- [3] P. A. R. Ade *et al.* [Planck Collaboration], Astron. Astrophys. **571**, A16 (2014).
- [4] G. Hinshaw *et al.* [WMAP Collaboration], Astrophys. J. Suppl. **208**, 19 (2013).
- [5] J.F. Navarro, C.S. Frenk and S.D. White, Astrophys. J. **462**, 563 (1996).
- [6] A. W. Graham, D. Merritt, B. Moore, J. Diemand and B. Terzic, Astron. J. **132**, 2685 (2006).
- [7] K. G. Begeman, A. H. Broeils, R. H. Sanders, MNRAS **249**, 523 (1991).
- [8] J. Diemand, B. Moore and J. Stadel, MNRAS **353**, 624 (2004).
- [9] A. Burkert, IAU Symp. **171**, 175 (1996) [Astrophys. J. **447**, L25 (1995)].
- [10] P. B. Tissera, S. D. M. White, S. Pedrosa and C. Scannapieco, MNRAS **406**, 922 (2010).

- [11] G. Bertone, D. Hooper and J. Silk, Phys. Rept. **405**, 279 (2005).
- [12] D. Hooper and S. Profumo, Phys. Rept. **453**, 29 (2007).
- [13] V. Silveira and A. Zee, Phys. Lett. B **161**, 136 (1985).
- [14] R. Barbieri, L. J. Hall and V. S. Rychkov, Phys. Rev. D **74**, 015007 (2006).
- [15] Y. G. Kim, K. Y. Lee and S. Shin, JHEP **0805**, 100 (2008).
- [16] T. Hambye, JHEP **0901**, 028 (2009).
- [17] L. J. Hall, K. Jedamzik, J. March-Russell and S. M. West, JHEP **1003**, 080 (2010).
- [18] C. E. Yaguna, JHEP **1108**, 060 (2011).
- [19] S. L. Glashow, Nucl. Phys. **22**, 579 (1961).
- [20] A. Salam, Conf. Proc. **C680519**, 367 (1968).
- [21] S. Weinberg, Phys. Rev. Lett. **19**, 1264 (1967).
- [22] Y. Fukuda *et al.* [Super-Kamiokande Collaboration], Phys. Rev. Lett. **81**, 1562 (1998).
- [23] Q. R. Ahmad *et al.* [SNO Collaboration], Phys. Rev. Lett. **87**, 071301 (2001).
- [24] E. Komatsu *et al.* [WMAP collaboration], Astrophys. J. Suppl. **192**, 18 (2011).
- [25] P. Gondolo and G. Gelmini, Nucl. Phys. B **360**, 145 (1991).

- [26] E.W. Kolb and M. Turner, *The Early Universe* (Westview Press, Boulder, 1990).
- [27] E. Aprile *et al.* [XENON100 Collaboration], *Phys. Rev. Lett.* **109**, 181301 (2012).
- [28] D. S. Akerib *et al.* [LUX Collaboration], *Phys. Rev. Lett.* **112**, 091303 (2014).
- [29] R. Agnese *et al.* [CDMS Collaboration], *Phys. Rev. D* **88**, 031104 (2013).
- [30] R. Agnese *et al.* [SuperCDMS Collaboration], *Phys. Rev. Lett.* **112**, 241302 (2014).
- [31] C. E. Aalseth *et al.* [CoGeNT Collaboration], *Phys. Rev. Lett.* **106**, 131301 (2011).
- [32] R. Bernabei *et al.* [DAMA Collaboration], *Eur. Phys. J. C* **56**, 333 (2008).
- [33] R. Bernabei *et al.* [DAMA and LIBRA Collaborations], *Eur. Phys. J. C* **67**, 39 (2010).
- [34] R. Bernabei *et al.* [DAMA Collaboration], *Eur. Phys. J. C* **74**, 3196 (2014).
- [35] E. Armengaud *et al.* [EDELWEISS Collaboration], *Phys. Lett. B* **702**, 329 (2011).
- [36] G. Angloher *et al.*, *Eur. Phys. J. C* **72**, 1971 (2012).
- [37] S. Archambault *et al.*, *Phys. Lett. B* **682**, 185 (2009).
- [38] C. Amole *et al.* [PICO Collaboration], *Phys. Rev. Lett.* **114**, 231302 (2015).
- [39] F. Aharonian *et al.* [HESS Collaboration], *Astrophys. J.* **636**, 777 (2006).
- [40] J. Albert *et al.* [MAGIC Collaboration], *Astrophys. J.* **674**, 1037 (2008).

- [41] T. C. Weekes *et al.*, *Astropart. Phys.* **17**, 221 (2002).[astro-ph/0108478].
- [42] [Fermi-LAT Collaboration], *Astrophys. J. Suppl.* **199**, 31 (2012).
- [43] M. Ageron *et al.* [ANTARES Collaboration], *Nucl. Instrum. Meth. A* **656**, 11 (2011).
- [44] R. Abbasi *et al.* [IceCube Collaboration], *Phys. Rev. Lett.* **102**, 201302 (2009).
- [45] M. Aguilar *et al.* [AMS Collaboration], *Phys. Rev. Lett.* **110** 141102 (2013).
- [46] O. Adriani *et al.* PAMELA Collaboration, *Nature* **458**, 607 (2009).
- [47] S. Ting, talk at AMS-02 days, April 15-17, CERN.
- [48] M. Ajello *et al.* [Fermi-LAT Collaboration], *Astrophys. J.* **819**, no. 1, 44 (2016).
- [49] Fermi Science Support Center, <http://fermi.gsfc.nasa.gov/ssc/data/access/>.
- [50] L. Goodenough and D. Hooper, arXiv:0910.2998 [hep-ph].
- [51] D. Hooper and L. Goodenough, *Phys. Lett. B* **697**, 412 (2011).
- [52] A. Boyarsky, D. Malyshev and O. Ruchayskiy, *Phys. Lett. B* **705**, 165 (2011).
- [53] D. Hooper and T. Linden, *Phys. Rev. D* **84**, 123005 (2011).
- [54] K. N. Abazajian and M. Kaplinghat, *Phys. Rev. D* **86**, 083511 (2012).
- [55] D. Hooper and T. R. Slatyer, *Phys. Dark Univ.* **2**, 118 (2013).

- [56] K. N. Abazajian, N. Canac, S. Horiuchi and M. Kaplinghat, Phys. Rev. D **90**, 023526 (2014).
- [57] R. Bartels, S. Krishnamurthy and C. Weniger, excess,” Phys. Rev. Lett. **116**, no. 5, 051102 (2016) [arXiv:1506.05104 [astro-ph.HE]].
- [58] S. K. Lee, M. Lisanti, B. R. Safdi, T. R. Slatyer and W. Xue, Phys. Rev. Lett. **116**, no. 5, 051103 (2016) [arXiv:1506.05124 [astro-ph.HE]].
- [59] T. Daylan, D. P. Finkbeiner, D. Hooper, T. Linden, S. K. N. Portillo, *et al.*, Phys. Dark Univ. **12**, 1 (2016).
- [60] F. Calore, I. Cholis and C. Weniger, JCAP **1503**, 038 (2015).
- [61] M. Ackermann *et al.* [Fermi-LAT Collaboration], Phys. Rev. Lett. **115**, 231301 (2015).
- [62] A. Drlica-Wagner *et al.* [Fermi-LAT and DES Collaborations], Astrophys. J. **809**, L4 (2015).
- [63] S. Chatrchyan *et al.* [CMS Collaboration], Phys. Lett. B **716**, 30 (2012).
- [64] G. Aad *et al.* [ATLAS Collaboration], Phys. Lett. B **716**, 1 (2012).
- [65] G. C. Branco, P. M. Ferreira, L. Lavoura, M. N. Rebelo, M. Sher and J. P. Silva, Phys. Rept. **516**, 1 (2012).
- [66] J. F. Gunion, H. E. Haber, G. L. Kane and S. Dawson, Front. Phys. **80** 1 (2000).
- [67] M. Aoki, S. Kanemura and O. Seto, Phys. Lett. B **685**, 313 (2010).

- [68] X. -G. He and J. Tandean, Phys. Rev. D **88**, 013020 (2013).
- [69] Y. Cai and T. Li, Phys. Rev. D **88**, 115004 (2013).
- [70] N. Okada and O. Seto, Phys. Rev. D **89**, 043525 (2014).
- [71] P. Ko and C. Yu, arXiv:1406.1952 [hep-ph].
- [72] A. Drozd, B. Grzadkowski, J. F. Gunion and Y. Jiang JHEP **1411**, 105 (2014).
- [73] N. Okada and O. Seto, Phys. Rev. D **90**, 083523 (2014).
- [74] R. Martinez, J. Nisperuza, F. Ochoa, J. P. Rubio and C. F. Sierra Phys. Rev. D **92**, 035016 (2015).
- [75] S. Baek, P. Ko and W. I. Park, JHEP **1202**, 047 (2012).
- [76] S. Baek, P. Ko, W. I. Park and E. Senaha, JHEP **1211**, 116 (2012).
- [77] Y. G. Kim and K. Y. Lee, Phys. Rev. D **75**, 115012 (2007).
- [78] J. F. Gunion and H. E. Haber, Phys. Rev. D **67**, 075019 (2003).
- [79] R. Harlander, M. Mühlleitner, J. Rathsmann, M. Spira and O. Stål
arXiv:1312.5571 [hep-ph].
- [80] G. Aad *et al.* [ATLAS Collaboration], Phys. Lett. B **726**, 88 (2013).
- [81] [CMS Collaboration], CMS PAS HIG-13-005.
- [82] A. Denner *et al.*, Eur. Phys. J. C **71**, 1753 (2011).

- [83] X. -G. He, T. Li, X. -Q. Li, J. Tandean and Ho-C. Tsai, Phys. Rev. D **79**, 023521 (2009).
- [84] [ATLAS Collaboration], ATLAS-CONF-2014-009.
- [85] [CMS Collaboration], CMS-HIG-13-001.
- [86] E. Ma, Phys. Rev. D **73**, 077301 (2006).
- [87] L. Lopez Honorez, E. Nezri, J. F. Oliver and M. H. G. Tytgat, JCAP **0702**, 028 (2007).
- [88] D. Majumdar and A. Ghosal, Mod. Phys. Lett. A **23**, 2011 (2008).
- [89] M. Gustafsson, E. Lundstrom, L. Bergstrom and J. Edsjo, Phys. Rev. Lett. **99**, 041301 (2007).
- [90] Q. -H. Cao, E. Ma and G. Rajasekaran, Phys. Rev. D **76**, 095011 (2007).
- [91] E. Lundstrom, M. Gustafsson and J. Edsjo, Phys. Rev. D **79**, 035013 (2009).
- [92] S. Andreas, M. H. G. Tytgat and Q. Swillens, JCAP **0904**, 004 (2009).
- [93] L. Lopez Honorez and C. E. Yaguna, JHEP **1009**, 046 (2010).
- [94] L. Lopez Honorez and C. E. Yaguna, JCAP **1101**, 002 (2011).
- [95] T. A. Chowdhury, M. Nemevsek, G. Senjanovic and Y. Zhang, JCAP **1202**, 029 (2012).
- [96] D. Borah and J. M. Cline, Phys. Rev. D **86**, 055001 (2012).

- [97] M. Fairbairn and R. Hogan, JHEP **1309**, 022(2013).
- [98] K. Kannike, Eur. Phys. J. C **72**, 2093 (2012).
- [99] J. Beringer et al. (Particle Data Group), Phys. Rev. D **86**, 010001 (2012).
- [100] A. Biswas, D. Majumdar, A. Sil and P. Bhattacharjee, JCAP **1312**, 049 (2013)
- [101] A. Arhrib, R. Benbrik and N. Gaur, Phys. Rev. D **85**, 095021 (2012).
- [102] B. Swiezewska and M. Krawczyk, Phys. Rev. D **88**, 035019 (2013).
- [103] A. Goudelis, B. Herrmann and O. Stal, JHEP **1309**, 106 (2013).
- [104] P. Posch, Phys. Lett. B **696**, 447 (2011).
- [105] G. Bhattacharyya, D. Das, P. B. Pal and M. N. Rebelo, JHEP **1310**, 081 (2013).
- [106] Y. Kajiyama, H. Okada and T. Toma, Eur. Phys. J. C **73**, 2381 (2013).
- [107] E. Aprile [XENON1T Collaboration], Springer Proc. Phys. **148**, 93 (2013).
- [108] [ATLAS Collaboration], ATLAS-CONF-2012-162,ATLAS-COM-CONF-2012-198.
- [109] C. Boehm, M. J. Dolan, C. McCabe, M. Spannowsky and C. J. Wallace, JCAP **1405**, 009 (2014).
- [110] T. Lacroix, C. Boehm and J. Silk, Phys. Rev. D **90**, 043508 (2014).
- [111] S. Ipek, D. McKeen and A. E. Nelson, Phys. Rev. D **90**, 055021 (2014).

- [112] K. Kong and J. C. Park, Nucl. Phys. B **888**, 154 (2014).
- [113] W. C. Huang, A. Urbano and W. Xue, arXiv:1307.6862 [hep-ph].
- [114] B. Kyae and J.-C. Park, Phys. Lett. B **732**, 373 (2014).
- [115] N. Okada and O. Seto, Phys. Rev. D **89**, 043525 (2014).
- [116] K. P. Modak, D. Majumdar and S. Rakshit, JCAP **1503**, 011 (2015).
- [117] E. Hardy, R. Lasenby and J. Unwin, JHEP **1407**, 049 (2014).
- [118] D. G. Cerde so, M. Peir s and S. Robles, JCAP **1408**, 005 (2014).
- [119] C. Boehm, M. J. Dolan and C. McCabe, Phys. Rev. D **90**, 023531 (2014).
- [120] P. Ko, W. I. Park and Y. Tang, JCAP **1409**, 013 (2014).
- [121] M. Abdullah, A. DiFranzo, A. Rajaraman, T. M. P. Tait, P. Tanedo and A. M. Wijangco, Phys. Rev. D **90**, 035004 (2014).
- [122] D. K. Ghosh, S. Mondal and I. Saha, JCAP **1502**, 035 (2015).
- [123] A. Martin, J. Shelton and J. Unwin, Phys. Rev. D **90**, 103513 (2014).
- [124] T. Mondal and T. Basak, Phys. Lett. B **744**, 208 (2015).
- [125] L. Wang and X. F. Han, Phys. Lett. B **739**, 416 (2014).
- [126] C. Arina, E. Del Nobile and P. Panci, Phys. Rev. Lett. **114**, 011301 (2015).

- [127] G. Belanger, B. Dumont, U. Ellwanger, J. Gunion and S. Kraml, *Phys. Lett. B* **723**, 340 (2013).
- [128] E. Witten, *Phys. Lett. B* **117**, 324 (1982).
- [129] S. Di Chiara and K. Tuominen, *JHEP* **1511**, 188 (2015).
- [130] L. Lopez-Honorez, T. Schwetz and J. Zupan, *Phys. Lett. B* **716**, 179 (2012).
- [131] M. Ackermann *et al.* [Fermi-LAT Collaboration], *Phys. Rev. D* **86**, 022002 (2012).
- [132] P. Agrawal, B. Batell, P. J. Fox and R. Harnik, *JCAP* **1505**, 011 (2015).
- [133] A. Geringer-Sameth, M. G. Walker, S. M. Koushiappas, S. E. Kuposov, V. Belokurov, G. Torrealba and N. W. Evans, *Phys. Rev. Lett.* **115**, 081101 (2015).
- [134] M. Ibe, H. Murayama and T. T. Yanagida, *Phys. Rev. D* **79**, 095009 (2009).
- [135] W. L. Guo and Y. L. Wu, *Phys. Rev. D* **79**, 055012 (2009).
- [136] M. Cirelli, G. Corcella, A. Hektor, G. Hutsi, M. Kadastik, P. Panci, M. Raidal and F. Sala *et al.*, *JCAP* **1103**, 051 (2011).
- [137] H. B. Jin, Y. L. Wu and Y. F. Zhou, *Phys. Rev. D* **92**, 055027 (2015).